This book attempts to cover the basic aspects of the electrical resistivity techniques. It includes a short introduction to electrical resistivity method and trying to provide a brief summary of the past and ongoing development for the techniques of this method. Presentation of the resistivity method is started always with the basic theoretical background, field measurement procedures, data processing, and interpretation, for one or more of the techniques of this method. Therefore, this book designed to cover all resistivity techniques with the most important studies that led to the development of these technologies and their applications.

Ahmed Srdah Kadhem Al-Zubedi (BSc. In Geology from Baghdad University, Iraq. MSc. and PhD. in geophysical from Baghdad University) is an author of a number of scientific papers dealing with geophysical subjects. Currently working as Geophysicist in General Commission for Groundwater, Ministry of Water Resources- Iraq.

978-3-659-78918-2

Electrical Resistivity Techniques

S. Al-Zeubedi

Ahmed S. Al-Zeubedi

Principles of Electrical Resistivity Techniques

LAP LAMBERT Academic Publishing

Ahmed S. Al-Zeubedi

Principles of Electrical Resistivity Techniques

Ahmed S. Al-Zeubedi

Principles of Electrical Resistivity Techniques

LAP LAMBERT Academic Publishing

Impressum / Imprint
Bibliografische Information der Deutschen Nationalbibliothek: Die Deutsche Nationalbibliothek verzeichnet diese Publikation in der Deutschen Nationalbibliografie; detaillierte bibliografische Daten sind im Internet über http://dnb.d-nb.de abrufbar.

Bibliographic information published by the Deutsche Nationalbibliothek: The Deutsche Nationalbibliothek lists this publication in the Deutsche Nationalbibliografie; detailed bibliographic data are available in the Internet at http://dnb.d-nb.de.

Coverbild / Cover image: www.ingimage.com

Verlag / Publisher:
LAP LAMBERT Academic Publishing
ist ein Imprint der / is a trademark of
OmniScriptum GmbH & Co. KG
Heinrich-Böcking-Str. 6-8, 66121 Saarbrücken, Deutschland / Germany
Email: info@lap-publishing.com

Herstellung: siehe letzte Seite /
Printed at: see last page
ISBN: 978-3-659-78918-2

This book attempts to cover the basic aspects of the electrical resistivity techniques. It includes a short introduction to electrical resistivity method and trying to provide a brief summary of the past and ongoing development for the techniques of this method. Presentation of the resistivity method is started always with the basic theoretical background, field measurement procedures, data processing, and interpretation, for one or more of the techniques of this method. Therefore, this book designed to cover all resistivity techniques with the most important studies that led to the development of these technologies and their applications.

This book consists of three chapters. The first chapter covers the theoretical aspect of the electrical resistivity method including basic principles of this method, electrical conductivity of the earth materials, array types, sensitivity function, the depth of investigation, and field instruments. The second one is devoted to the 1D resistivity techniques with some applications. The 2D and 3D resistivity techniques are covered in last chapter; it includes the development of these techniques with some applications such as, 2D azimuthal resistivity imaging, cross-borehole surveys, 4D and time-lapse surveys. The array optimization methods and electrode arrays characteristics in 2D imaging surveys also covered in this chapter. The text is presented in clear and simple language, aided by numerous illustration figures. The book-layout is designed to serve as a teaching manual for university students and staff members of geophysical exploration companies.

Author

Dedication

Messenger of God Mohammed (peace be upon him and his family) said:-

If a human died his works end, except three of them, continuous Science or beneficial work or virtuous son prays to God for him.

Oh my lord, I beg you to make this work as a beneficial science and its reward is for me, my parents, my brothers, my wife, my sons, my teachers and for all Muslims and believers……. and I hope it will be in the balance of my goods on the show day and accept these from us……. you are hearing and replying.

Ahmed

CONTENTS

Chapter Three - 2D and 3D Resistivity Techniques

1-1 Introduction.

Surface geophysical techniques provide a relatively quick and inexpensive data to characterize the subsurface. It measures the physical properties of the subsurface such as electrical conductivity or resistivity, dielectric permittivity, magnetic permeability, density, or acoustic velocity. These techniques can be influenced by chemical and physical properties of soils, rocks, and pore fluids. Interpretation from these measurements can be used to image the distribution of physical properties of different materials in the subsurface.

The resistivity method is one of the oldest geophysical techniques, it is basing on passing artificial electrical current in the earth through the ground via a pair of electrodes and a resulting potential difference is measured between a second pair of potential electrodes. This method has been used for many decades in hydrogeological, mining, geotechnical, archeological, environmental and engineering investigation. The resistivity method has been used since early 1900s, when it was initially applied for qualitative interpretations by locating conductive anomalies by moving a potential electrode pair while keeping the current electrodes fixed. According to Dahlin, (2001), such work was carried out in Sweden in 1906. While Conrad Schlumberger started his pioneering work on electrical prospecting in 1912, and approximately at the same time Wenner developed the same idea in the USA.

Since the first commercial use of the resistivity method in the early 1920's (Burger et al., 2006) and right up to the late 1980's, it has been used essentially as a one-dimensional (1D) resistivity technique, (Loke et al., 2013). The 1D resistivity technique was carried out doing Constant Separation Traverse (CST), Vertical Electrical Sounding (VES) and Combined VES/CST techniques. As a result advances in field equipment design capability and computer algorithms led to appearance 2D and 3D resistivity techniques in the 1990s. The basic theory of resistivity method and some applications of it will be discussed in the present chapter.

1-2 Basic principles.

The resistivity method is based on the response of the earth to the flow of electrical current. Where electrical current is passing into the ground surface by two current electrodes and the potential difference is measured between second couples of electrodes. In fact, the current is flowing between two electrodes (A and B) in the subsurface earth and the current lines will take semi-circle shapes, while the equipotential lines are perpendicular on it, as shown in figure (1-1), so that any changes in the conductivities of the subsurface material lead to change the current flow lines, as a result that equipotential lines will be disturbed, because they flow vertically on the current lines. Thus, the measurement values will change on the ground surface. However, the potential difference (ΔV) at any point which is caused by two current electrodes (A and B) measured between the potential electrodes (M and N) is given by:-

$$\Delta V = V_M - V_N = \frac{\rho I}{2\pi}\left(\frac{1}{AM} - \frac{1}{BM} - \frac{1}{AN} + \frac{1}{BN}\right) \quad \ldots\ldots\ldots\ldots(1)$$

Where:-

V_M = potential at M due to A and B.

V_N = potential at N due to A and B.

I = Electrical current.

ρ = Resistivity.

AM, BM, AN, BN = Distances between the electrodes.

From equation (1)

$$\rho = \frac{2\pi}{\left(\frac{1}{AM} - \frac{1}{BM} - \frac{1}{AN} + \frac{1}{BN}\right)} \frac{\Delta V}{I} \quad \ldots\ldots\ldots\ldots(2)$$

Equation (2) is a fundamental equation in the direct - current (dc) method of electrical prospecting.

The factor $\left\{\frac{2\pi}{\left(\frac{1}{AM} - \frac{1}{BM} - \frac{1}{AN} + \frac{1}{BN}\right)}\right\}$ is called the geometric factor of the electrode arrangement and generally is designated by the letter (K).

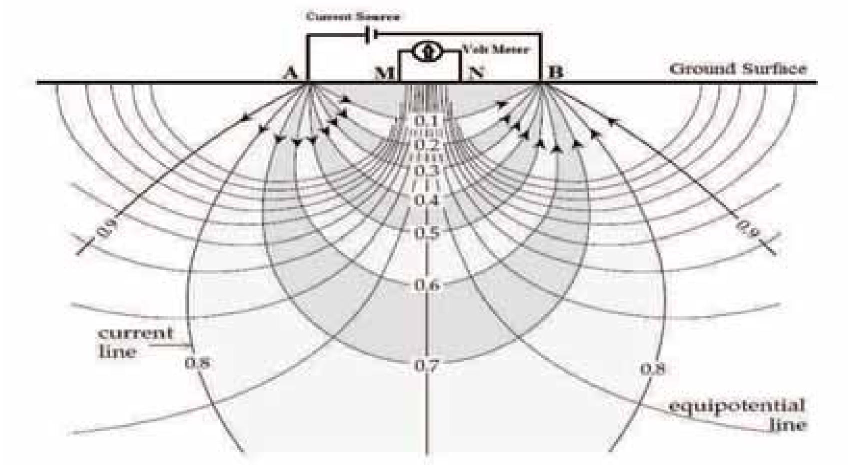

Figure (1-1):- Schematic illustrating basic concept of electrical resistivity measurement, (Lowrie, 2007).

Therefore:-

$$\rho = K\frac{\Delta V}{I} \qquad \text{.........(3)}$$

If the measurement of **(*ρ*)** is made over semi–infinite space of homogeneous and isotropic material, then this value is called resistivity **(*ρ*)** of the material. However, if the medium is inhomogeneous and/or an- isotropic then the resistivity computed from equation (2) is called an apparent resistivity **(*ρa*).** Then the general equation is:-

$$\rho_a = K\,R \qquad \text{............(4)}$$

Where:-

R = Resistance of Material= (**ΔV / I**)

The value of the apparent resistivity is a function of several variables such as, porosity, permeability, water saturation, the concentration of dissolved solids in the pore water, isotropic properties and other characteristics of the subsurface materials, (Keller and Frischknecht, 1966; Bhattacharya and patra, 1968; and Zohdy, 1974). As well as orientation of the array with respect to the bodies even the orientation of the traverse line with respect to the subsurface features, (Habberjam and Watkins, 1967). Its unit is ohm.m, or (Ω.m), and the unit of conductivity is mhos/m, or more commonly given as millimhos/m.

1-3 Electrical Conductivity of The Earth Materials.

The electric current flows into the earth by two electrodes depending on two main types of conduction. The first is electronic conduction; the current flows by free electrons, such as in metals. The second is electrolytic conduction where the current flows by the movement of ions in groundwater, (Keller and Frischknecht, 1966; Zohdy, 1974). In the areas where the water table lies near the earth's surface, the electrolytic conduction is probably the more common mechanism. In areas where the water table is deep, the electronic conduction will depend on the conductive minerals present, (Zohdy et al, 1974).

The relation between geology and resistivity depends on the physical and chemical properties of rocks and soils. Therefore, the rocks and soils have a large range of resistivity, (Keller and Frischknecht, 1966).

For sedimentary rocks, which are usually more porous and have higher water content, normally have lower resistivity values compared to igneous and metamorphic rocks. In general, the resistivity values range from (1) to about (10000 Ω.m). As on example, wet soils and fresh groundwater have even lower resistivity values. Clayey soil normally has a lower resistivity value than sandy soil .The resistivity of groundwater varies from (10) to (100 Ω.m), depending on the concentration of dissolved salts. Note that the low resistivity about (0.2 Ω.m) of sea water is due to the relatively high salt content, (Zohdy et al, 1974; Lowrie 2007; Loke, 2012).

This wide range of values is at the same time the strength and the weakness of electrical prospecting. It is the strength because it facilities distinction types of rocks; it is a weakness because it sometimes means variation in measurements that have no relation to the problem under consideration, (kunetz 1966).

The resistivity values of several rocks, sediments and water are given in figure (1-2).

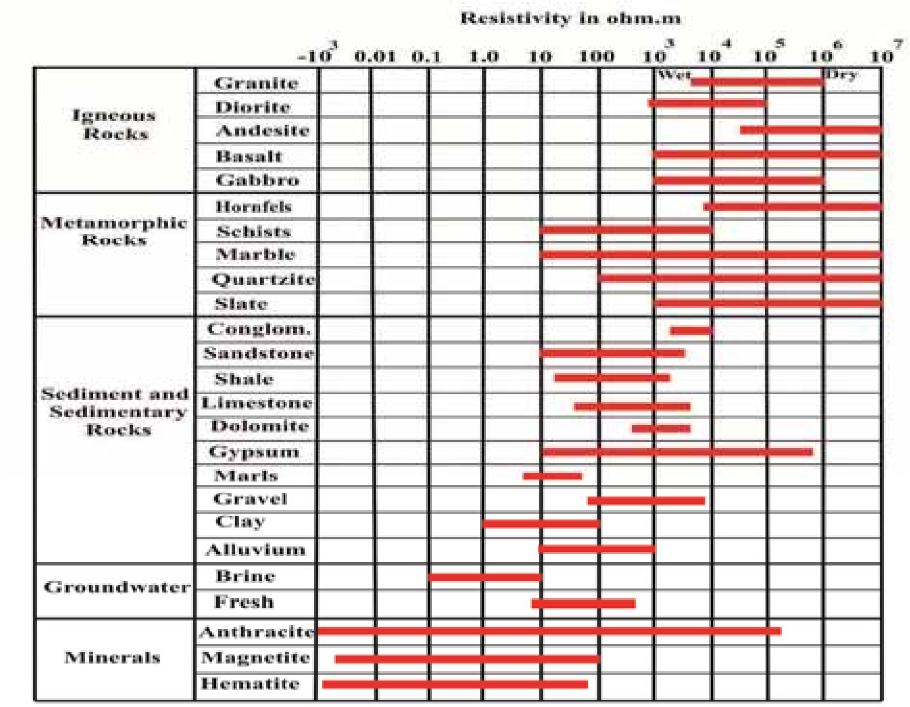

Figure (1-2):- The resistivity of rocks, sediment and minerals modified from (Loke, 2012).

1- 4 Electrodes Arrays.

There are 92 array used in the electrical resistivity method, (Szalai and Szarka, 2008). But the types of electrical arrays that are most commonly used do not exceed ten arrays. These arrays are Schlumberger, Wenner, Dipole – dipole, Pole-dipole, Pole-pole, Square, Offset Wenner, Wenner-Schlumberger and Multiple gradient arrays. The choice of best array for a field survey depends on different factors, such as the investigation depth, sensitivity function of array that is connected with the type of structure to be mapped, vertical and horizontal data coverage and the resolution of the array, in addition to, the sensitivity of resistivity meter and background noise level (Roy, and Apparao, 1971; Loke, 2012).

1-4-1 Schlumberger Array.

In the 1D resistivity techniques that is the Schlumberger array is the most widely used for deep sounding due to it is easy in application, especially in VES technique to investigate the groundwater aquifers, (Kunetz, 1966; Lashkaripour and Nakhaei, 2005). It is adopted by Conrad schlumberger in his pioneer works (Kunetz 1966). In this array, four electrodes (A,M,N and B) are placed along a straight line on the earth surface in the same direction (Kunetz, 1966). The spacing between the current electrodes (MN) is given as (a), while (n) is the distance between the current and potential electrodes (A and M or N and B), as shown in figure (1-3).

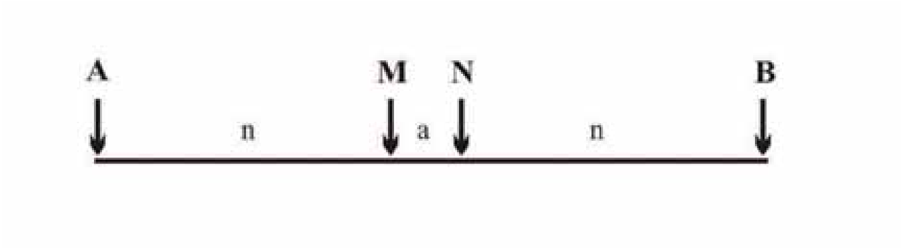

Figure (1-3):- The geometry of the Schlumberger array.

This array is high sensitive to vertical changes in the subsurface resistivity below the center point of the array, and relatively less sensitive to horizontal changes in earth layers. The value of the apparent resistivity in this array can be calculated by the equation:-

$$\rho_a = K\,R \qquad \text{.............(5)}$$

The (**K**) factor can be calculated by two equations, the first is called practical equation, and it is represent practical case of the array.

$$K_{pr} = \pi\left[(AB\backslash 2)^2/MN - MN/4\right] \qquad \text{.............(5-1)}$$

As for second is called theoretical equation, and it is represent theoretical case of the Schlumberger array.

$$K_{th} = \pi(AB\backslash 2)^2/MN \qquad \text{...............(5-2)}$$

The difference between these equations are appeared during derivation of the geometrical factor of this array, where the equation (5-1) involve derivation (**K**) when the (MN) distance not equal zero, but it is small in comparison with the (AB) distance, and it is represent practical case in the field . While the equation (5-2) involves derivation (**K**) when the (MN) distance equal zero approximately, that is the array in this case is represent theoretical case, which does not application in the field.

1-4-2 Wenner Array.

This array consists of four electrodes (A, B, M and N) placed at the surface of the ground along a straight line. Where (A B) are current electrodes, and (M N) are potential electrodes.The electrode distance (MN) is equal to electrode spacing (a) or (1/3 AB). The (ρ_a) values for this array can be calculated by equation (6), (Keller and Frischknecht, 1966; Kunetz, 1966; Zohdy, 1974).

$$\rho a = 2\pi a R \qquad \text{............(6)}$$

This array is relatively less sensitive to vertical changes in the subsurface resistivity below the center point of the array, and it is good in resolving horizontal changes in earth layers, especially near earth surface. Among the common arrays, the Wenner array has the strongest signal strength, so this can be an important factor if the survey is carried in areas with high background noise, (Zohdy, 1974; Loke, 2012). However, many of the early 2D imaging techniques were carried out with Wenner array (Loke, 1999). It is the most commonly used in resistivity method. It is an array which was popularized by the pioneering works of the research group of the University of Birmingham (Griffiths and Turnbull, 1985; Griffiths et al., 1990). However, there are three different arrangements can be used for Wenner array as: Wenner-Alpha, Wenner-Beta and Wenner- Gamma, figure (1-4). The Wenner- Alpha is considered to be the standard Wenner array (Carpenter and Habberjam, 1956).

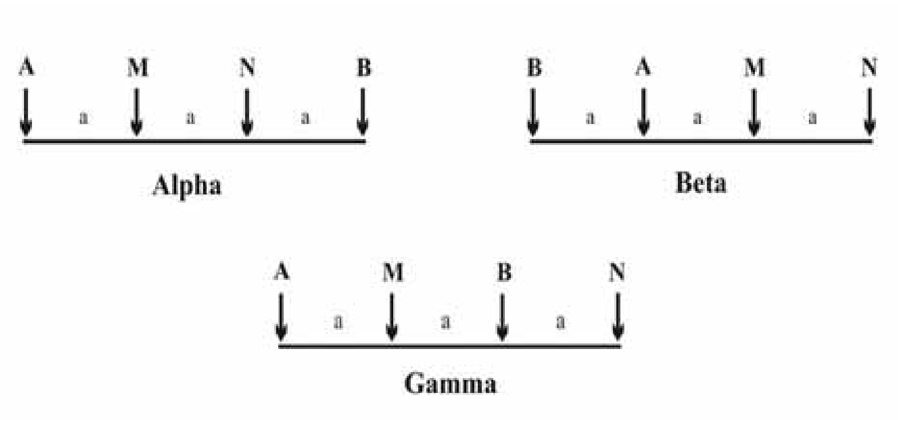

Figure (1-4):- The geometry types of the Wenner array, modified from (Loke, 2012).

1-4-3 Dipole – Dipole Array.

There are different types of Dipole – dipole array such as Equatorial, Azimuthal, Parallel, Perpendicular, Radial, and Polar or Axial array (AL-pine, 1950; Kunetz, 1966; Keller and Frischknecht, 1966), figure (1-5).

The Polar dipole–dipole array is the most widely used in 2D imaging technique, because it is easy applying in the fieldwork. The arrangement of the electrodes of this array is shown in figure (1-6). The spacing between the current electrode pair, AB, is given as (a) which is the same as the distance between the potential electrode pair (MN), (n) is the distance between the (A and M) electrodes, which controls the depth of investigation (AL-pine, 1950; Kunetz, 1966; Keller and Frischknecht, 1966).

This array is very sensitive to horizontal changes in resistivity, but relatively insensitive to vertical changes, which means it is good in mapping vertical structures, such as faults, but relatively poor in mapping horizontal structures such as sedimentary layers, (Loke, 2012).

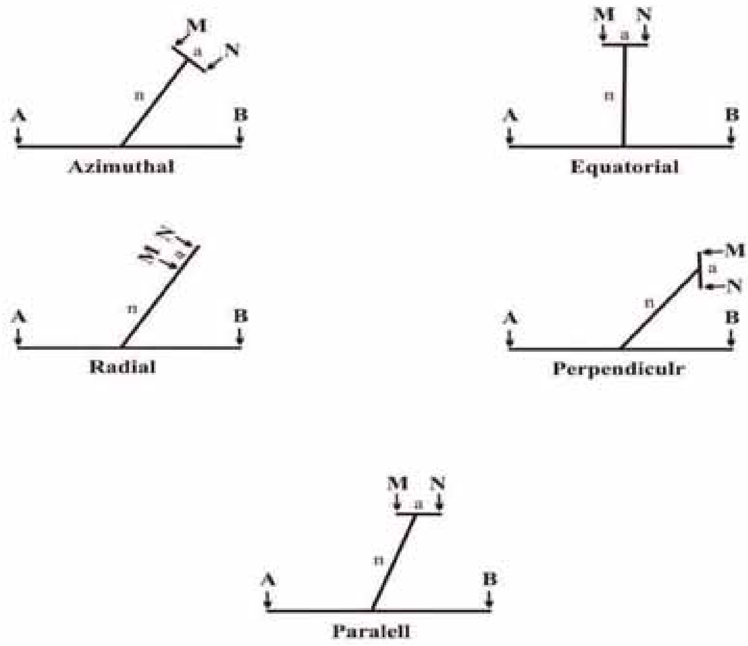

Figure (1-5):- The geometry types of dipole – dipole array, (AL-pine, 1950).

The apparent resistivity (ρ_a) value for Polar dipole–dipole can be calculated by equation (7), (AL-pine, 1950; Kunetz, 1966; Keller and Frischknecht, 1966).

$$\rho_a = \pi \, an \, (n+1) \, (n+2) \, R \qquad \text{...............(7)}$$

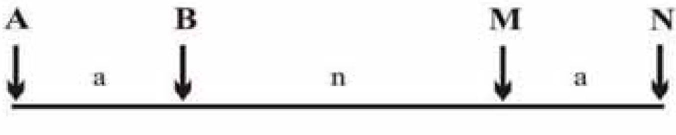

Figure (1-6):- The geometry of the Polar dipole – dipole array, (AL-pine, 1950).

1-4-4 Pole –pole Array.

The simplest array is one in which one of the current electrodes and one of the potential electrodes are placed so far away that they can be considered at infinity, figure (1-7).

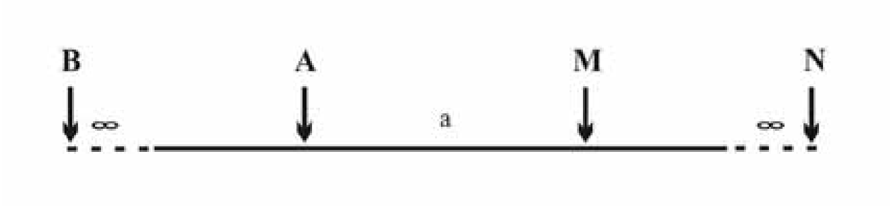

Figure (1- 7):- The geometry of the Pole – Pole array, modified from (Loke, 2012).

This array is not as commonly used as the Schlumberger, Wenner and dipole-dipole arrays. However, the second current and potential electrodes (B and N) must be placed at a distance that is more than 20 times the maximum separation between (A and M) electrodes used in the survey. The effect of the (B) and similarly for the (N) electrode is approximately proportional to the ratio of the (A-M) distance to the (B-N) distance. If the effects of the (B) and (N) electrodes are not taken into account, the distance of these electrodes from the survey line must be at least 20 times the largest (A-M) spacing used to ensure that the error is less than 5%, (Loke, 2012) . One drawback of this array is that it can pick up a large amount of telluric noise which can severely degrade the quality of the measurements. Thus this array is mainly used in surveys where relatively small electrode spacings (less than 10 m) are used. Therefore, this array not commonly used in 2D imaging technique, but it is commonly used for 3D imaging technique (Li and Oldenburg 1992). However, it has the widest horizontal data coverage and the deepest depth of investigation, (Loke, 2012).

The apparent resistivity (ρ_a) values for this array can be calculated by equation (8) and as following:-

$$\rho_a = 2\pi a R \qquad \text{...............(8)}$$

1-4-5 Pole-Dipole Array.

The pole-dipole array contains four collinear electrodes. One of the current electrodes is installed at an effective infinity distance, which is approximately five to ten times the survey depth. The other current electrode is placed in the vicinity of the two potential electrodes, (AL-pine, 1950; Kunetz, 1966; Keller and Frischknecht, 1966).

The pole-dipole array also has relatively good horizontal coverage, but it has a significantly higher signal strength compared with the dipole-dipole array and it is not as sensitive to telluric noise as the pole-pole array, (Loke, 2012). There are two types of this array, forward and reverse pole-dipole arrays, as shown in figure (1-8).

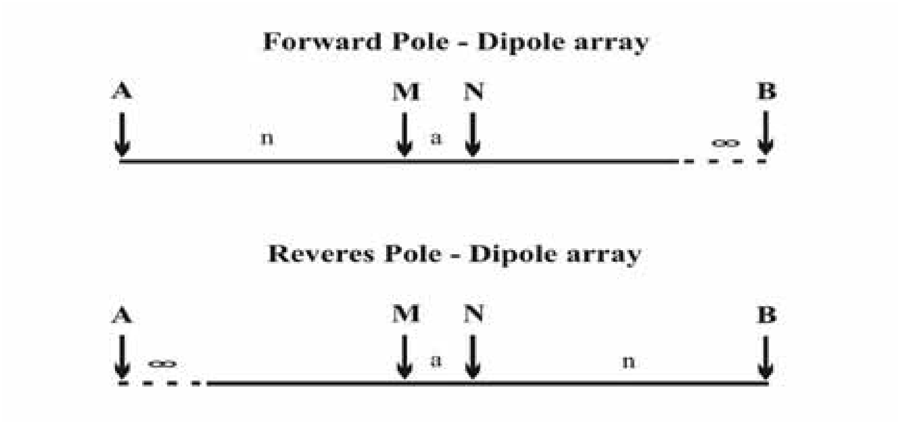

Figure (1- 8):- The forward and reverse pole-dipole arrays, modified from (Loke, 2012).

According to Loke, (2012), the signal strength for the pole-dipole array decreases with the *square* of the (*n*) factor. While this effect is not as severe as the dipole-dipole array, it is usually not advisable to use (*n*) values of greater than 8 to 10. Beyond this, the (*a*) spacing between the (MN) dipole pair should be increased to obtain stronger signal strength. The ratio of the depth of investigation to the array length does not increase significantly for (*n*) values beyond 4 or 5. Thus to increase the depth of investigation, it is better to increase the (*a*) spacing rather than to keep increasing the (*n*) value when it reaches 5. There is another interesting effect when the (*n*) factor is increased that is frequently not appreciated, and leads to an interesting pitfall in field surveys.

1-4-6 Square Array.

This array consists of four electrodes (A, B, M and N) placed at the surface of the ground on a square shape. Where (A B) are current electrodes, and (M N) are potential electrodes, figure (1-9). The location of a measurement is assigned to the center point of the square. The array size (a) is the length of the side of the square. The array is expanded symmetrically about the center point, in increments of ($a\sqrt{2}$) (Habberjam and Watkins, 1967). There are three types of square array, (alpha α, beta, β and gamma, γ).The α and β measurements provide information on the directional variation of the subsurface apparent resistivity (ρ_a). The γ measurement serves as a check on the accuracy of the α and β measurements.

In a homogeneous anisotropic medium:-

$$\rho_a \alpha = \rho_a \beta + \rho_a \gamma \qquad \text{.........(9)}$$

And in an isotropic medium:-

$\rho_a \gamma = 0$ therefore

$$\rho_a \alpha = \rho_a \beta \qquad \text{........(10)}$$

The apparent resistivity is determined using the equation:

$$\rho_a = K R \qquad \text{.........(11)}$$

$$K = 2\pi a / 2 - 2\sqrt{2} \qquad \text{.........(12)}$$

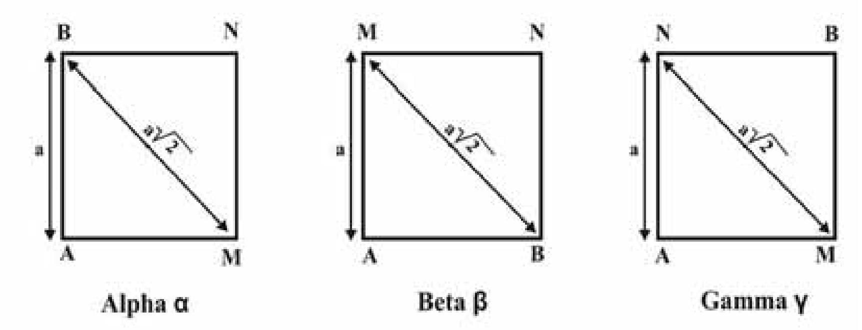

Figure (1-9):- The geometry types of Square array, (Habberjam and Watkins, 1967).

1-4-7 Wenner – Schlumberger Array.

This array is one of the important arrays used in 2D imaging technique, it is a combination of the Wenner and Schlumberger arrays (Pazdirek and Blaha, 1996). It is a new hybrid array that modified from these arrays, figure (1-10), and arising out of relatively recent work with resistivity imaging surveys. The advantage of this array is that it can be used with the electrodes system arranged with a constant spacing, hence it is easier than Schlumberger array. The purpose of using this array is that they are moderately sensitive to both horizontal and vertical structures, (Loke, 2012).

In areas with limited open space for a long survey line, the conventional Wenner array has a disadvantage, because there is a large reduction in horizontal coverage when the electrode spacing is increased in order to achieve a deeper depth of investigation, (Loke, 2010). However, the apparent resistivity value for the Wenner-Schlumberger array is given by:-

$$\rho_a = \pi \, n \, (n + 1) \, a \, R \qquad \text{..........(13)}$$

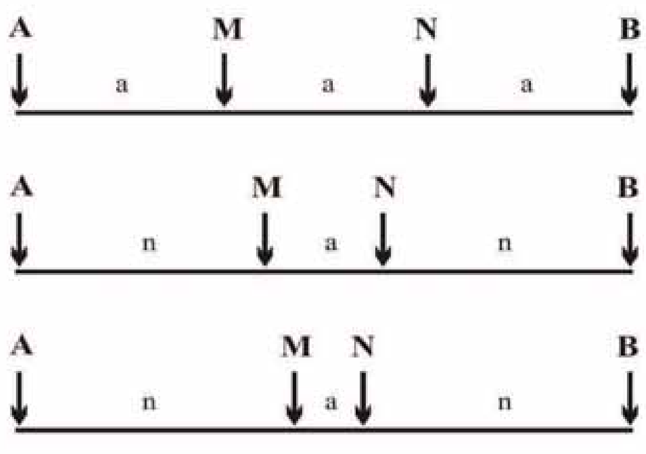

Figure (1-10):- The geometry of the Wenner-Schlumberger array, modified from (Loke, 2012).

1-4-8 Gradient Array.

This is a relatively new array developed primary for multi-channel resistivity meter systems (Dahlin and Zhou 2006). A multi-channel system can make several measurements simultaneously with the potential electrode pairs at different location but with the same positions of the current electrodes, figure (1-11). In the multiple gradient arrays, different sets of measurements are made with the current electrodes at different locations. The results obtained by this array is comparable to those obtained by the dipole-dipole and pole-dipole arrays (Dahlin and Zhou 2004) while it has more favorable noise characteristics.

One interesting minor problem associated with this array is the plotting method for the pseudosection and profiles. The vertical position can be easily determined by using the median depth of investigation which can be numerically determined. The main issue is the horizontal position of the plotting point.

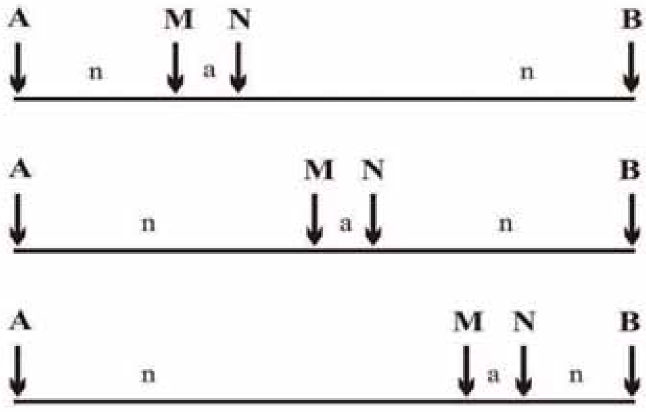

Figure (1-11):- The geometry of the gradient array, modified from (Loke, 2012).

1-5 The Sensitivity Function and The Depth of Investigation.

The major factors that affect on the accuracy of the resistivity measurements is sensitivity function of array used. The sensitivity function basically tells us the degree to which a change in the resistivity of a section of the subsurface will influence the potential measured by the array, (Loke, 2012). The higher the value of the sensitivity function, the greater is the influence of the subsurface region on the measurement, and it depends on the relative positions of the electrodes. In other words, it is the resolution and the depth of investigation for each array, (Chitea and Georgescu, 2009; Loke, 2010).

Mathematically, the sensitivity function of a homogenous half-space is given by the Frechet derivative (McGillivray and Oldenburg, 1990). They consider the simplest possible array configuration is pole-pole array as shown in figure (1-12) with just one current located at the origin (*0,0,0*) and one potential electrode located at (*a,0,0*), i.e. both electrodes are (*a*) meters apart. A current is injected into the ground through the current electrode (A) that results in a potential Φ observed at the potential electrode (M).

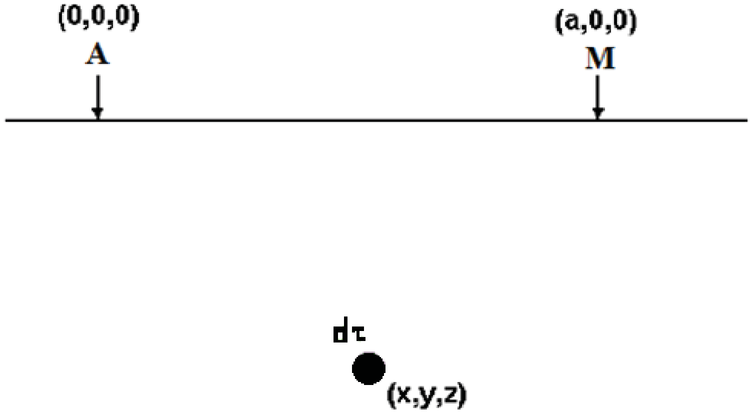

Figure (2-12):- Sensitivity function calculation at a point d_T(x,y,z) within a half-space, (Modified from Loke, 2010).

Suppose the resistivity of a volume of subsurface material, located at $d\tau(x,y,z)$, figure (1-12) is changed by a small amount, δρ. What would be the corresponding change in the potential, δϕ, measured at (M) that this is given by (Loke and Barker 1995, from loke,2012):-

$$\delta\phi = \frac{\delta\rho}{\rho^2}\int_V \nabla\phi \cdot \nabla\phi' \, d\tau \qquad \text{.......... (14)}$$

Hence, the parameter ϕ is the potential resulting from a current electrode located at the position of the (M) potential electrode can be calculated as:-

$$\phi = \frac{\rho}{2\pi\left(x^2 + y^2 + z^2\right)^{0.5}} \qquad \text{.......... (15)}$$

and similarly for ϕ'

After differentiating the above equations to obtain the divergence, and substituting into equation (14) we get:-

$$\frac{\delta\phi}{\delta\rho} = \int_V \frac{1}{4\pi^2} \cdot \frac{x(x-a) + y^2 + z^2}{\left[x^2 + y^2 + z^2\right]^{1.5}\left[(x-a)^2 + y^2 + z^2\right]^{1.5}} dxdydz \text{.. (16)}$$

The 3D Frechet derivative is then given by the integrand of Equation (16), namely:

$$F_{3D}(x,y,z) = \frac{1}{4\pi^2} \cdot \frac{x(x-a) + y^2 + z^2}{\left[x^2 + y^2 + z^2\right]^{1.5}\left[(x-a)^2 + y^2 + z^2\right]^{1.5}} \text{... (17)}$$

Equation (16) gives the 3D Frechet derivative, or the general sensitivity function for the pole-pole array. Figure (1-13) shows 1D sensitivity function for the pole-pole array.

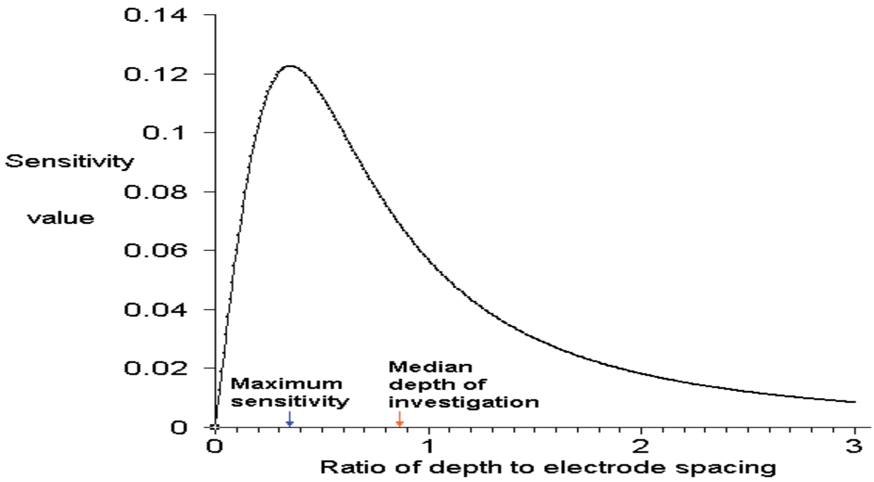

Figure (1-13):- A plot of the 1-D sensitivity function for the pole-pole array. Note that the median depth of investigation (red arrow) is more than twice the depth of maximum sensitivity (blue arrow), (Loke, 2012).

To obtain the Frechet derivative for a general four electrodes array consisting of two current electrodes and two potential electrodes as shown in figure (1-14), equation (17) can be used, (Tamssar, 2013).

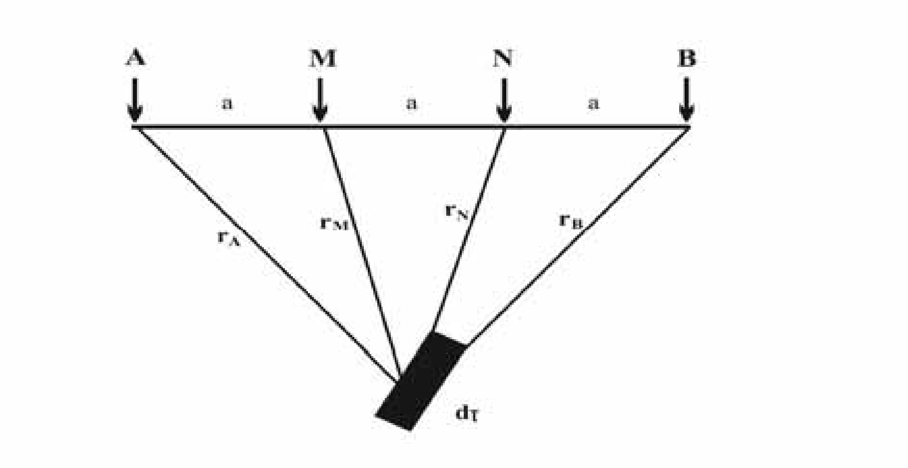

Figure (1-14):- Sensitivity function calculation at a point d_T(x,y,z) within a half-space for a general four electrodes array,(Modified from Tamssar, 2013).

$$F_{3D}(x,y,z) = \frac{1}{4\pi^2}\left[\frac{(x-x_A)(x-x_N)+(y-y_A)(y-y_N)+(z-z_A)(z-z_N)}{(r_A r_N)^3} + \frac{(x-x_B)(x-x_N)+(y-y_B)(y-y_N)+(z-z_B)(z-z_N)}{(r_B r_N)^3} + \frac{(x-x_A)(x-x_M)+(y-y_A)(y-y_M)+(z-z_A)(z-z_M)}{(r_A r_M)^3} + \frac{(x-x_B)(x-x_M)+(y-y_B)(y-y_M)+(z-z_B)(z-z_M)}{(r_B r_M)^3}\right]$$

The depth of investigation in a homogeneous half-space can be obtained mathematically by integrating the sensitivity function formula or the Frechet derivative of the array.If the subsurface is assumed to consist of horizontal layers, each with different resistivities, the change in the potential measured by the array on the surface can be determined. For a horizontal layer, the *x* and *y* limits of the layer extends from $-\infty$ to $+\infty$. Thus the sensitivity function for a thin horizontal layer is obtained by integrating the 3D sensitivity function given in equation (17) in the *x* and *y* directions, (Loke, 2012).

$$F_{1D}(z) = \frac{1}{4\pi^2}\int_{-\infty}^{+\infty}\int_{-\infty}^{+\infty}\frac{x(x-a)+y^2+z^2}{\left[x^2+y^2+z^2\right]^{1.5}\left[(x-a)^2+y^2+z^2\right]^{1.5}}\,dxdz \quad \textbf{... (19)}$$

The above equation has a simple analytical solution (Roy and Apparao, 1971), which is given by:

$$F_{1D}(z) = \frac{2}{\pi}\cdot\frac{z}{\left(a^2+4z^2\right)^{1.5}} \quad \textbf{... (20)}$$

The above equation (20) is also known as the depth of investigation for 1D resistivity sounding surveys. Figure (1-15) shows 1D sensitivity function for the Wenner array.

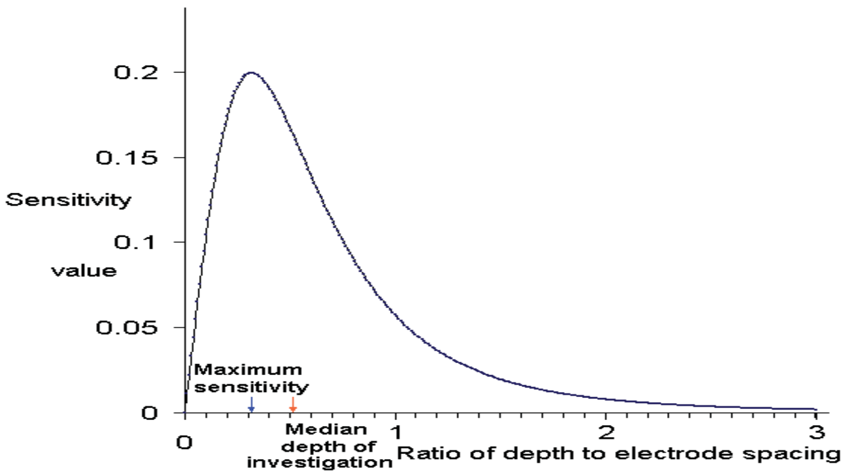

Figure (1-15):- A plot of the 1-D sensitivity function and median depth of investigation for the Wenner array, (Loke, 2012).

To study the suitability of the different arrays for 2D surveys, we need to go one step beyond the simple 1D sensitivity function, i.e. the 2D sensitivity function. In this case, for a particular (*x*,*z*) location, we add up the contribution from all points for *y*-values ranging from +∞ to −∞. This involves the integration of the 3D sensitivity function in equation (9) with respect to *y*. The integrate of equation (18) has an analytic solution that is given in terms of elliptic integrals (Loke and Barker 1995). The complete solution is:-

$$F_{2D}(x,z) = \pi\left[\frac{1}{2\alpha^3} - \frac{3a^2}{16\alpha^5}\right], \quad \text{with } \alpha = 0.25a^2 + z^2 \qquad \textbf{... (21)}$$

Equation (21) is also known as the depth investigation characteristic and has been used by many authors to determine the properties of various arrays in resistivity sounding surveys (Edwards 1977, Barker 1991, Merrick 1997). Edwards (1977) and

Barker (1991) have considered the (median depth of investigation) is a more robust estimate. The median depth of investigation is determined by integrating the sensitivity function with depth. Therefore Edwards (1977) gives a table includes the median depth of investigation (ze) for the different arrays, table (1-1). This table gives an idea of the depth to which are can map with a particular array. However, the depth of investigation does not depend on the measured apparent resistivity or the resistivity of the homogeneous earth model (Loke, 1999). Also, if there are large resistivity contrasts near the surface, the actual depth of investigation could be somewhat different.

To determine the maximum depth mapped before carrying out the particular survey, we can find it by multiplying the maximum (a) electrode spacing, or maximum array length (L) by the appropriate depth factor given in the table (1-1). For example, if the maximum electrode spacing (a) used for the Wenner array is 190 m, or maximum array length (L) =570 m, then the maximum depth mapped will be given as either:

Maximum depth= Electrode spacing x Ze/a = 190 x 0.519 = 98.61 m

or

Maximum depth = Total array length x Ze/L = 570 x 0.173 = 98.61 m

Table (1-1):- The median depth of investigation (Ze) for the different arrays (After Edwards, 1977), modified from (Loke, 2012).

Array		*ze/a*	*ze/L*	Geometric Factor
Wenner Alpha		0.519	0.173	6.2832
Wenner Beta		0.416	0.139	18.850
Wenner Gamma		0.594	0.198	9.4248
Dipole-dipole	n = 1	0.416	0.139	18.850
	n = 2	0.697	0.174	75.398
	n = 3	0.962	0.192	188.50
	n = 4	1.220	0.203	376.99
	n = 5	1.476	0.211	659.73
	n = 6	1.730	0.216	1055.6
	n = 7	1.983	0.220	1583.4
	n = 8	2.236	0.224	2261.9
Equatorial dipole-dipole				
	n = 1	0.451	0.319	21.452
	n = 2	0.809	0.362	119.03
	n = 3	1.180	0.373	367.31
	n = 4	1.556	0.377	841.75
Wenner - Schlumberger				
	n = 1	0.519	0.173	6.2832
	n = 2	0.925	0.186	18.850
	n = 3	1.318	0.189	37.699
	n = 4	1.706	0.190	62.832
	n = 5	2.093	0.190	94.248
	n = 6	2.478	0.191	131.95
	n = 7	2.863	0.191	175.93
	n = 8	3.247	0.191	226.19
	n = 9	3.632	0.191	282.74
	n =10	4.015	0.191	345.58
Pole-dipole	n = 1	0.519	0.296	12.566
	n = 2	0.925	0.308	37.699
	n = 3	1.318	0.330	75.398
	n = 4	1.706	0.341	125.66
	n = 5	2.093	0.349	188.50
	n = 6	2.478	0.354	263.89
	n = 7	2.863	0.358	351.86
	n = 8	3.247	0.361	452.39
Pole-Pole		0.867		6.28319

1- 6 Parameters Controlling Investigation Depth.

The depth of investigation in any electrode system is determined by the position of current and potential electrodes and not by the current electrode only. In general and according to (Roy and Apparao, 1971), the depth of investigation depends on:-

A-The contrast in resistivities for different layers and their relative thicknesses.

B-The length of the transmitting line (AB) and on the separation between the transmitting (AB) line and the receiving (MN) line. At larger (A, B) length, the deeper the penetration of the current.

C- From a practical point of view, the depth of investigation depends on the measurability of the (V_{MN}) potential which can be expressed as ($V_{MN} = \rho \times I_{AB} / K$) as well. For large investigation depths, the electrodes have to be far away from each other, the (K) coefficient has thus an important value and the (V_{MN}) signal becomes small, possibly difficult to measure.

D-Type of rocks and sediments, where the high rocks resistivity or sediments has led to decrease the penetration of the current, consequently the depth of investigation.

E-The intensity of the current which can be expressed as ($I_{AB} = V_{AB} / R_{AB}$) where the resistivity systems are usually characterized by a maximum current, a maximum voltage and a maximum power, one of these three parameters determining the intensity of the current which can really be transmitted into the ground in relation with the value of the ground resistance (R_{AB}).

F- A highly sensitive meter, with filtering capability including stacking / averaging process for noise rejection (Self Potential, drift of SP, power lines fields, other industrial or natural electromagnetic interferences,…), which makes it possible to measure an additional a low (V_{MN}) magnitude.

For the above reasons it is impossible to indicate a definite maximum depth of investigation and this depth in any electrode array is smaller than what is generally assumed.

1-7 Field Instruments.

presently and in the typical survey, the data acquisition systems generally consists of a resistivity instrument, a relay switching unit, a computer, electrode cables, various connectors and electrodes (Overmeeren and Ritsema, 1988; Griffiths et al., 1990; Dahlin, 2001).In some cases two or more components are housed in the same box, e.g. a computer integrated with the instrument. Some systems employ intelligent switches at each electrode take-out instead of a central switching unit,(Dahlin, 2001).

There are two types of resistivity instruments. The first one is static type while the second is dynamic type. Most instruments are of the static type where electrodes are connected to a cables (or multi-electrode cable as in 2D and 3D imaging techniques) and planted into the ground during the survey, as shown in figures (1-16) and (1-17).

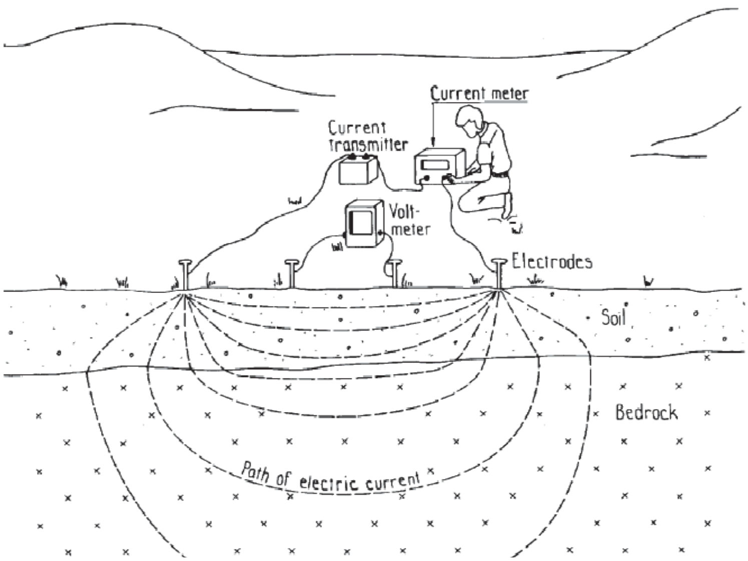

Figure (1-16):- Static instrument type from (Robinson and Coruh, 1988).

The dynamic type uses a small number of electrodes but move the entire specific system to obtain a wide coverage. A cable with a number of electrodes is used, where one electrode pair is used for transmitting current while other electrodes are used for measuring the potentials. A combination of normal and reciprocal Wenner and Schlumberger, and other arrays, may be used. The initial types of these instruments are used in 1D resistivity techniques. The advantage of this concept is a possibility of high speed of surveying and high lateral resolution, but limited depths cover for logistical reasons, (Dahlin, 2001). As a result advances in field equipment design capability and computer algorithms led to of appearance new dynamic types of instruments used in 2D and 3D resistivity techniques. In these instruments two electrodes are used as current electrodes, while six electrodes are used for the potential measurements and one is used as a ground electrode. This type relies on the current being injected into the ground by direct contact, so it can only be used in open ground, such as farmlands in Northern Europe, (Loke, 2012). Panissod et al. (1998) use an approach where the wheels of a carriage towed behind a vehicle are used as electrodes.

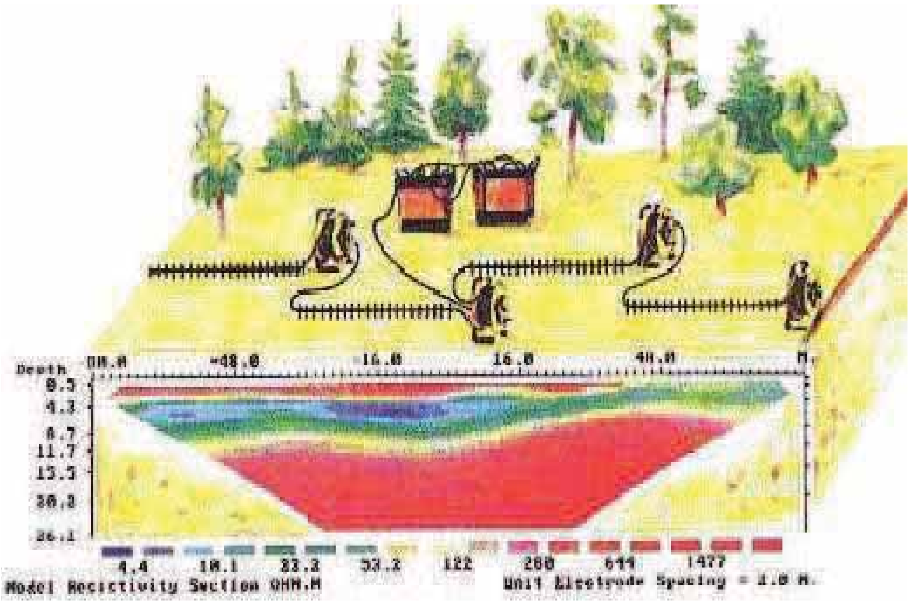

Figure (1-17):- Static instrument type of ABEM Imaging Lund System. Each mark on the cables indicates an electrode position. The cables are placed along a single line (the sideways shift in the figure is only for clarity), SISC Group, www.sisc.com.vn.

Another dynamic type that does not require direct contact with the ground but uses capacitive coupling (Gerard and Tabbagh 1991, Shima et al. 1996, Panissod et al. 1998, Loke et al. 2011a) to induce the flow of current in the ground. This system can be used in areas that are paved, such as roads and city areas. One such type shown in figure (1-18) in is the Geometrics OhmMapper type where a cable with 4 to 6 electrodes attached to a measuring unit is pulled by a single operator, (Loke, 2012).

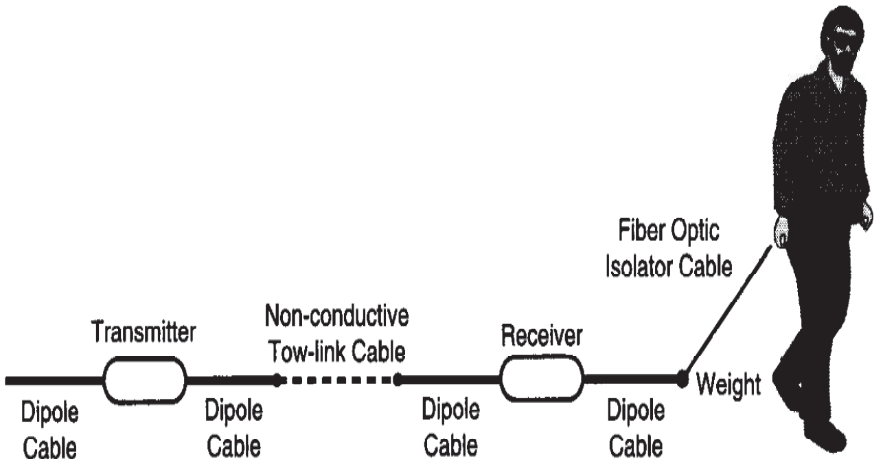

Figure (1-18):- The Geometrics OhmMapper type using capacitive coupled electrodes. (Courtesy of Geometrics Inc.), from (Loke, 2012).

2-1 Introduction.

The electrical resistivity method used to determine the subsurface resistivity distribution by making measurements on the ground surface. From these measurements, the true resistivity of the subsurface can be calculated and displayed as model,(Loke, 2012). From the 1920's to the late 1980's there were essentially three techniques used. These techniques are: constant separation traversing (CST), vertical electric sounding (VES), and Combined VES/CST techniques. Over the last 25 years, there have been revolutionary improvements to the resistivity method where two-dimensional (2D) technique is now routinely conducted. Three-dimensional (3D) technique is widely used in areas with complex geology, while there have been significant interest and developments in four-dimensional (4D) technique (Loke et al., 2013). This has been made possible by recent developments in field instrumentation, automatic interpretation algorithms, and computer software. With the new tools, complex variations of the subsurface resistivity in both space and time can now be accurately mapped.

This chapter includes a short introduction to 1D resistivity techniques and attempts to provide a brief summary of the past and ongoing development of these techniques. It includes short descriptions of the procedures used for data acquisition, the methods used to process data and how resistivity techniques are constructed and interpreted.

2-2 One-Dimension (1D) Resistivity Techniques.

2-2-1 Constant Separation Traverse (CST) or Horizontal Profiling Technique.

In this technique, fixed electrode spacing is chosen while the whole electrode array is moved along a profile after each measurement, figure (2-1). The profile gives measurements of resistivity along horizontal line at apparent depth, which will vary depending on depth function which is determine from electrode geometry of the array, therefore, the best apparent resistivity anomalies are obtained by orienting the profiles at right angles to the strike of the geologic structure.

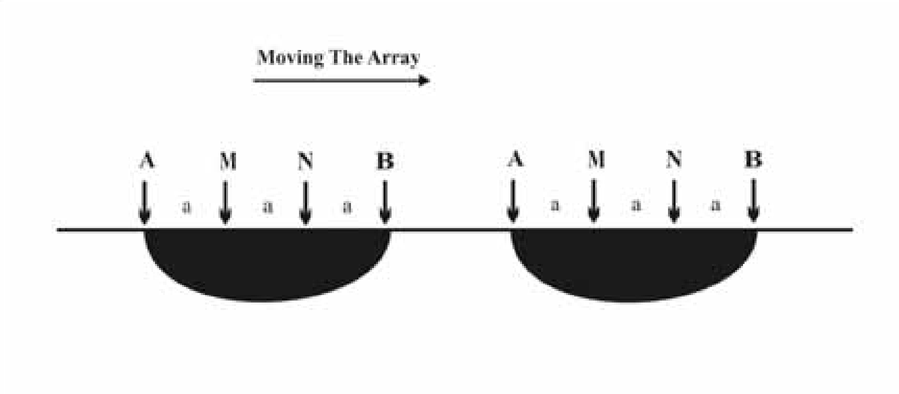

Figure (2-1):- Sketch showing the data acquisition by Constant separation traverse (CST) technique.

The interpretation of horizontal profiling data is mainly qualitative as horizontal resistivity profiling or horizontal resistivity maps. In the case of horizontal resistivity profiling, with one or more electrode separation, it will be one curve for each electrode separation used. Where the midpoint of the array at each measurement is plotted on the abscissa and the apparent resistivity values is plotted on the ordinate using liner or logarithmic scale as appropriate, (figure 2-2). In the case of horizontal resistivity maps, the results of group of profiles can be showed in the form of map, one for each measurement is plotted and the corresponding value of apparent resistivity contours are then drawn representing points of equal resistivity, (Kunetz, 1966; Zohdy, 1974).However, this technique gives some information about lateral changes in the subsurface apparent resistivity, but it cannot detect vertical changes in the resistivity, (Loke, 2010).

In general, all types of electrode arrays have been used in this technique, but the most commonly used are polar dipole – dipole and Wenner array, According to (Kunetz, 1966; Zohdy, 1974).

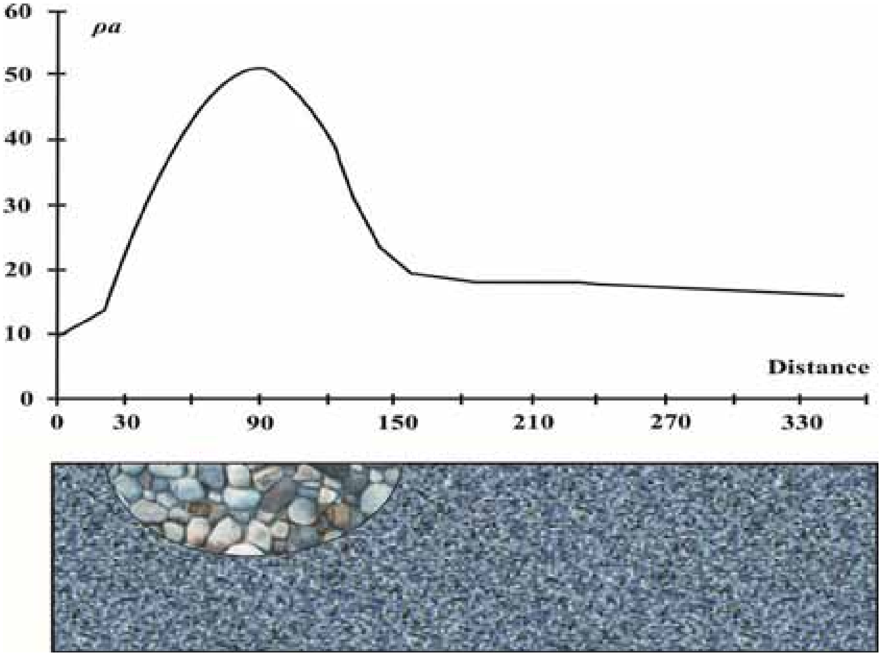

Figure (2-2):- Constant separation traverse (CST) or Horizontal profiling over gravels lens within sand deposits for Wenner array.

2-2-2 Vertical Electrical Sounding (VES) Technique.

A Vertical Electrical Sounding technique has been used since 1912 and went through major developments during the 1980s. It is designed to provide vertical profiles of resistivity versus depth. This technique is based on the general observation that current penetrates deeper into the subsurface with increasing separation of electrodes.

In this technique, the center point of the electrode array remains fixed, but the spacing between the electrodes is increased to obtain more information about the deeper section of the subsurface. The results of (VES) data are represented in log-log graph paper in which the half length of array (AB/2) is plotted on the abscissa and the corresponding apparent resistivity is plotted on the ordinate (Kunetz 1966),figure (2-

3). This technique can be use by any electrical resistivity array, but the Schlumberger array is more widespread in VES, because, it offers better control over lateral resistivity variation close to the potential electrodes. This technique was used for groundwater and shallow engineering studies, (Keller and Frischknecht, 1966; Zohdy, 1974).

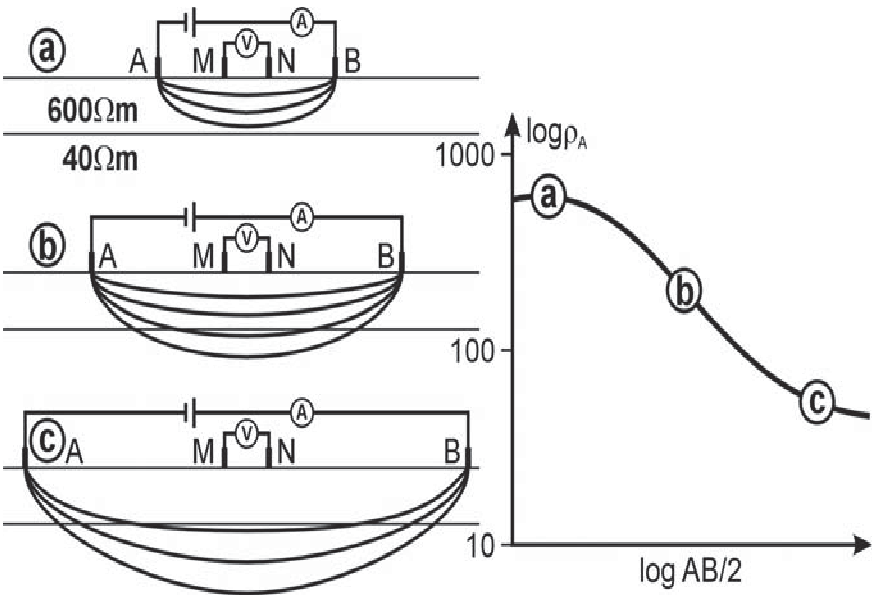

Figure (2-3):- Apparent resistivity measurements, with increased current electrode spacing, are leading to increased penetration depths of the injected current. Results are compiled in the sounding curve (Kirsch, 2006).

2-2-2-1 Field Curves of Schlumberger Array.

In the Vertical Electrical Sounding technique that is the Schlumberger array is the most widely used for deep sounding, especially in investigation of groundwater aquifers, (Kunetz, 1966; Lashkaripour and Nakhaei, 2005). Four electrodes (AMNB) are placed along a straight line on the earth surface in the same direction (Kunetz, 1966), when taking measurements the potential electrodes remain fixed, while the current electrodes expanding to various distances, until the potential difference between (M N) drops to such degree, that it can not be measured. In this case it is necessary to increase the distance between potential electrodes.

The vertical distribution of resistivity within a particular volume of earth is called a geo-electrical section. For many purposes, the subsurface geology can often be approximated by a geo-electrical section consisting of a sequence of uniform horizontal layers. The (VES) procedure is best suited to this of section (Orellana and Mooney, 1966). However, the following figure (2-4) shows a section of this type in two-dimensional representation, where layer thicknesses are designated by $\mathbf{h_1, h_2}$, … Depths to the bottom of successive layers will then be given by $\mathbf{h_1, h_1+ h_2}$,… True resistivities of the individual layers are designated $\boldsymbol{\rho_1}$, $\boldsymbol{\rho_2}$,… The last or n'th layer in considered to have a very great thickness.

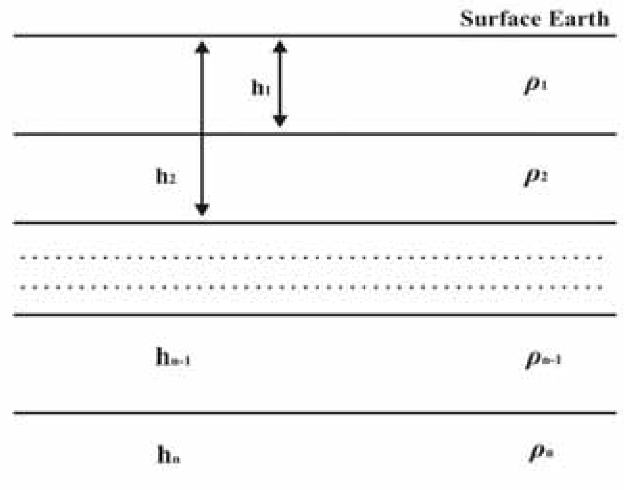

Figure (2-4):- An n- layer geo-electrical section, (Orellana and Mooney, 1966).

The electrical properties of such a geo-electrical section may be represented graphically, as shown in the following figure (2-5). Comparison of curves leads to the recognition of the type curves and enable the curves to be divided into groups. However, the multi-layers curves can be grouped into many types by depending on the resistivity variation between them with depth, as follows:-

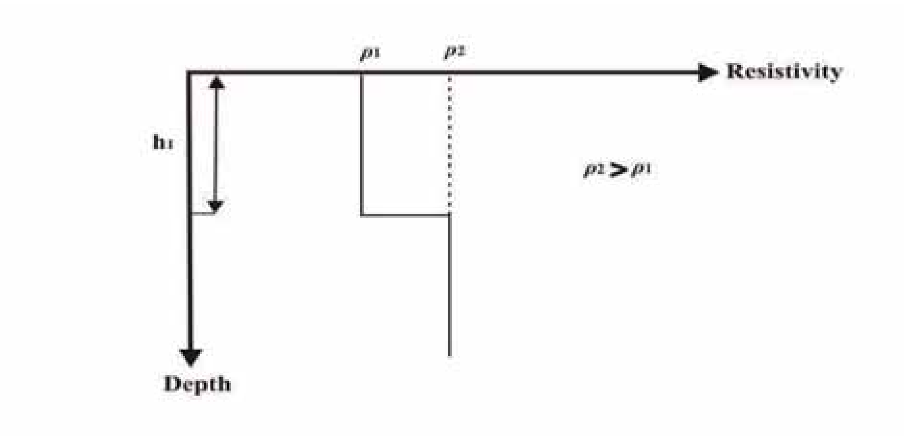

Figure (2-5):- Two-layer section, (Orellana and Mooney, 1966).

a- Two –layer curves.

There are two types from these curves, and as follows:-

First type: in this type $\rho_2 > \rho_1$

Second type: in this type $\rho_2 < \rho_1$

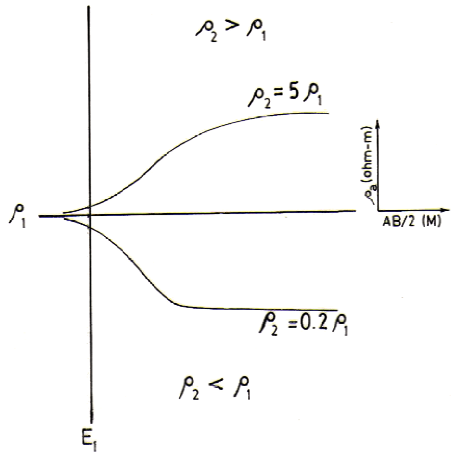

Figure (2-6):- Two-layer curves type, (Bhattacharya and patra, 1968).

b- Three –layer curves.

The apparent resistivity curve for a three-layer structure generally has one of four typical shapes, determined by the vertical sequence of resistivities in the layers as following, figure (2-7):

A-type curve: Shows some changes in gradient but the apparent resistivity generally increases continuously with increasing electrode separation, indicating that the true resistivities increase with depth from layer to layer, ($\rho_1 < \rho_2 < \rho_3$).

K-type curve: Rises to a maximum then decreases, indicating that the intermediate layer has higher resistivity than the top and bottom layers, ($\rho_1 < \rho_2 > \rho_3$).

H-type curve: Shows the opposite effect; it falls to a minimum then increases again due to an intermediate layer that is a better conductor than the top and bottom layers, ($\rho_1 > \rho_2 < \rho_3$).

Q-type curve: Exhibits the opposite effect; it decreases continuously along with a progressive decrease of resistivity with depth, ($\rho_1 > \rho_2 > \rho_3$).

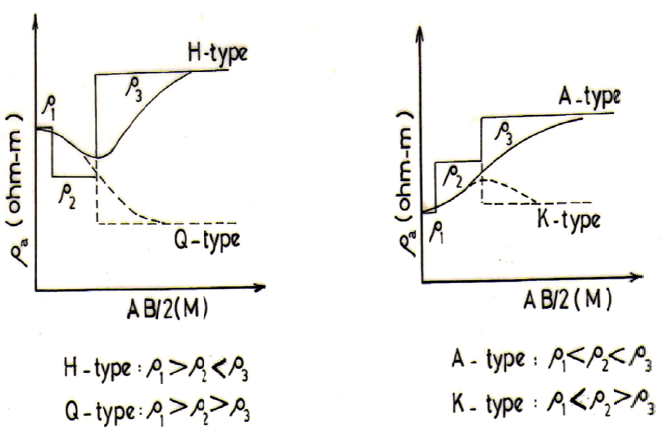

Figure (2-7):- Three-layer curves type,(Bhattacharya and patra, 1968).

c- Four –layer curves.

Four-layer curves can be grouped into eight types as shown in figure (2-8).

AA type: in this type $\rho_1 < \rho_2 < \rho_3 < \rho_4$

AK type: in this type $\rho_1 < \rho_2 < \rho_3 > \rho_4$

HA type: in this type $\rho_1 > \rho_2 < \rho_3 < \rho_4$

HK type: in this type $\rho_1 > \rho_2 < \rho_3 > \rho_4$

KH type: in this type $\rho_1 > \rho_2 < \rho_3 < \rho_4$

KQ type: in this type $\rho_1 < \rho_2 > \rho_3 > \rho_4$

QQ type: in this type $\rho_1 > \rho_2 > \rho_3 > \rho_4$

QH type: in this type $\rho_1 > \rho_2 > \rho_3 < \rho_4$

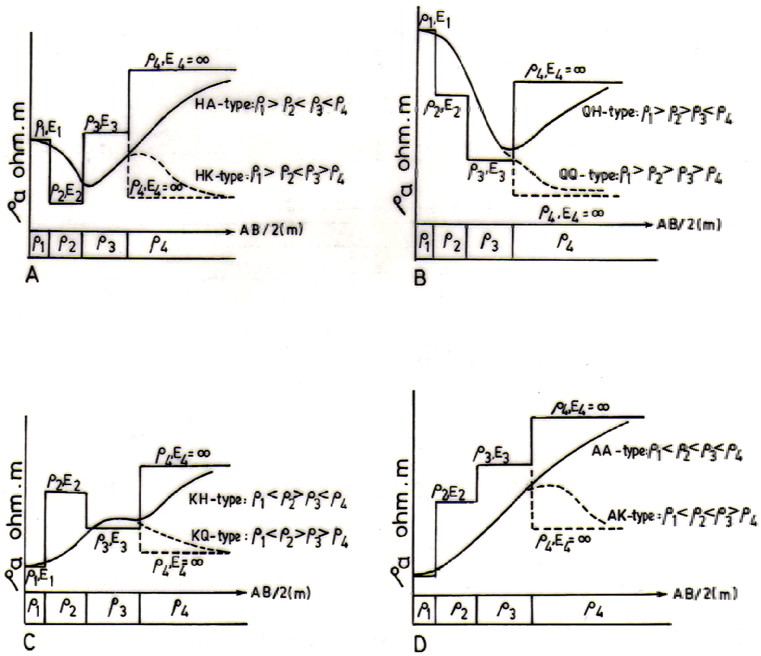

Figure (2-8):- Four-layer type curves (A) HA and HK types, (B) QH and QQ types, (C) KH and KQ types, (D) AA and AK types, (Bhattacharya and patra, 1968).

In general, an n-layer of curve can be grouped into ($\mathbf{2^{n-1}}$) types and identified by (n-2) letters from the three-layer classification, for example if the number layers of curve equal (5) , that is:-

$$\mathbf{2^{n-1} = 2^{5-1} = 2^4 = 16}$$

Thus, can be seen that there are sixteen (16) types from five-layer curves, and indicate them (5-2) = 3 letters from types of three-layer curves, for example:- **HAA, HKH, QHA, QQQ…** etc, and as shown in figure (2-9).

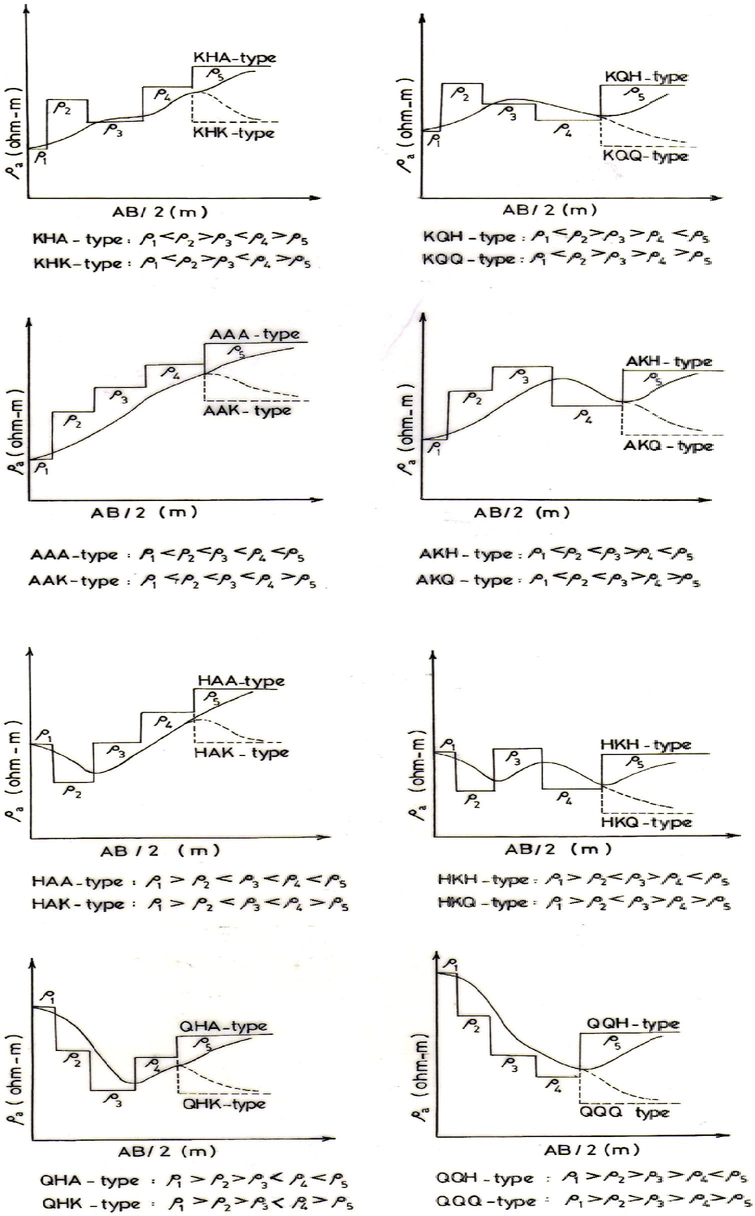

Figure (2-9):- Five-layer type curves, (Bhattacharya and patra, 1968).

2-2-2-2 Data Processing of Vertical Electrical Sounding (VES).

After completing the vertical electrical surveys (VES) in any field work that carried out by Schlumberger array, the results of the apparent resistivity values are plotting on log- log paper to form apparent field curves, this curves will show many distortion in the shapes. These distortions are generally caused by the lateral inhomogenities in the lithology of ground, errors in measurements, or by equipment failure (Zohdy, 1974).

The interpretation of VES points depend on (**ρa**) measurements. Therefore, we must remove the distortions from apparent resistivity field curves through the processing of smoothing, which is represented the first step in interpretation. However, this distortion phenomena that appears on the field curves are cusps, scattering (**ρa**) values and sharp maximum, as well as the displacement in the field curves branches (Zohdy, 1974).

A-The Distortion Phenomena.

1- Formation of Cusps.

The formation of cusps in the field curves is generally caused by lateral inhomgenities in the ground, such as the presence of fractures or lithological changes. It is clearly appeared in the figuer(2-10).

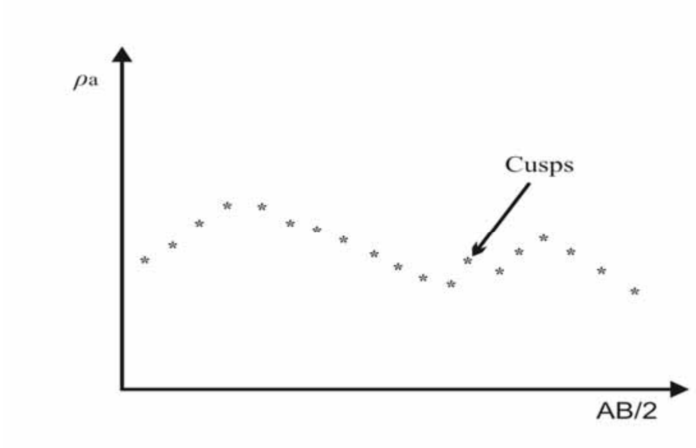

Figure (2-10):- Appearance of Formation of Cusp in the field curve.

2- Scattering (*ρ*a) Values.

The scattering (**ρa**) values generally caused by high lateral inhomgenities in the ground, such as the presence of cavities. It is clearly appeared in the figuer (2-11).

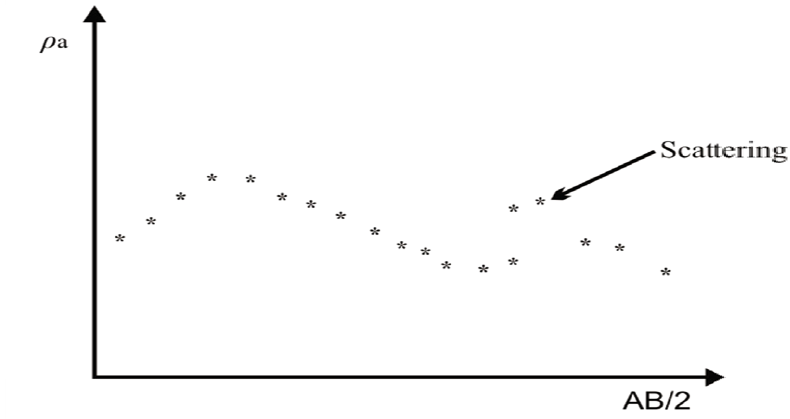

Figure (2-11):- Appearance of Scattering (**ρa**) values in the field curve.

3- Sharp Maximum.

The maximum or peak value on a K-type sounding curve is always gentle and broad, and should never have a sharp curvature where the ground is horizontally homogeneous. The formation sharp peak generally is indicative of the limited lateral extent of the buried (middle) resistive layer (Zohdy, 1974). These distortions must be removing from field curves.

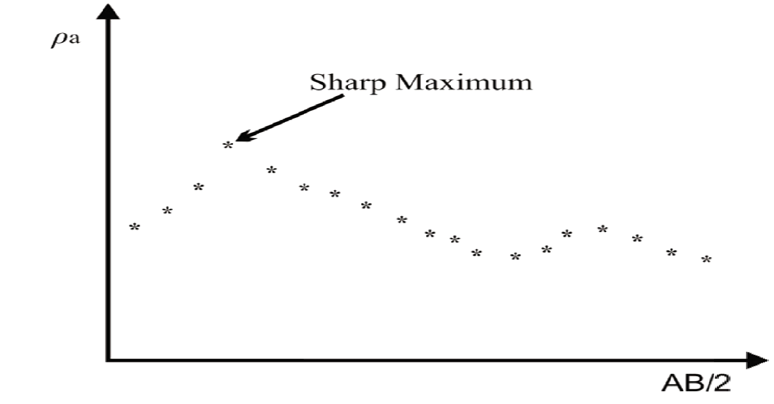

Figure (2-12):- Appearance of Sharp Maximum in the field curve.

B- The Displacement of Field Branches.

There are two types of displacement or discontinuities, and which are:-

1- Theoretical Displacement.

This type is caused by theoretical affect due to enlarging the spacing between potential electrodes (MN) with constant spacing of current electrodes (AB) or increasing the ratio (MN/AB) to (1/4) or (1/3). Al-Zubedi (2009) modified table (2-1) from (Bhattacharya and patra, 1968; AL –Ane, 1998).

Table (2-1):- Show electrode distances for (ρ**a**) measurements, (Al-Zubedi, 2009).

NO.	AB/2	MN/2	MN/AB	ρ a Ω.m
1	1.5	0.25	1/6	
2	2	0.25	1/8	
3	3	0.25	1/12	
4	3	0.5	1/6	
5	4	0.5	1/8	
6	5	0.5	1/10	
7	6	0.5	1/12	
8	5	1	1/5	
9	6	1	1/6	
10	8	1	1/8	
11	10	1	1/10	
12	8	2	1/4	
13	10	2	1/5	
14	15	2	1/7.5	
15	20	2	1/10	
16	25	2	1/12.5	
17	20	5	1/4	
18	25	5	1/5	
19	30	5	1/6	
20	40	5	1/8	
21	50	5	1/10	
22	40	10	1/4	
23	50	10	1/5	
24	60	10	1/6	
25	80	10	1/8	
26	100	10	1/10	
27	100	20	1/5	
28	120	20	1/6	
29	140	20	1/7	
30	160	20	1/8	
31	200	20	1/10	
32	200	40	1/5	
33	250	40	1/6.25	

This table was designed to avoid the ratio (MN/AB) equal to (1/3) and (1/4), as much as possible, to reduce the theoretical displacements in the field curve branches.

2- Inhomogeneities Displacement.

This type is caused by lateral inhomogeneities of surface lithology near the potential electrodes (M) and (N), (Zohdy, 1974). This type appears in most field curves of Schlumberger array as displacements between the field branches, figure (2-13).

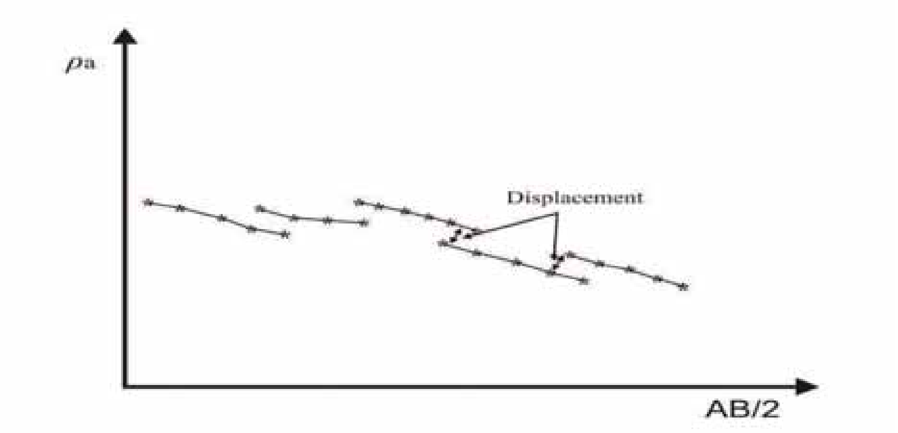

Figure (2-13):- Appearance of displacement in the field curve.

With a clear existence of such displacements between the field branches, the processes which is widely used is to determine a branch of field curves that has minimum distortion, then the other branches are shifted vertically and parallel to (***ρ*****a**) axis until connecting all branches to form one smooth field curve.

2-2-2-3 Interpretation of (VES) Data.

The measurements of vertical electrical sounding are plotted and Processing, then interpreted using two methods of interpretations; the first method is called qualitative interpretation, which is included primary evaluation of the apparent resistivity values by using many techniques,(Zohdy, 1974), such as:-

A – Study the Curve Types of VES.

B – Apparent resistivity pseudo cross – section.

C – Apparent resistivity Profiles.

D – Apparent resistivity maps.

The second method is called quantitative interpretation which includes determination of the resistivities and thicknesses of electrical horizons for VES field curves by using two techniques. The first one is manually by using curve matching, and the second by using the computerized programs. Usually both techniques are used together. However, the results of interpretation must be consolidated by geological and hydro-geological information available from maps and drilled wells to obtain a more reliable geologic picture of the subsurface.

2-2-2-3-1 Qualitative Interpretation Method.

A- Study of the Curves Types of VES.

In this technique, the field curves are distributing on the geological map and categorized into groups depended on the types of field curves, where the type (shape) can reflect the vertical variations of the apparent resistivity distribution of the subsurface in the survey area. Therefore, this technique of interpretation are gives elementary information about number of electrical horizons for every curve, where the increase and decrease in the resistivity values for every horizon compared with other, can be observed through inflection point in the field curve, and which are reflecting changes in the electrical properties (Griffiths and King , 1981).

B - Apparent Resistivity Pseudo cross - Section.

The apparent resistivity section or pseudo cross - section, is one of many techniques that have been used in the qualitative interpretation, where gives preliminary information about the changes in the apparent resistivity values with increasing of the half current electrodes separations (AB/2). This information forms the two - dimension image, where the horizontal dimension (x-axis) represents locations of vertical electrical soundings VES points, while the vertical dimension (y-axis) represents the half current electrode separation (AB/2) as shown in figure (2-14), which is drawn on linear scale instead of logarithmic scale in most cases, for the purpose of reducing the effect of near surface layers. However, the apparent resistivity values will be a function of both (AB/2) and their VES position on the surface.

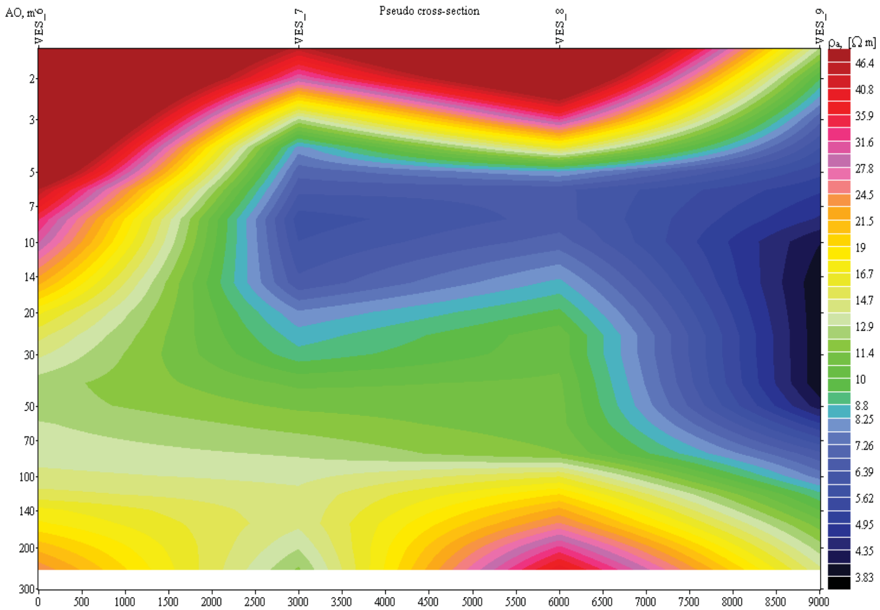

Figure (2-14):- The apparent resistivity section (pseudo cross – section), (Al-Zubedi, 2009).

C- Apparent Resistivity Profiles.

The apparent resistivity profiles are drawn on linear scale, where the horizontal axis (x-axis) represents locations of vertical electrical soundings VES points, while the vertical axis (y-axis) represents the apparent resistivity values as shown in figure (2-15). This technique gives preliminary information about the changes in the apparent resistivity values with increasing of the half current electrodes separations (AB/2), it is being used for investigation about faults in most time.

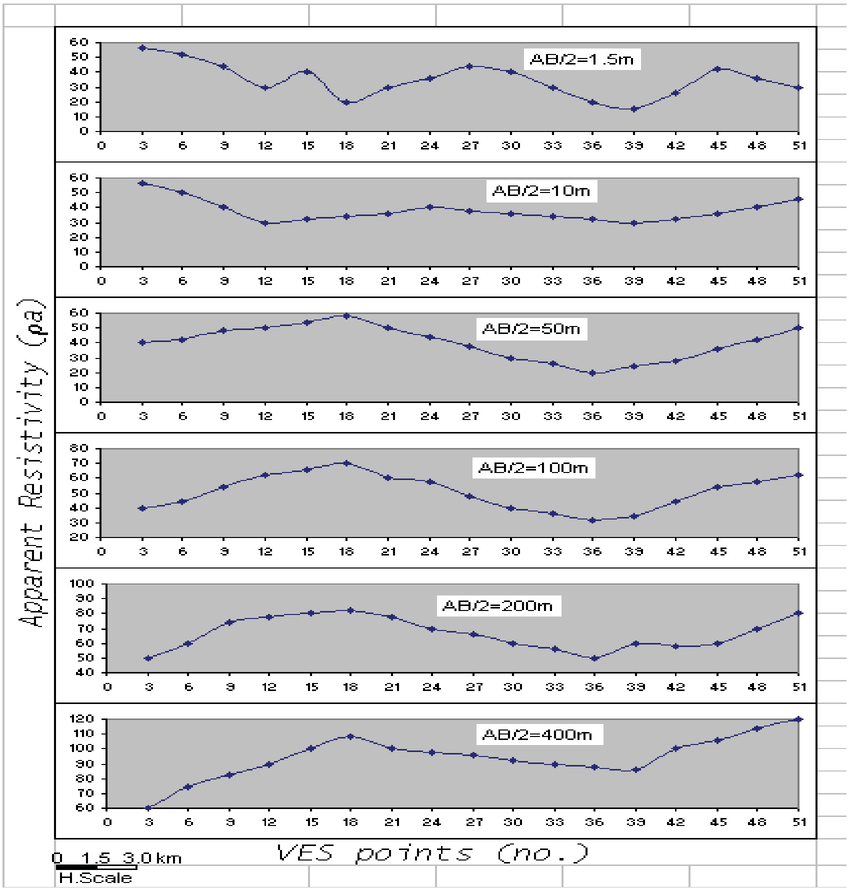

Figure (2-15):- Apparent resistivity profile,(Amin,2008).

D- Apparent Resistivity Maps.

The Apparent resistivity map is prepared by plotting the apparent resistivity values, as registered on the sounding curves, at a given electrode spacing (common to all soundings), and contouring the results, (Zohdy, 1974).

2-2-2-3-2 Quantitative Interpretation Method.

The quantitative interpretation of VES data have been used for determine the resistivity and thicknesses with depths of different electrical horizons from the apparent resistivity field curves.

There are two techniques can be used in the quantitative interpretation of (VES) data. Both techniques are based on comparison between the field curves and theoretical master curves. The first one is manually by using curve matching, and the second by using the computerized programs. The curve matching techniques include two methods. The first method is complete curve matching, which requires a large number of theoretical master curves, so it is rarely used in comparison with the second method, which called the partial curve matching. This method requires a few numbers of theoretical master curves. However most theoretical master curves, which are used in the manual interpretation can be found in the following references (Compagnie General de Geophysique, 1963; Orellana and Mooney, 1966). The second technique is computerized programs that can be used by many software, such as: IPI2win software, IX1D software, VES software, and Resist software.

A- Complete Curve Matching Method.

This method is based on comparison between the field curves and theoretical master curves, and is usually carried out by using the sets of two and three layers theoretical master curves in most times, to apply the complete curve matching method to the interpretation of three–layers field curve , proceed as follow:-

1- Plot the field curves on a double –logarithm transparent graph sheet with a modulus of 62.5mm, and determine the type of curve (A,H,K,Q) by inspection and select the applicable set of theoretical master curves.

2-Superpose the transparent paper containing the field curve onto the master curves sheet.

3-Move one sheet with respect to other, keeping the vertical axes parallel, until the field curve fits one of the master curves, interpretation between curves is permitted.

4- Determine the position cross on the transparent paper, which indicate to coordinate origin of the theoretical master curves, and also resistivity mark (ρ_2) and (ρ_3). Then determine the thickness ratio **(E_2/E_1)** from the master curve which mach with field curve, and determine the resistivity ratio of layers.

5- The thickness of the first layer **(E_1)** will be equal to the cross abscissa on the field graph (represent the horizontal axes of center coordinate), and the thickness of the second layer **(E_2)** can be calculated from the ratio **(E_2/E_1)**.

6-The resistivity of the first layer (ρ_1) will be equal to the cross ordinate on the field graph. The resistivity of the second layer (ρ_2) will be equal to the reading on the field graph corresponding to the position of the (ρ_2) resistivity mark, and similarly for the resistivity of the third layer using the (ρ_3) resistivity mark.

7- A perfect match will rarely be obtained, but interpolation between master curves will usually be satisfactory, as mentioned in (Orellana and Mooney, 1966; Keller and Frischnicht , 1966).

An example of this interpretation procedure is given in figure (2-16).

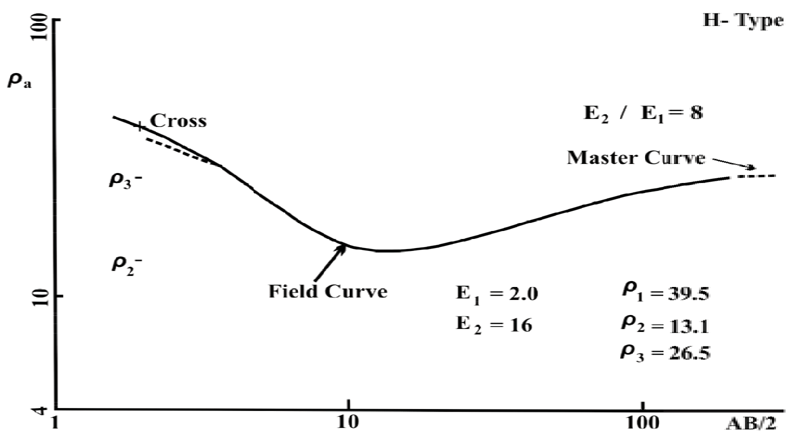

Figure (2-16):-Interpretation of three–layers field curve by complete curve matching, (Bhattacharya and patra, 1968).

B- Partial Curve Matching Method.

The partial curve matching method or (Auxiliary point method) includes two methods; the first is Orellana, while the second is Ebert method. Both methods are carried out using the sets of two and three layers theoretical master curves. In general the theoretical basis of the partial curve matching method depend on lessening the layers number of field curve during the interpretation process (Orellana and Mooney, 1966 ; Keller and Frischnicht , 1970). However, the Orellana method is rarely used in comparison with Ebert method, which is often used in the quantitative interpretation.

Orellana and Mooney (1966) have shown that the asymptotic behavior of **H** and **A** type curve depends only upon (1) resistivity in the deepest layer , and (2) longitudinal conductance (S), of the overlying section. Based upon this, they have introduced a graphic interpretation procedure for **H** and **A** type three-layer field curves. To apply the Orellana method to the interpretation of **H** and **A** type three–layers field curve , proceed as follow:-

1- The left-hand portion of field curve matches with two-layer master curves, figure (2-17), put a cross (1) on the field curve which indicate to coordinate origin of the two-layer theoretical master curves, and also other mark (ρ_2). The values **(E_1)** and (ρ_1) of first layer are calculated where they are represent horizontally and the vertical axes for cross (1) respectively, as for mark (ρ_2), it is represented (ρ_2).

2-On the transparent paper containing the field curve, draw a horizontal line at the ordinate of (ρ_2).

3- Superpose the transparent paper onto the two-layer master curves sheet. Keep axes parallel at all times.

4- Move one sheet with respect to other (Keep axes parallel) until the right-hand portion of the field curve matches one of the master curves. Put a cross (2) on the field curve which indicate to coordinate origin of the two-layer theoretical master curves, and also other mark (ρ_3).

5- Superpose the transparent paper containing the field curve onto a blank sheet of the logarithmic paper to the same scale. Place the first cross at the origin (coordinate 1-1) of one of the cycles of the logarithmic paper (Keep axes parallel).

6- Read the coordinate on the logarithmic paper corresponding to the position of cross. The horizontal coordinate will be designated (X), the vertical coordinate (Y). Therefore the thickness of second layer equal:-

$$\mathbf{E_2=(X\text{-}Y)\ E_1}$$

(E_2) may also be computed graphically as follows: with the field curve sheet still superposed on the blank sheet as in step (5), read the abscissa value on the field curve sheet corresponding to the **(X-Y)** value on the blank sheet, this give **(E_2)**, (for more details, please refer to (Orellana and Mooney 1966). An example of this interpretation procedure is given in figure (2-18).

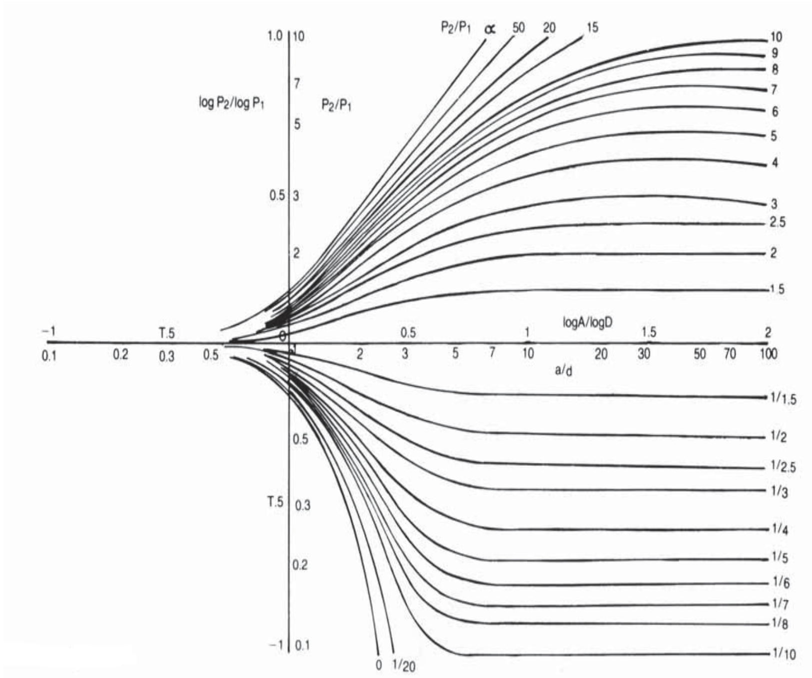

Figure (2-17):- Two-layer master curves, (USGS,2010).

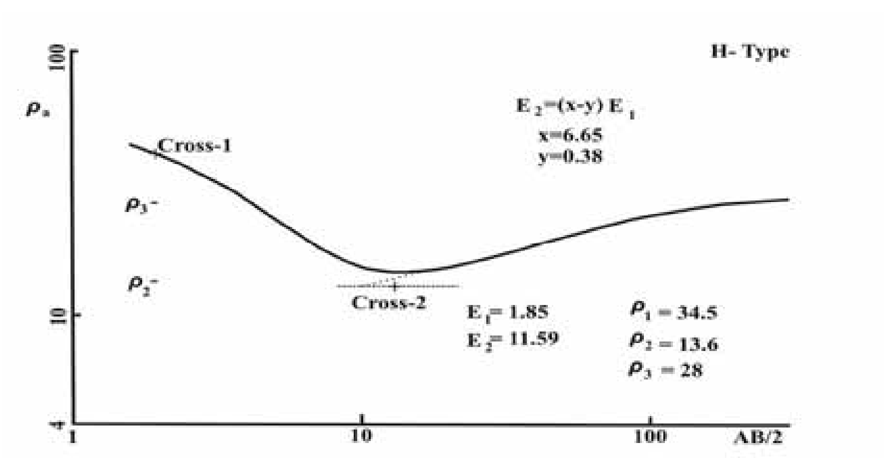

Figure (2-18):-Interpretation of three–layers field curve by Orellana method, (Orellana and Mooney, 1966).

Ebert method is carried out using the sets of two and three layers theoretical master curves with the help of the auxiliary graph of (A , Q , H , K) types, (Zohdy ,1965). In general the theoretical basis of the partial curve matching method depend on lessening the layers number of field curve during the interpretation process, through merging two layers or more in a fictitious layer, it has fictitious resistivity and thickness, (Orellana and Mooney, 1966 ; Keller and Frischnicht , 1970). To apply the Ebert method to the interpretation of type three-layer field curve, proceed as follow and as shown in figure (2-19) :-

1- Identify the field curve from its shape as to type **(A, K, Q, or H)**. Select the corresponding auxiliary point diagram, which accompanies the master curve set.

2- Match the left-hand portion of the field curve with a two-layer master curve. During this step, the position of the cross (1) and of the resistivity mark should be marked onto the transparent paper containing the field curve. This yield $\mathbf{E_2}, \boldsymbol{\rho_1}$ and an estimate of $\boldsymbol{\rho_2}$. Read $\boldsymbol{\rho_1}/\boldsymbol{\rho_2}$.

3- Superpose the transparent paper containing the field curve onto the auxiliary point diagram, figures (2-20 and 2-21). Keep axes parallel at all times. For **Q** and **H** type curves, place the cross (1) over the coordinate origin of the auxiliary diagram. As for **A** and **H** type curves, place the first cross over the left-hand vertical axis of the auxiliary diagram, at a vertical position corresponding to the value of $\boldsymbol{\rho_1}/\boldsymbol{\rho_2}$.

4- Select the curve on the auxiliary diagram which (a) corresponding to the value of $\boldsymbol{\rho_1}/\boldsymbol{\rho_2}$ and (b) starts from the position of the cross (1). Superpose the transparent paper containing the field curve onto the two-layer master curves sheet.

5- Move one sheet with respect to other (Keep axes parallel) until the right-hand portion of the field curve matches one of the master curves. During this process, keep the cross (origin of coordinates of the two-layer master curves sheet) in coincidence at all times with the auxiliary curve previously drawn.

6- On the transparent paper containing the field curve, mark the position of cross (2) and of the resistivity mark from master curves sheet. The position of the resistivity mark gives $\boldsymbol{\rho_3}$, the resistivity of third layer.

7- Superpose the field curve once again onto the auxiliary diagram. Place the cross in the same position as for step (4). The cross (2) will now lie on or close to one of the dashed lines. The dashed line will be indentified by a number, which equals $\mathbf{E_2}/\mathbf{E_1}$.

8- From $\mathbf{E_1}$ and $\mathbf{E_2}/\mathbf{E_1}$ compute $\mathbf{E_2}$.

For more details, please refer to (Orellana and Mooney, 1966; Keller and Frischnicht, 1970).

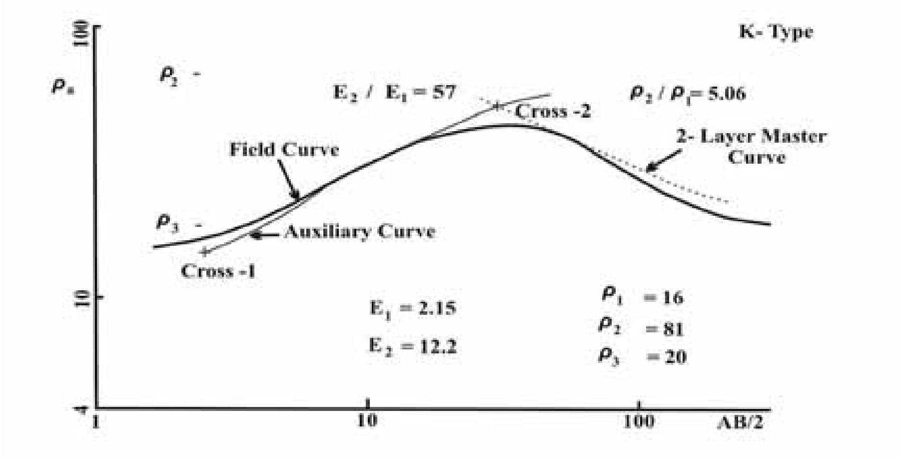

Figure (2-19):- Interpretation of 3-lyare filed curve uses 2-lyare master (Ebert method).

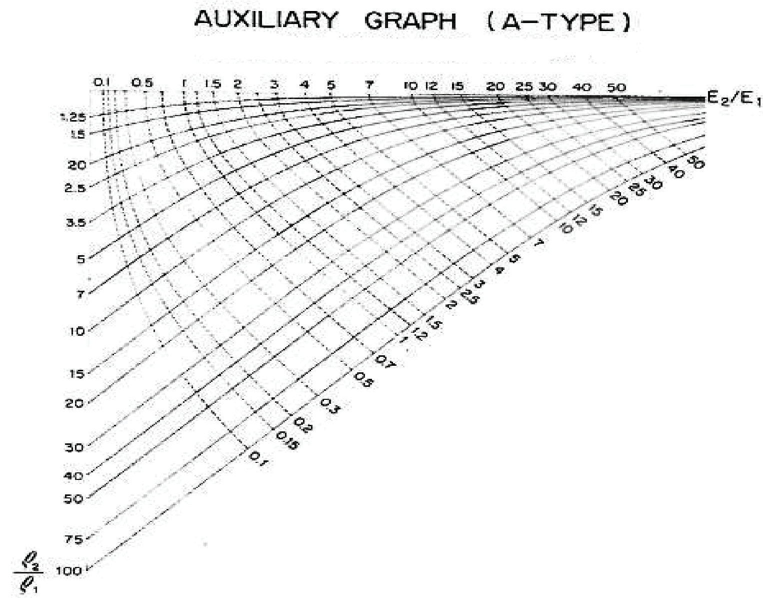

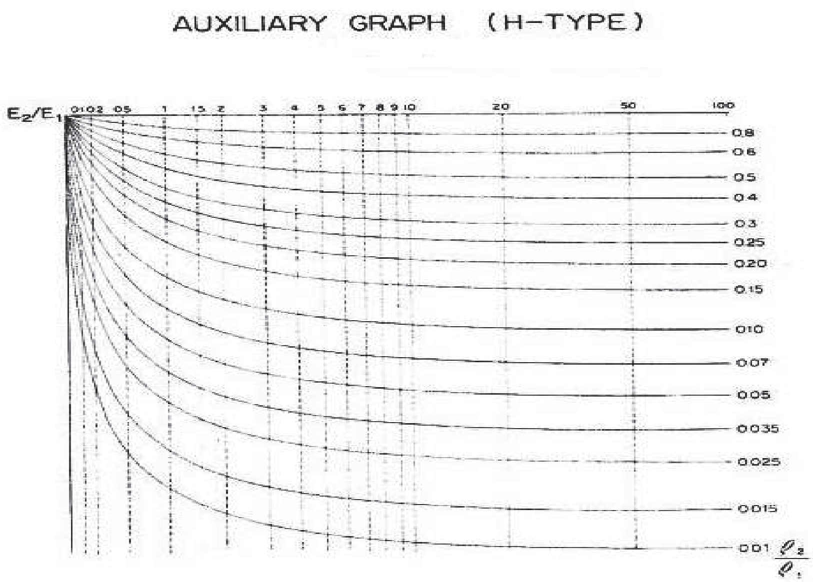

Figure (2-20):- Auxiliary graph of (A, H) types, (Keller and Frischnicht, 1966).

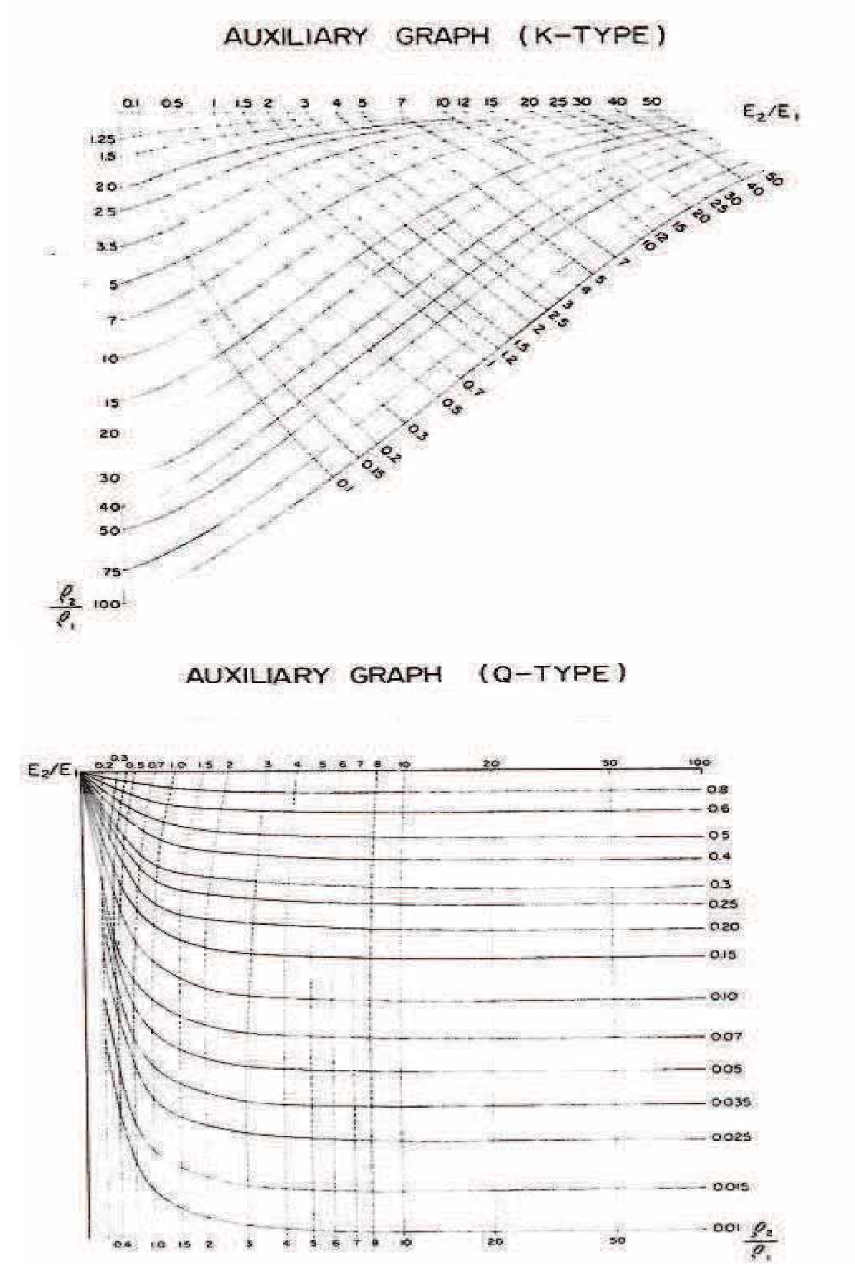

Figure (2-21):- Auxiliary graph of (k, Q) types, (Keller and Frischnicht, 1966).

C- Cumulative plot $\sum \rho_a$.

This method is used for interpretation of the curves of vertical electrical sounding by Wenner array. It is gives the good estimation for shallow depths, but it is not given good results about thick layers. This method is usually using for interpretation when the increase of electrode separation is small and constant in comparison with layers thickness. To apply this method, proceed as follow:-

1- Plot the value of ρ_a on vertical axis (represents summation of the apparent resistivity values) with value of (*a*) on the horizontal axis.

2- Plot the straight lines through the points, which was determined in the previous step. Then the intersection between the lines is dropped on the horizontal axis to determine the depths of borderlines between layers, as shown in the following figure (2-22), as mentioned in (Telford et al., 1976).

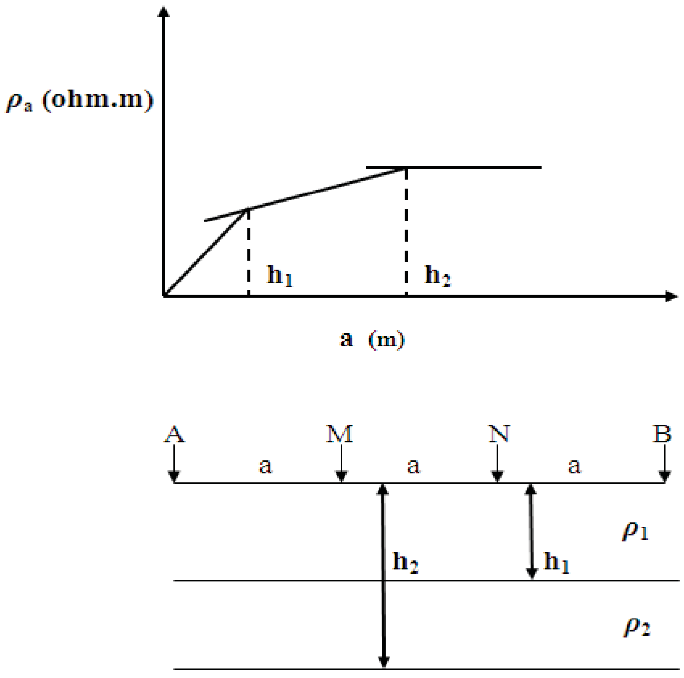

Figure (2-22):- Cumulative plot Wenner array, (Telford et al., 1976).

D- The Quantitative Interpretation by Computerized Programs.

There are many computerized programs using in quantitative interpretation, but, according to the most studies which were carried out during the last years, the IPI2win program is the more used program in the qualitative and quantitative interpretation. This program is designed for interpretation one dimension vertical electrical sounding (VES) and induced polarization data curves along single profile. Targeting at the geological result is the specific feature distinguishing IPI2win among other popular programs of automatic inversion, (Bobachev, 2002). With respect to qualitative interpretation, this program is designed for showing the measurements of VES interpretation as a pseudo - cross section. While the quantitative interpretation, this program includes two methods.

The first method is forward calculation and the second is inverse modeling. It is also capable of showing the results of VES quantitative interpretation in the form of geo-electrical sections. However the forward calculation method of quantitative interpretation includes entering the values of apparent resistivity and (AB/2) by the key board of the computer, then the program gives the resistivity and thicknesses of the best fitting between field curve and the theoretical master curves. While the inverse modeling method includes entering the resistivity and thicknesses of the field curve which are obtained from manual interpretation into the software, the program will altered the manual interpretation results for lessens the percent of deviation between the field curve and one of the theoretical curves, where the quantity of layers is not altered.

According to (Bobachev, 2002), this method is used for checking of manual interpretation results. In the following, some notes about forward calculation and inverse modeling methods are given as.

1 - Good interpretation results are depend on the good smoothing of the field curve. It was observed the equality almost in the interpretation results for both methods, when the field curve was good smoothing, as shown in figure (2 - 23).

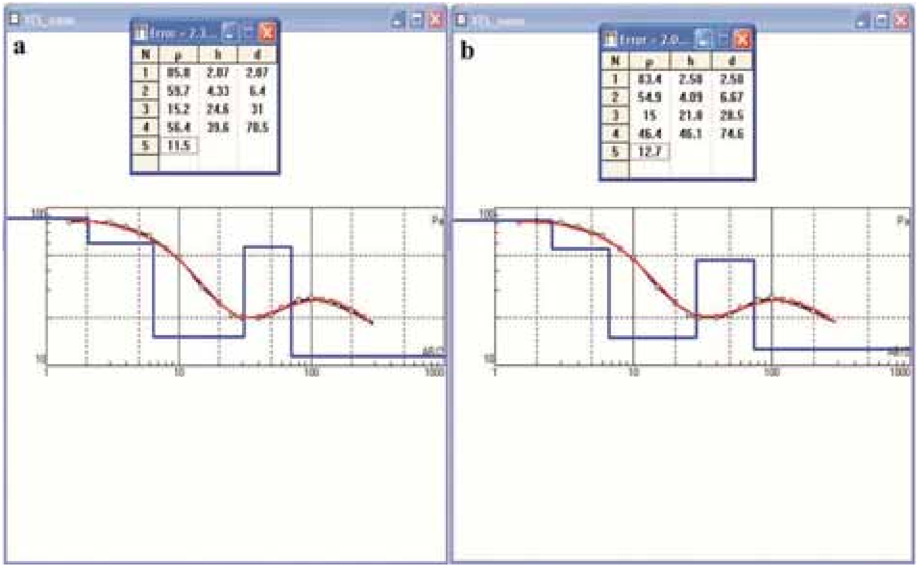

Figure (2-23):- Shows the interpretation results (a) forward calculation method, (b) inverse modeling method, (Al-Zubedi, 2009).

2 -The reduced capability can be clearly observed in the interpretation results for both methods, when the field curve includes sudden changes in the apparent resistivity values, in the inflection point on the field curve , as observed the forward calculation method is the least capability, where gives imaginary values of some horizons for the field curve that do not agree with wells lithological sections, as shown in the apparent resistivity values of the sixth horizon of field curve, as show in figure (2-24a).

Comparison with figure (2-24b) which represents the results of inverse modeling method, therefore the interpreter should have a role in the interpretation process, especially when using forward calculation method through the comparison between the interpretation results and the initial information of lithological sequence in the area under investigation.

3-The inverse modeling method can be used also for checking (Bobachev, 2002), and improving the interpretation results for some field curves so as to agree with layer boundaries of the lithological sections from wells, within the principle of equivalence that permits to change of the thicknesses and resistivity values for each layer of the field curve within specific limits without change the field curve shape.

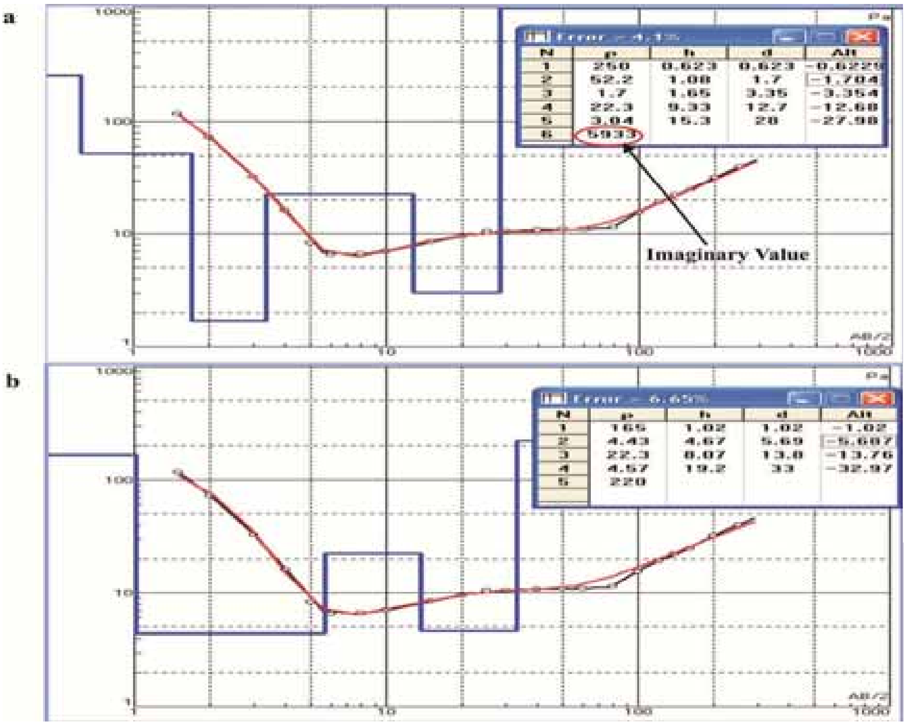

Figure (2 -24):- Shows the results of forward calculation (a), and inverse modeling (b) methods, (Al-Zubedi, 2009).

2-2-2-4 Ambiguity in Electrical Resistivity Method.

As can be seen in other geophysical methods, ambiguity in electrical resistivity interpretation procedures may also appeared due to the presence of the following important principles. This ambiguity may lead to produce an erroneous in results. Following are the most important source of ambiguity:-

A- Principle of Equivalence.

The principle of equivalence concerns the beds for which the resistivity is either greater, or less than, both beds above and below. It is found that a resistant bed between two more conductive beds manifests itself mostly by its transverse resistance or the product of its resistivity with its thickness. On the other hand, a conductive bed, between two or more resistant beds, shows essentially its longitudinal conductive or the product of its conductivity to its thickness, of course it is also the thickness divided by the resistivity. In other words, it will be difficult if not impossible to distinguish between two resistant beds of different thicknesses and resistivity, if the product of the thickness and resistivity are the same. Similarly, two conductive beds can not be distinguished if the ratio of the thickness to the resistivity are the same. The effect of this principle becomes low as layer thickness increases (Flathe, 1955: Kunetz, 1966).

B - Principle of Suppression.

The principle of suppression relates to those layers whose resistivities are intermediate between the resistivity of the enclosing beds. Such layers as long as they do not have a great enough thickness, have practically no influence on the resistivity curve. When the thickness of the intermediate layer begins to grow, it appears its affect on the resistivity curve. This failure to define beds of intermediate resistivity is met frequently in ground water studies in which there is a surface layer of dry alluvium, then wet alluvium, both reposing on a conductive sub-stratum of shale layer. In such a case, it becomes impossible to determine the depth of sub-stratum.

2-2-2-5 Representation of Quantitative Interpretation Results.

A- The Geo-electrical Sections.

The geo-electrical section is one of the important forms for displaying the results of the quantitative interpretation of vertical electrical sounding. It is drawn with reliance on the resistivity contrast between the different electrical horizons, and is usually supported by the wells lithological sections to obtain good geo-electrical sections, (Van Overmeeren, 1989). In these sections, the vertical axis represents the electrical horizons thickness, while the horizontal axis represents the distance between (VES) points. The electrical horizon may represents group from geological layers have approximate resistivity values cannot separated between them at field curves interpretation. The following figure (2-25) showed the geo-electrical section.

B- The Resistivity Maps.

The true resistivity values concluded from the quantitative interpretation results are drawn on form the resistivity map. It is not the apparent resistivity map because it is represented the distribution of true resistivity values under ground in the surveys areas, which may be is reflecting the presence the faults or geologic structures. This method usually is carried out by computerized programs such as Surfer program.

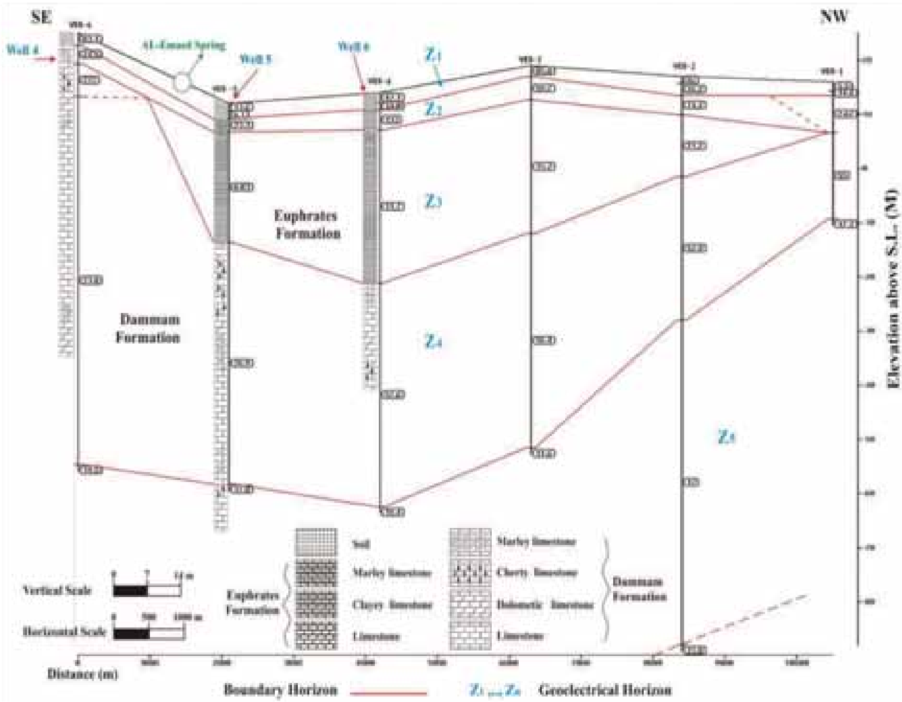

Figure (2-25):- Shows the geo-electrical section, (Al-Zubedi and Thabit, 2014).

2-3 Geo-electrical parameters.

A geological section consists of one or more than one sequence layered rocks, with quite different textures. It differs from a geo-electrical section when the boundaries between geologic layers do not coincide with the boundaries between layers characterized by different resistivities (Zohdy, 1974), because uniform electrical layers can be combined into a single unit of geo-electrical section. For example, when the salinity of ground water in a given type of rock varies with depth, several geo-electrical layers may be distinguished within lithologically homogeneous rocks. In the opposite situation, layers of different lithology or ages or both may have the same resistivity and thus form a single geo-electrical layer.

The average electrical properties of each unit in a layered geo-electrical section may be described with five parameters, on the bases of resistivity (ρ_i) and thickness (h_i) of the geo-electrical unit, (Zohdy, 1974). These parameters are called Dar-Zarruok Parameters, (Maillet, 1947).

The electrical well logs provide virtually the only certain method for determining the electrical parameters describing a geo-electrical section (Keller and Frischkecht, 1982).

The following are the most important parameters controlling geo-electrical section:-

1- Transverse resistance (R_T)

It is the total resistance through a (1m2) column cut perpendicular to the bedding planes of sequence of layers (n) with resistivities (***ρ**$_n$*) and thickness (**h$_n$**), it is given by:-

$$R_T = \sum_{i=1}^{n} \rho_i h_i \qquad ....(22)$$

2-Transverse resistivity (ρ_{Tr})

It is the average resistivity normal to the bedding planes of (n) layers with total thickness (**H**), or is the transverse resistance divided by the total thickness of layers, as follow:-

$$\rho_{Tr} = R_T / H \qquad ……….(23)$$

It is always greater than the longitudinal resistivity.

3- Longitudinal conductance (S_L)

It is the total conductance along the direction of the bedding planes of (n) layers, which are equal to total thickness of layers (H) divided by the total resistivities of layers, is given by:-

$$S_L = \sum_{i}^{n} h_i / \rho_i \qquad ………(24)$$

4- Longitudinal resistivity (ρ_L).

It is the average resistivity along the bedding planes, or equal to the total thickness (H) divided by the longitudinal conductance (S_L), as follow:-

$$\rho_L = H / S_L \qquad ……… (25)$$

5- Coefficient of anisotropy (λ).

It is defined by taking the square root of the ratio of the resistivities measured in the two principles directions, across the bedding plane (ρ_{Tr}) and along bedding plane (ρ_L), as shown in figure (2-26). Which is given by:-

$$\lambda = \sqrt{\rho Tr / \rho L} = \sqrt{RT.SL / H} \qquad \text{...........(26)}$$

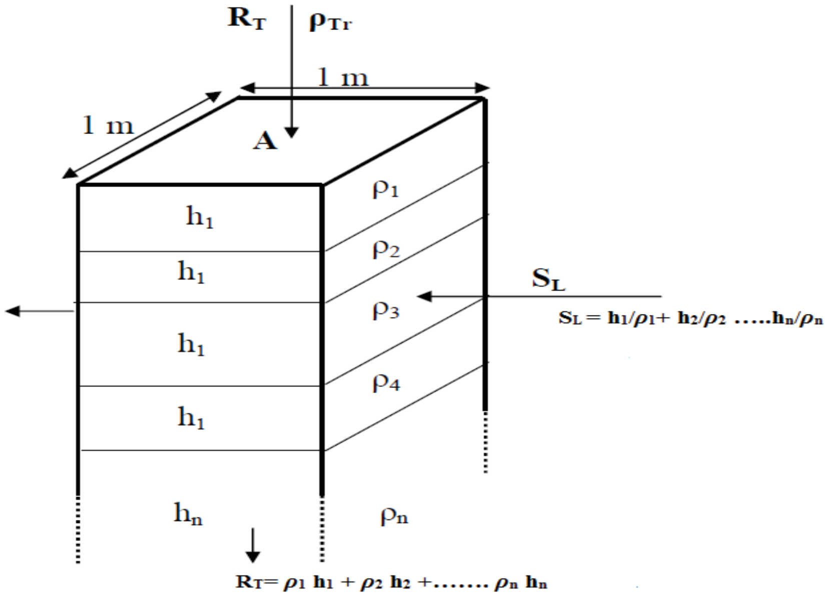

Figure (2-26):- Isometric diagram showing geo-electrical parameters of (n) layers of the Earth, (Zohdy, 1974).

Principle of showing different physical properties such as resistivity value in more than one direction, when we suppose to specify the potential distribution in anisotropic media, and as known that the electrical resistivity appears maximum value along transverse resistivity (ρ_{Tr}) direction, and minimum value along longitudinal resistivity (ρ_L), which is perpendicular to the previous direction. Accordingly, the distribution of equipotential surface can be described through the use of the ratio of (λ), (Maillet, 1974). It also can be found that the current lines are not perpendicular to the equipotential surfaces of anisotropic media, (Kunetz, 1966).

2-4 1D Azimuthal Resistivity Survey.

1D Azimuthal resistivity survey is one of the electrical resistivity surveys being used for identification and characterization of fractured rocks. It has been adopted as a fast and effective surface method for determining the directions of the anisotropy that are directly related to structural or lithological changes in the subsurface (Leonard, 1984; Taylor and Fleming, 1988; Hagrey, 1994; Busby, 2000; Busby and Jackson, 2006). The variation in the apparent resistivity values is measured as a function of azimuth by using Vertical Electrical Sounding (VES) or Constant Separation Traverse (CST) techniques. An electrode array is rotated about its center so that the apparent resistivity is observed for several directions (Taylor and Fleming, 1988).However; there are two types of array rotation in the azimuthal resistivity survey:-

2-4-1 Symmetrical 1D Azimuthal Resistivity Survey.

This survey is carried out using the same electrodes array spacing and the center of the electrodes spreading is fixed at the same position, as in figure (2-27).

Each successive spread is oriented in a different direction or azimuth until 180 degrees are covered in increments of 45 degrees. A full 360 degrees do not need surveyed at the setup of 0 degree. However, the 0 degree gives the same result of 180 degree and 45 degree gives the same result as 225 degree, etc, (Taylor and Fleming, 1988).

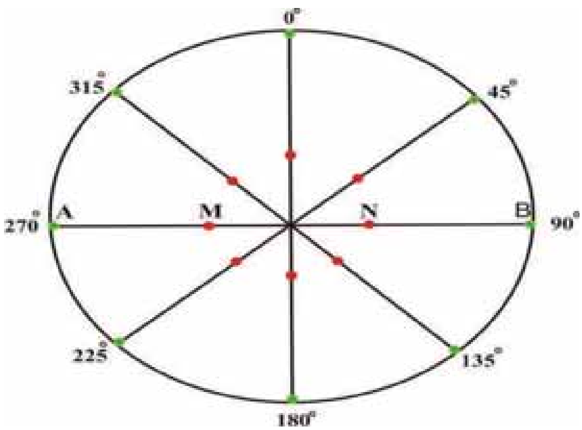

Figure (2-27):- Symmetrical 1D azimuthal resistivity survey by Wenner array with rotated 45 degrees clockwise, (Taylor and Fleming, 1988).

2-4-2 Non-Symmetrical 1D Azimuthal Resistivity Survey.

This survey is collocated by using the same electrodes array spacing, but the center of the array is changed with changing the all spread direction. This survey can be carried out by two methods. The first method includes changing the position of all the four electrodes, as in figure (2-28).

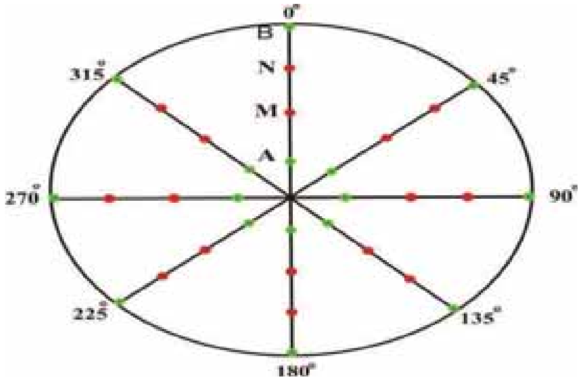

Figure (2-28):- Non-symmetrical 1D azimuthal resistivity survey. The position of all the four electrodes moved out, (Taylor and Fleming, 1988).

The second method, one of the current electrodes keeps fixed and the other electrodes move out to next positions at a new direction, (Taylor and Fleming, 1988), as in figure (2- 29).

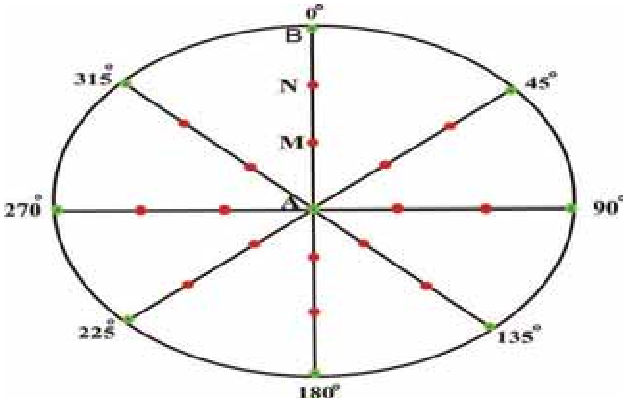

Figure (2-29):- Non-symmetrical 1D azimuthal resistivity survey. One of the current electrodes keeping fixed, (Taylor and Fleming, 1988).

2-4-3 Display 1D Azimuthal Resistivity Data.

The azimuthal resistivity data can be displayed by several methods, one of them is given by (Nunn et al., 1983). In this method the data are plotted as a function of azimuth in Cartesian coordinates, as example figure (2- 30).

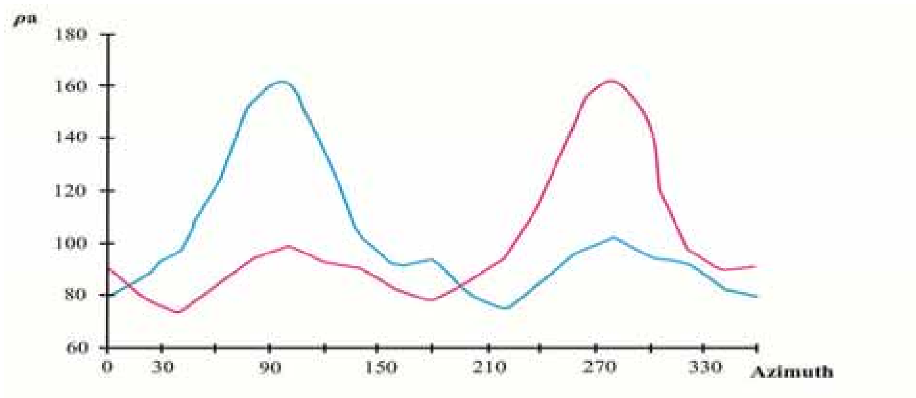

Figure (2-30):- 1D Azimuthal resistivity diagram, (Nunn et al., 1983).

Another method is most commonly used for displaying the azimuthal data, where the apparent resistivity is recorded for all electrodes spacing and plotted along the azimuth on a polar diagram. Each point plotted at a distance from the diagram's center along the same azimuth with definite linear scale. All points are connected with a curve, as in figure (2-31), (Taylor and Fleming, 1988).

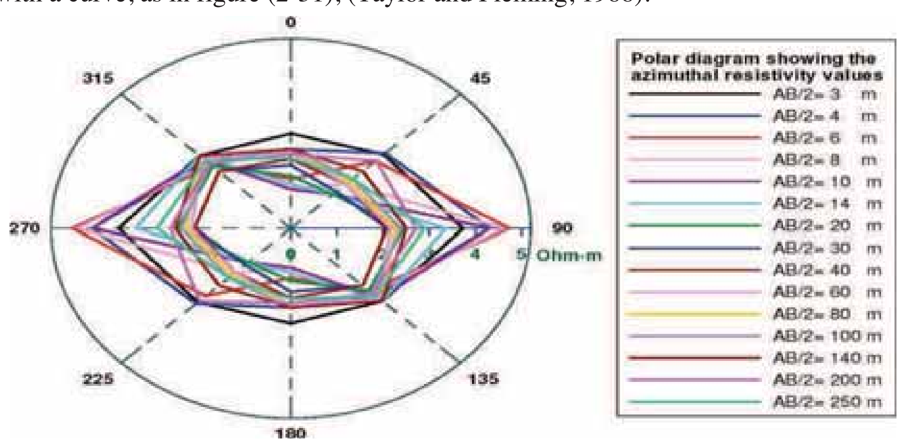

Figure (2-31):- 1D Azimuthal resistivity measurements in polar diagram from (Massoud et al., 2009).

A circular apparent resistivity anomaly implies heterogeneity, fault zone or the volume of rock investigated was too thick to reveal the presence of anisotropy .An ellipsoidal plot of the resistivity anomaly may indicate the presence of a structural feature such as a fault along its azimuthal direction. For collinear arrays, the major axis of the ellipse is coincident with the strike of the fault, whereas in the case of nonlinear arrays, such as square array (Habberjam and Watkins, 1967), the minor axis of the ellipse is parallel to the fault strike.

The azimuthal resistivity measurements which obtained by Vertical Electrical Sounding (VES) are displayed and interpreted qualitatively and quantitatively, (Leonard, 1984).The following figure (2-32) shown azimuthal resistivity by (VES) technique.

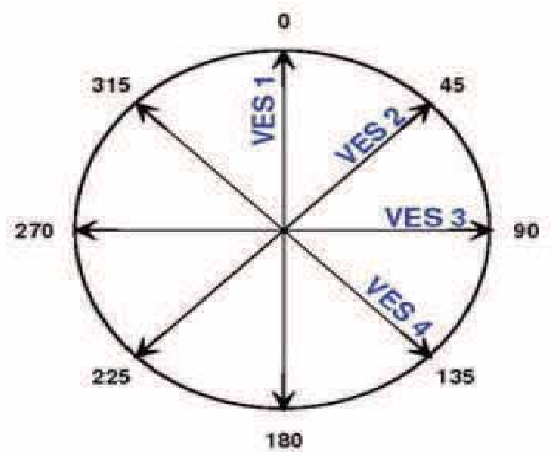

Figure (2-32):- 1D azimuthal resistivity survey by (VES) technique with rotated 45 degrees clockwise from (Massoud et al., 2009).

1D Azimuthal resistivity surveys are used to determine the anisotropic in soils or rocks. There are many methods that can be used for determining the anisotropic, one of them was given by (Steinich et al., 1997). In this method the anisotropy (λ) is calculated from the ratio between the largest apparent resistivity (ρ_a max) and the smallest apparent resistivity (ρ_a min) in the azimuthal resistivity curve as:

$$\lambda = \frac{\rho_a \max}{\rho_a \min} \qquad \text{………..} \textbf{(27)}$$

Thus the value of (1) for (λ) is an index characterizing the eccentricity of the curve with respect to a circle, which would be expected for an isotropic medium and for which the value of (1) would be unity. However, the results of 1D azimuthal resistivity surveys in both Vertical Electrical Sounding (VES) and Constant Separation Traverse (CST) techniques are not separate between anisotropy types and this lead to erroneous conclusions, where azimuthal variations in apparent resistivity may be result from the presence of dipping stratigraphy or other lateral changes in formation resistivity (Watson and Barker, 1999).

2-5 Combined VES/CST Technique (Pseudosection Technique).

A pseudosection is a display technique devised by Hallof (1957) which involves plotting resistivity traverse data as a depth section. It includes using the Vertical Electrical Sounding (VES) and Constant Separation Traverse (CST) techniques together to determine the lateral and vertical changes of subsurface apparent resistivity in the same time. The obtained data of ($\boldsymbol{\rho}_{\mathbf{a}}$) values are plotted to form a pseudosection. In this case, each measurement is represented the mid – point of electrodes set used to make that measurement for linear array. The vertical location of the plotting point is placed at a distance (depth), which proportional to the separation distances between the electrodes or this distance represents depth function of each electrode array, (Edwards, 1977; Barker, 1992).

One common method is to place the plotting point of ($\boldsymbol{\rho}_{\mathbf{a}}$) measurements at the intersection of two lines starting from the mid-pint of the (AB) and (MN) dipole pairs, with an angle equal (45º) to the horizontal, as shown in figure (2-33).

The interpretation of pseudosection data is mainly qualitative and it gives very approximate and not actual image of the true subsurface resistivity distribution, (Loke, 2004).However, the pseudosection is mainly using for mineral investigation and the detailed surveys about the under ground structures, (Edwards, 1977). In the last years, this technique is used in the 2D imaging surveys, which represents the modern technique in the electrical resistivity surveys.

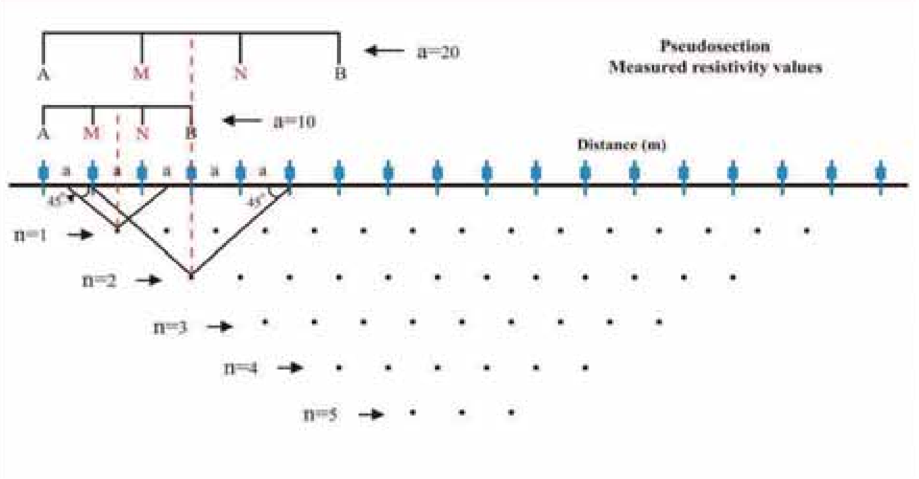

Figure (2-33):- The measurement sequence for building up pseudosection for Wenner array.

3-1 Introduction.

The development in the field equipment design capability and computer algorithms led to appearance of 2D and 3D resistivity imaging techniques in the 1990s,(Loke et al., 2013).The 2D resistivity imaging technique has become one of the most significant electrical resistivity techniques for investigating underground structures, (Kemna et al., 2002; Zhou et al., 2004; Loke et al., 2013; Al-Zubedi and Thabit, 2014). It is based on an old technique called Pseudosection. This technique includes using the Vertical Electrical Sounding (VES) and Constant Separation Traverse (CST) techniques together to determine the lateral and vertical changes of subsurface apparent resistivity in the same time, (Edwards, 1977; Barker, 1992). A three-dimensional 3D geoelectrical resistivity imaging should, in theory, give a more accurate and reliable picture of the subsurface, especially in highly heterogeneous subsurface commonly associated with environmental and engineering investigation sites, (Aizebeokhai and Olayinka, 2010).

3-2 2D Resistivity Imaging Technique.

The 2D resistivity imaging technique provides a more realistic model of the subsurface information and not available by 1D techniques. Where the maximum limitation of the resistivity 1D sounding resistivity is that it does not take into account horizontal changes in the subsurface resistivity. A more accurate model of the subsurface is a two dimensional (2D) model where the resistivity changes in the vertical direction, as well as in the horizontal direction along the survey line. At the present time, 2D resistivity imaging technique is the most practical economic compromise between obtaining very accurate results and keeping the survey costs down, (Dahlin, 1996).

3-2-1 Field Measurement Procedures.

In 2D resistivity imaging technique, we need to use a large number of electrodes (25) or more, linked to a multi node unit or a multi – core cable. A laptop microcomputer together with an electronic switching unit is used to select automatically the relevant electrodes for each measurement, figure (3-1), (Barker, 1992; Loke, 2014).

Loke (1999) give a description of the field measurement procedures of the 2D resistivity technique, where all electrodes are inserted into the ground along a straight line attached to a multi-core cable. Normally a constant spacing between adjacent electrodes is used .The multi-core cable is attached to an electronic switching unit that is connected to a laptop computer.

The sequence of measurements to take the type of array to use and other survey parameters (such the current to use) is normally transferred to resistivity meter from the computer.

To obtain a good picture of the subsurface, the coverage of measurements must be 2D as well. As an example, (figure 3-1) shows a possible sequence of measurements for the Wenner electrode array for a system with (20) electrodes.

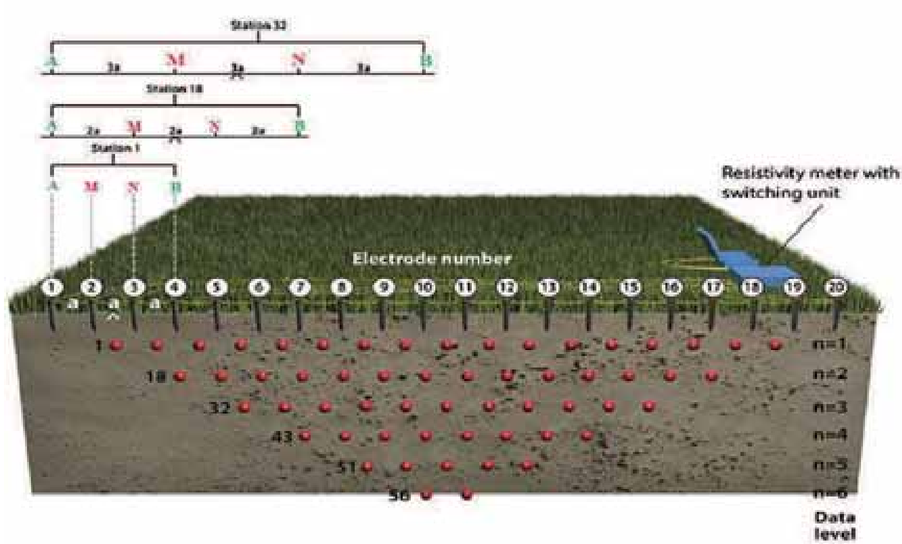

Figure (3-1):- Shows the arrangement of electrodes for 2D resistivity survey and the sequence of measurements, (Loke et al., 2013).

In this example, the spacing between adjacent electrodes is (a). The first step is to make all the possible measurements with the Wenner array of electrode spacing of (a).

For the first measurement, electrodes numbers (1, 2, 3 and 4) are used. Notice that electrode (1) is used as the first current electrode (A), electrode (2) as the first potential electrode (M), electrode (3) as the second potential electrode (N) and electrode (4) as the second current electrode (B). For the second measurement, electrodes number (2, 3, 4 and 5) are used for (A, M, N and B) respectively. This is repeated down the line of electrodes until electrodes (17, 18, 19 and 20) are used for the last measurement with (1a) spacing. For a system with (20) electrodes, note that there are 17 (20 - 3) possible measurements with (a) spacing for the Wenner array. After completing the sequence of measurements with spacing, the next sequence of measurements with (2a) electrode spacing is made. First electrodes (1, 3, 5 and 7) are used for the first measurement. The electrodes are chosen so that the spacing between adjacent electrodes is (2a). For the second measurement, electrodes (2, 4, 6 and 8) are used.

This process is repeated down the line until electrodes (14, 16, 18 and 20) are used for the last measurement with spacing (2a). For a system with (20) electrodes, note that there are 14 (20-2x3) possible measurements with (2a) spacing. The same process is repeated for measurements with (3a), (4a), (5a) and (6a) spacing, (Barker, 1992; Loke, 1999). To get the best results, the measurements in a field survey should be carried out in a systematic manner so that, as far as possible, all the possible measurements are made. This will affect on the quality of interpretation model obtained from the inversion of the apparent resistivity measurements. One technique used to extend horizontally the area covered by the survey, particularly for a system with a limited number of electrodes, is the roll-along technique (Loke, 2012). After completing the sequence of measurements, the cable is moved past one end of the line by several unit electrode spacings. All the measurements that involve the electrodes on part of the cable that do not overlap the original end of the survey line are repeated, (Loke, 2012), as shown in figure (3-2).

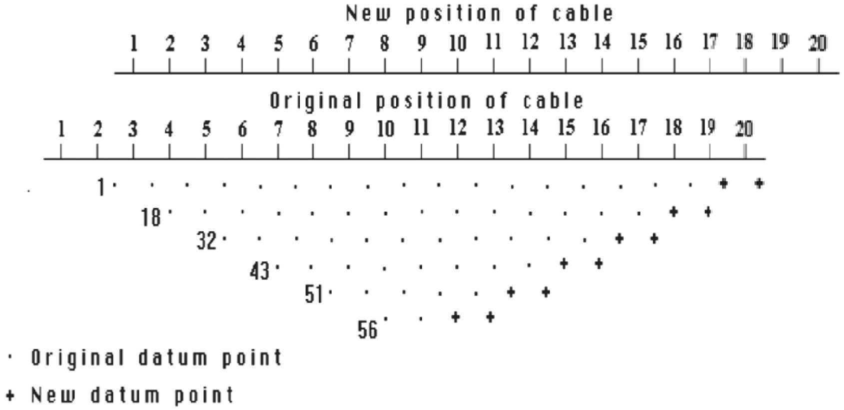

Figure (3-2):- The use of the roll-along technique to extend the area covered by a 2D survey,(Loke, 2012).

If the resistivity meter was old and not involve multi- core cable, the 2D imaging technique can be carried out manually, where the current and potential cables are moved from pole to another along the survey line, and then the data input manually to the interpretation programs through IPI2win or any text editor programs such as Notepad, WordPad and Microsoft Office Excel program, more information about this can be found in (AL-Zubedi, 2009).

3-2-2 Create 2D Imaging Sequences.

Before the fieldwork the multi-core cable is attached to an electronic switching unit that is connected to a laptop computer. Then the sequences (or protocol) of measurements are created and upload to the resistivity meter. There are many programs designed to create the sequences of different electrode arrays before carrying out fieldwork. Different resistivity meters used different formats for sequence files.

The main object of these programs is to select the suitable sequence to achieve real subsurface imaging. They give the approximately information about the maxim depth of investigation, number of level, number of readings and estimated acquisition time. The most important parameters in these programs to create the sequences of 2D imaging are *a*-spacing and *n*-factor for array used. These parameters are played major role to improve the data quality for resistivity surveys by using overlapping data levels with different combinations of (*a* and *n*) parameters, particularly in noisy areas for the Wenner-Schlumberger, dipole-dipole and pole-dipole arrays, (Loke, 2014). For example, The Wenner-Schlumberger array of 60 electrodes, used to create the sequences of 2D imaging with *a*-spacing (unit electrode spacing) equal to (10m) between them and *n*-factor equal to (6n) by ELECTRE pro program (from IRIS-Company-France), as shown in figure (3-3). Therefore, the created sequence gives maximum investigation depth equal to (110m), while the numbers of levels are (30). This means for each *a* there is (6) levels, where (*a*) is 5, while the *n*-factor is 6 (5x6 = 30) as shown in figure (3-4). It is indicated to good horizontal and vertical coverage data. With respect to the estimated acquisition time it is 1:02 hour, while the number of readings (measurements) 789. However, after completing the sequences, the data are exported from the computer to the resistivity meter to carry out the fieldwork.

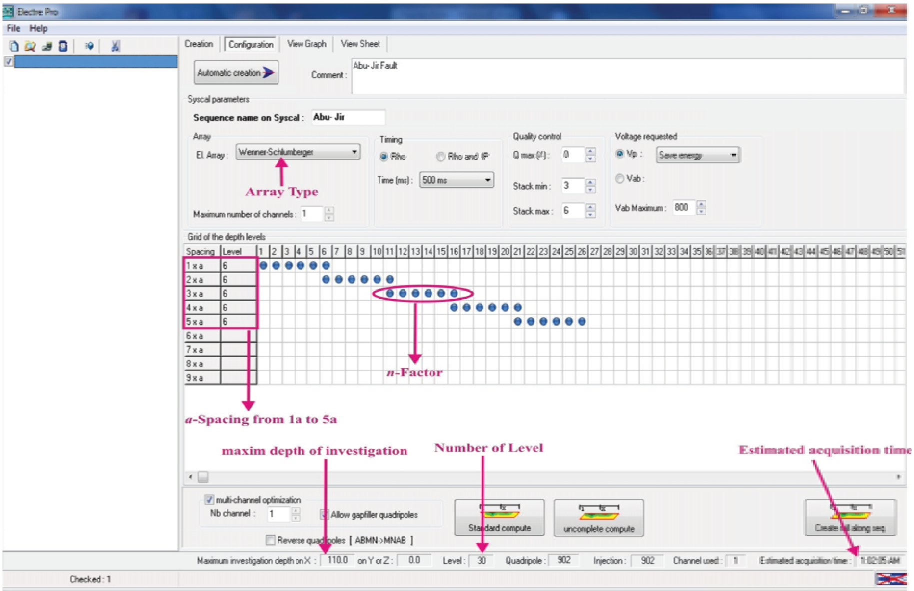

Figure (3-3):- Shows the sequences creation of Wenner-Schlumberger array, (Al-Zubedi 2015).

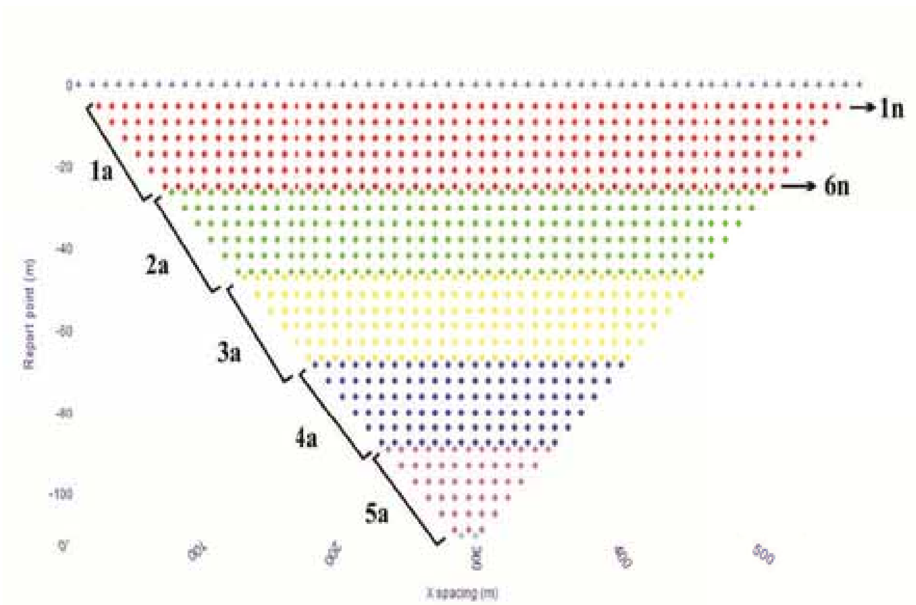

Figure (3-4):- Shows pattern of levels and *a*-spacing from 1*a* to 5*a* and *n*-factor from 1*n* to 6*n*.

3-2-3 Data Processing.

After completing the field work of 2D surveys, the data measurements are exported from the resistivity meter memory to the computer with the assistant software. In some these software (such as Prosys, from IRIS- Company-France), there are many options can be used for data displaying and processing, before exporting it to any interpretation software. The data processing can be carried out through many filters. These filters are specified for filtering abnormal recorded potential, resistivities, and injection current, where the interpreter can look at the whole recorded data for each 2D imaging line and decide whether it is necessary to pass the data over some suitable filter or not.

The abnormal (or bad) data are caused by two categories from noise, (systematic) and (random) noise. According to Loke (2014), the Systematic noise is usually caused by some sort of failure during the survey such that the reading does not represent a true resistivity measurement. Examples are including breaks in the cable, very poor ground contact at an electrode such that sufficient current cannot be injected into the ground, forgetting to attach the clip to the electrode, connecting the cables in the wrong direction etc. Systematic noise is fairly easy to detect in a data set as it is usually present in limited number of readings, and the bad values usually stick out like sore thumbs. Random noise include effects such telluric currents that affects all the readings, and the noise can cause the readings to be lower or higher than the equivalent noise-free readings. However, most interpretation program have some options can be used for data processing such as RES2DINV program. In this program there is (Edit data) on the top menu bar followed by the (Exterminate bad data points) option can be used to remove the bad data points manually by clicking them with the mouse.

If the data set contains more than a thousand data points. In some cases, the (RMS error statistics) option can be used to remove the bad data points automatically, (this option is used after carrying out the trial inversion), (Loke, 2014).

3-2-4 Data Interpretation.

The large amounts of data produced by multi-electrode systems require automated data handling and processing. Automatic inverse numerical modeling techniques (inversion) based on the finite difference or finite element methods for the forward calculations, (Dahlin, 2001). In the forward modeling problem, the subsurface resistivity distribution is specified and the purpose is to calculate the apparent resistivity that would be measured by a survey over such a structure. A forward modeling subroutine is in fact also an integral part of any inversion program since it is necessary to calculate the theoretical apparent resistivity values for the model produced by the inversion routine to see whether is agrees with the measured values or not, (Loke, 2014).

The contoured data can be modeled using a two-dimensional (2D) finite element or finite difference algorithm (Dey and Morrison, 1979) to calculate the 2D forward response of the model.

In 2D forward modeling the subsurface resistivity distribution is described by a 2D model extended in infinity in the third direction. It is important to notice, however, that the sources, the current electrodes, are modeled as 3D sources. If not, they would obviously be mistakenly described as line electrodes.

The forward modeling finds a solution to the current flow equations in inhomogeneous ground for a given resistivity distribution and current source configuration. The solution includes the potential field in the investigated 2D section, from which calculation of the apparent resistivities from the configuration of the potential electrodes are straightforward.

The simplified equation for 2D is typically solved numerically by dividing the subsurface in a number of finite elements and solves by matrix inversion techniques. The most common numerical methods are the finite differences or the finite element method. The method of finite differences has been used as default except for when topography is included then the finite element method is preferred due to more flexibility in arranging the cells.

The inversion programs are used to convert the field apparent resistivity measurements into a resistivity model section that can be used for geological interpretation. The inversion of resistivity data is non - linear process and non - unique results, (Dahlin and Loke, 1998). Because the RES2DINV program is the more use in the interpretation of 2D imaging data, we restricted to describe the inversion routines which is used in this program.

This program can give the model depending on the mathematical relation ship, which is a link between the model parameter and the model response for the 2D resistivity and is provided by the finite – difference or finite – element methods (Loke & Barker, 1995).

The 2D model used by this program divides the subsurface into a number of rectangular blocks, (figure 3-5).The purpose of the program is to determine the resistivity of the rectangular blocks that will produce an apparent resistivity pseudosection that agrees with the actual measurements.

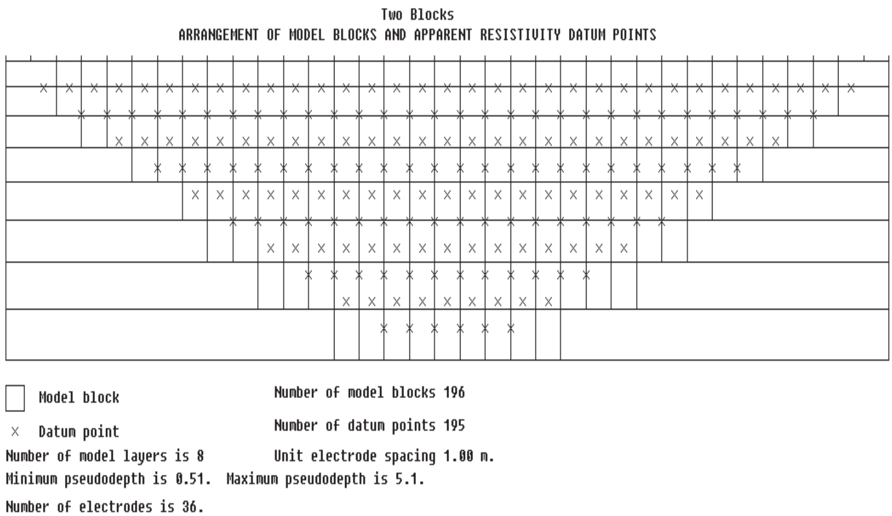

Figure (3-5):- Shows subdivide the subsurface into a number of rectangular block, (Loke, 2004).

The arrangement of the blocks is loosely tied to the distribution of the data points in the pseudosection .The program automatically chooses the optimum inversion parameters for a data set.

The optimization method tries to reduce the difference between the calculated and measured apparent resistivity values by adjusting the resistivity of the model blocks.

A measure of this difference is given by the root-mean squared (RMS) error. However, the model with the lowest possible (RMS) error can sometimes show large and unrealistic variations in the model resistivity values and might not always be the "best" model for a geological perspective. In general, the most approach is choosing the model at the iteration after which the (RMS) error does not change significantly.

This usually occurs between the 3rd and 5th iterations, (Loke, 2004). Figure (3-6) shows the output from the RES2DINV software.

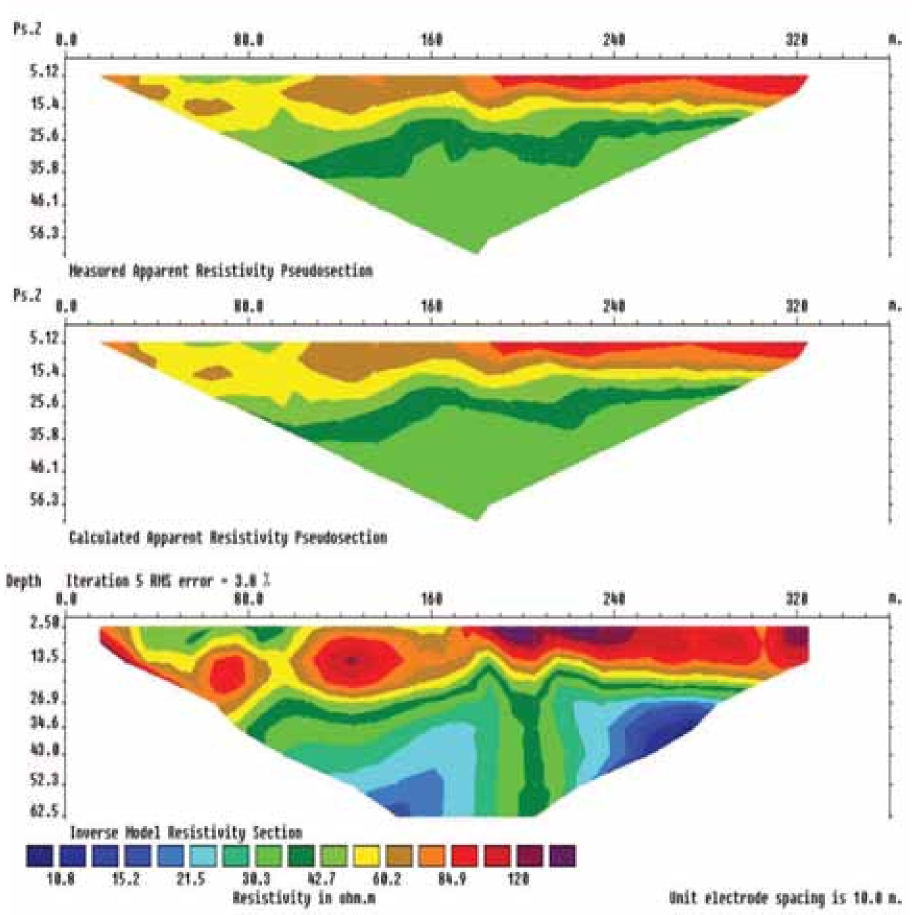

Figure (3-6):- shows the 2D models by RES2DINV program.

The inversion routine is based on the smoothness constrained least-squares method (deGroot-Hedlin and Constable, 1990; Sasaki, 1992; Loke and Barker, 1996a). More information about this program can be found in (Tutorial: 2D and 3D electrical imaging surveys of Loke, 1996- 2014).

The inversion procedure of measured data to create 2D imaging model can be summarized in a flow chart as in figure (3-7).

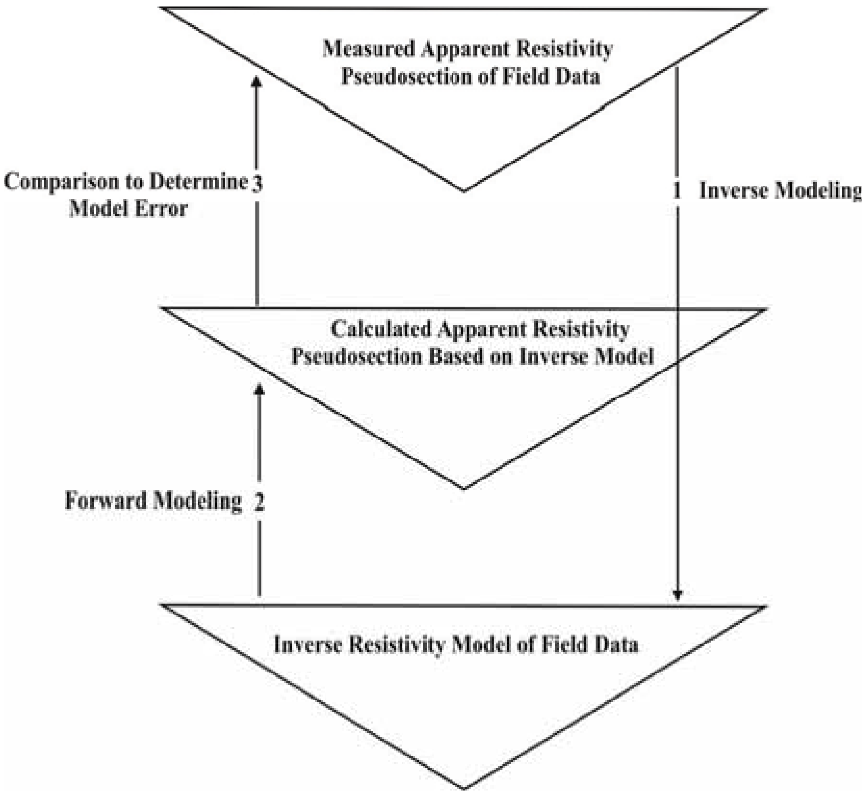

Figure (3-7):- Overview of resistivity imaging inversion process.

3-2-5 2D Azimuthal Resistivity Imaging Survey.

A 2D Azimuthal resistivity imaging survey is one of the electrical resistivity surveys being used by 2D imaging technique for identification and characterization of fractured rocks. It is initially used by Al-Zubedi (2015) to determine the subsurface fracture characteristics in Dammam aquifer within and out of Abu-Jir fault zone, central Iraq.

The 2D azimuthal imaging survey was carried out by Al-Zubedi (2015) through four 2D imaging lines in different directions (N- S, E-W, NE-SW and NW-SE) with a coverage equal to 45 degrees and by Wenner-Schlumberger array. Each 2D imaging line consisted of (60) electrodes with the unit electrode spacing (a) 10m, as shown in figure (3-8).

The results showed that the 2D azimuthal technique was successful in imaging the subsurface fractures extension in all directions. Therefore, this technique can be useful in determining the structures extension, especially in the unknown areas that characterizing by hidden geological and structural setting, particularly in deep investigations.

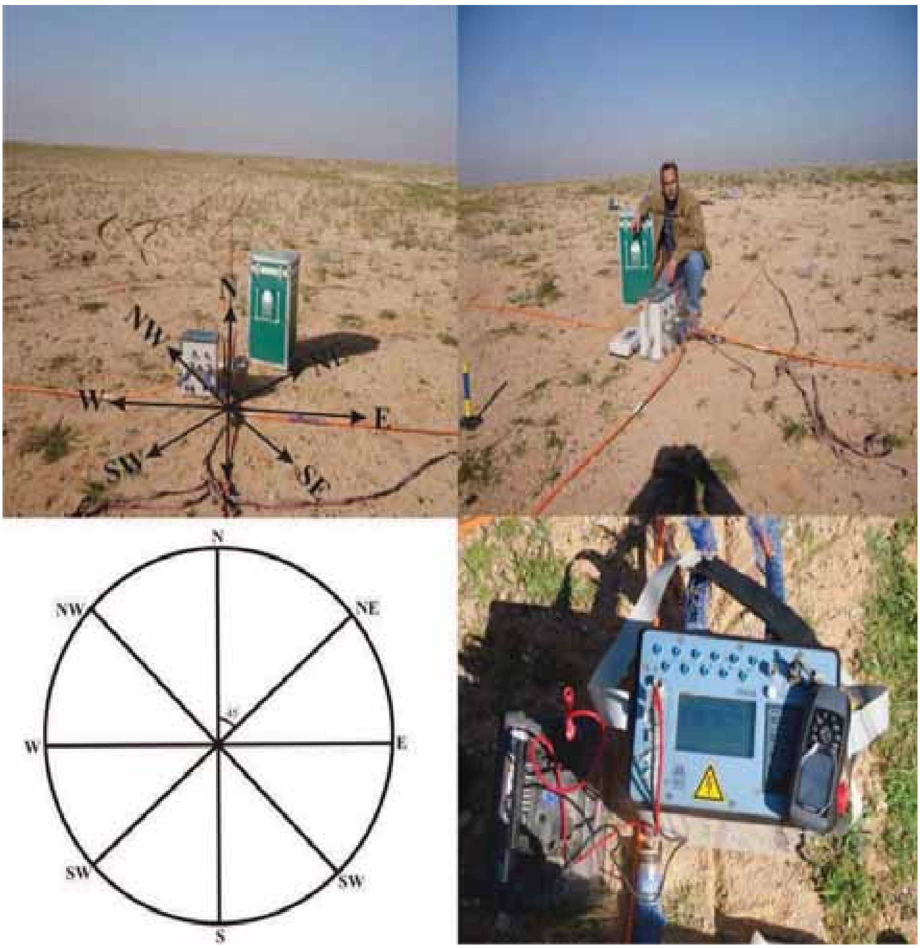

Figure (3-8):- Data acquisition by 2D azimuthal resistivity imaging survey, (Al-Zubedi, 2015).

3-2-6 Cross-Borehole Imaging Surveys.

Typically, the 2D resistivity imaging technique used to determine the subsurface resistivity distribution by making measurements on the ground surface, where all electrodes are inserted into the ground along a straight line attached to a multi-core cable. In some cases this technique can be used in boreholes and it is named cross-borehole surveys. In these surveys, any array that is used for normal surface surveys can be adapted for cross-borehole surveys. However, there are three possible configurations of these surveys by four electrode arrays, as shown in figure (3-9). In the first configuration, all electrodes can be in the same borehole. In the second configuration, the electrodes can be in different boreholes, where the third configuration has two electrodes on the surface and other electrodes in borehole.

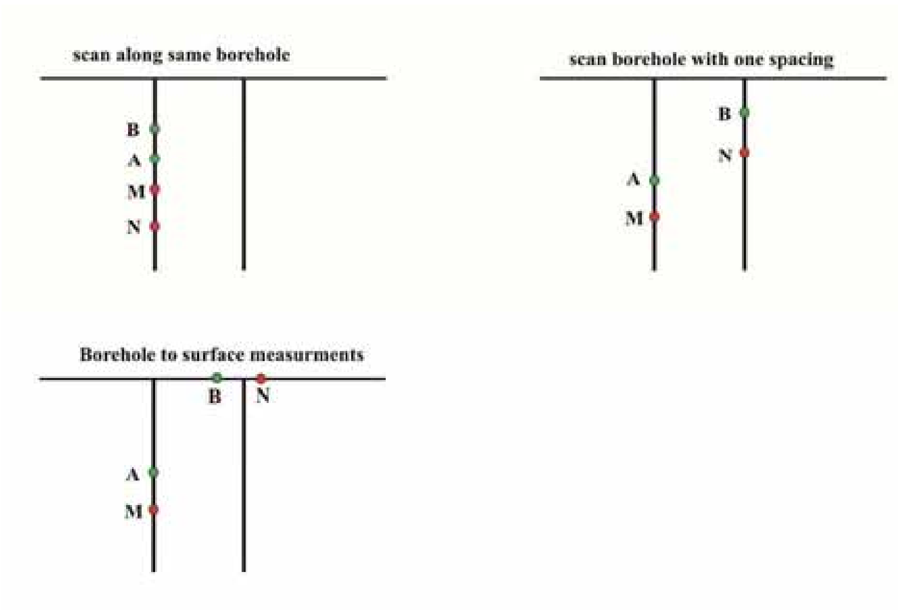

Figure (3-9):- Possible measurement sequences using the four electrodes array, modified from (Loke, 2014). Other possible measurements sequences are described in the paper by Zhou and Greenhalgh (1997).

In some situations, only a single borehole is available. In this case, only the borehole to surface measurements is possible and this named single borehole surveys, (Loke, 2014). There are two possible configurations of these surveys by four electrode arrays, as shown in figure (3-10). The first configuration has only one electrode in borehole and other electrodes on the surface, while the second configuration has two electrodes on the surface and other electrodes in borehole. More information about two electrodes and three electrode arrays that used in the single and cross-borehole surveys can be found in Loke (2014).

The cross-borehole surveys are used for shallow investigations. Therefore, they are widely used in engineering projects. However, there are many publications on such surveys; such as by Zhao et al. (1986), Sasaki (1992), Slater et al. (1997) , Zhou and Greenhalgh (2000), Oldenborger et al. (2005), Chambers et al (2007), Wilkinson et al (2008) and Nimmer et al (2008).

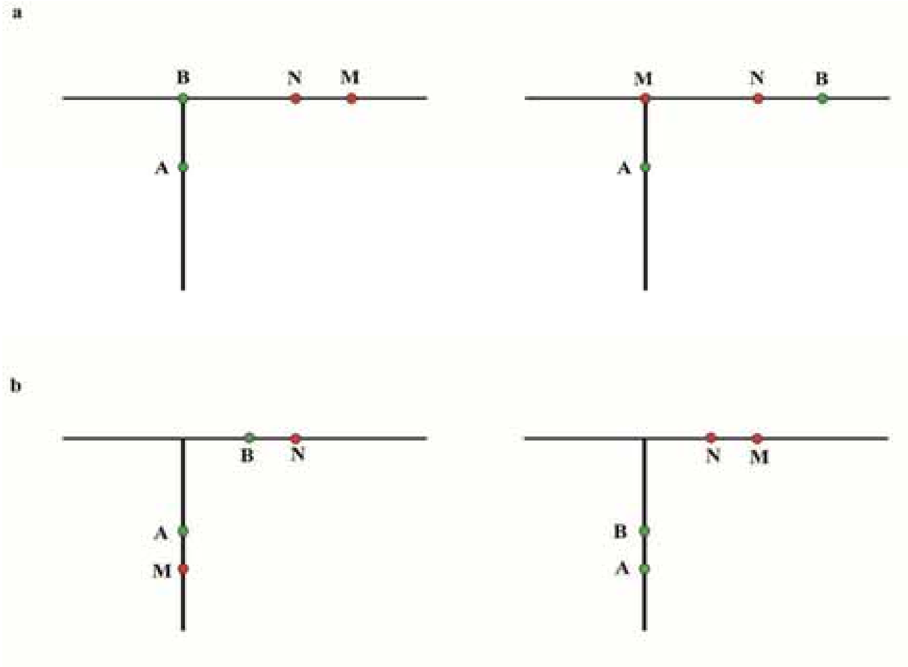

Figure (3-10):-Several possible configurations of four electrodes array with a single borehole, a- one electrode in borehole, b- two electrodes in borehole.

3-3 3D Resistivity Imaging Technique.

The earth often shows three-dimensional characteristics, which can limit a 2D interpretation. As multi-electrode systems were developing rapidly, e.g., by the use of multichannel recorders, it became more and more interesting to carry out measurements allowing for a three-dimensional reconstruction. There are two current developments that should make 3D surveys more cost-effective option in the near future. One is the development of multi-channel resistivity meters that enable more than one reading to be taken at a single time. This is important to reduce the survey time.

The second development is faster microcomputers to enable the inversion of very large data sets (with more than 8,000 data points and survey grids of greater than 30 by 30) to be completed within a reasonable time, (Loke, 2014).

3-3-1 Field Measurement Procedures.

The field measurement procedures were described by Loke and Barker (1996b). The initial suggestion involved the deployment of one multi - core cable in snake-lines across a regular grid of electrodes, as in figure (3-11). The use of measurements in two perpendicular directions helps to reduce any directional bias in the data. This survey mode only used for shallow investigation, because it is involved grid least 16 by 16, (Loke, 2012). It is usually carried out by arrays that have sensitivity function decreasing with increasing the investigation depth, such as pole-pole, pole-dipole and dipole-dipole arrays.

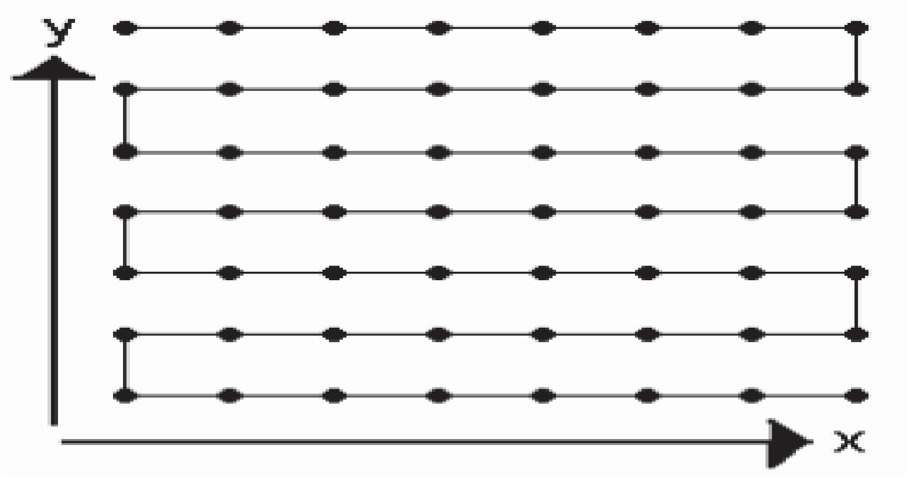

Figure (3-11):- The arrangement of the electrodes for 3D survey, (Loke, 2012).

According to Loke, (2012), for larger coverage and more depths by 3D surveys, measurements are made only in two perpendicular or parallel 2D survey lines (X and Y). The 3D data set consists of a number of parallel 2D lines, (Rucker et al., 2009a).

The data from each 2D survey line is initially inverted independently to give a series of 2D cross-sections as in figure (3-12).In this case, the spacing between the electrodes must be equaled or smaller than the spacing between the 2D lines to reduce banding effects ,(Loke, 2010). Al-Zubedi (2015) indicated that the 3D imaging technique that carried out through parallel 2D imaging lines not give a good image about subsurface structures, whether the (Y- spacing) equaled electrode spacing (a) or larger than 4*a*, especially if the survey is carried out for deep investigation . This is agreed with previously mentioned by (Loke, 2014), the model will be constructed from the series of 2D inversions along parallel lines is not a true 3D inversion model.

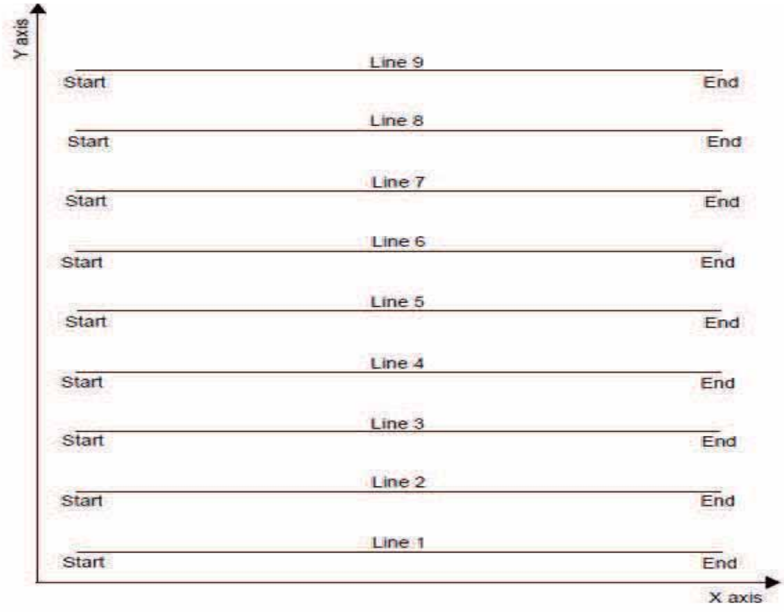

Figure (3-12):- 3D imaging technique by parallel 2D lines, from (ABEM, 2010).

The parallel 2D lines are used because it is useful for surveys with any electrode arrays, (Loke, 2012). However, some authors such as (Pavlova and Shevnin , 2013) consider the cross 2D imaging lines (perpendicular lines) that used to construct 3D model is the 2D azimuthal resistivity imaging survey. The cross 2D imaging lines do not represent the 2D azimuthal resistivity imaging survey because the principles of this survey based on measuring the variation of the resistivity values in different directions and not only in two directions (Taylor and Fleming, 1988).

One method to survey such large grids with a limited number of electrodes is to extend the roll-along technique used in 2D surveys to 3D surveys (Dahlin and Bernstone 1997). Figure (3-13) shows an example of a survey using a multi-electrode resistivity-meter system with 50 electrodes to survey a 10 by 10 grid, (Loke, 2014). However, numerous authors have been noted several suggestions to help migrate 2D imaging data to 3D acquisition (Loke and barker, 1996b; Dahlin and Bernstone, 1997; Dahlin et al., 2002; Bentley and charibi, 2004; Gunther et al., 2006; Loke and Dahlin 2010).

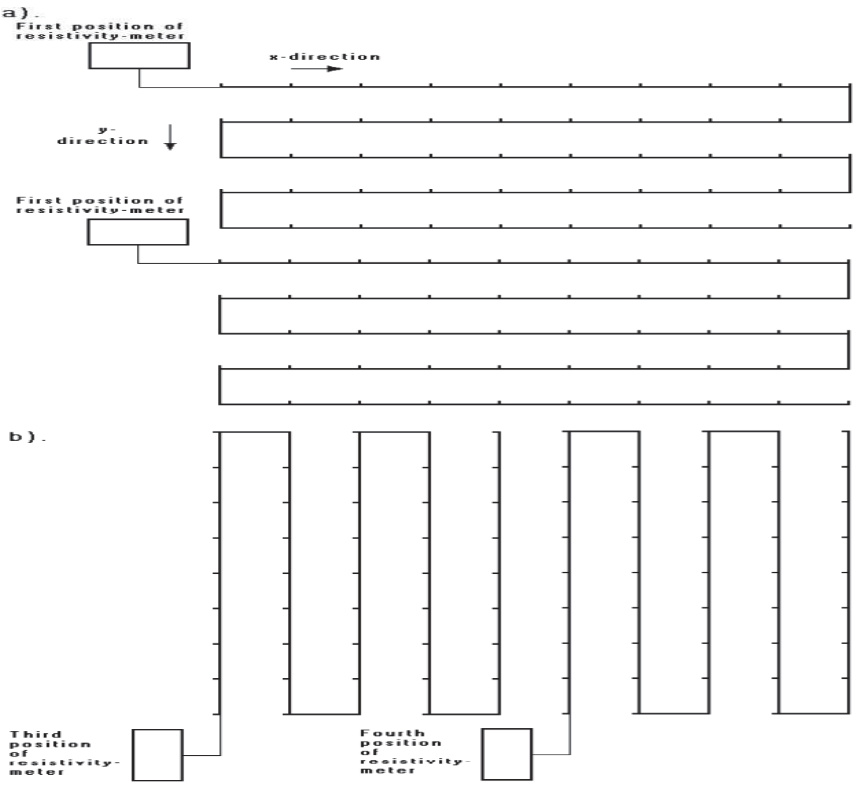

Figure (3-13):- Using the roll-along method to survey a 10 by 10 grid with a multi-electrode system with 50 nodes. (a) Surveys using a 10 by 5 grid with the lines orientated in the *x*-direction. (b) Surveys with the lines orientated in the *y*-direction, (Loke, 2014).

The principles of create Sequences and data processing are the same as those for the 2D case, (Li, 1992; Oldenburg and Li, 1994; Loke and Barker, 1996b). However, to display the data that obtained from parallel 2D survey lines to 3D image. The data file must be set in a format that can be read by RES3DINV program which is intended to be used for inversion processes.

There are two methods that can be used to combine 2D imaging data into a 3D data set, (Loke, 2004). The first is used through RES2DINV program that has an option to combine the data from a number of parallel 2D survey lines into a 3D data set with the format required by the RES3DINV program. In the following table (3-1) is an example script file from Loke (2012), (for more details, please refer to the manual for the RES2DINV program).

Table (3-1):- Shows the file Collate_2D_3D.TXT., (Loke, 2012).

COLLATE_2D_3D.TXT file	Comments
Conversion of RES2DINV data file	Title
Number of files to collate	Header for no. of data files
3	Number of data files
File 1 parameters	Header for first file
Name of data file in RES2DINV format	Header for name of file
d:\test\FILE2D_1.DAT	Full name plus path of file
X and Y location of first electrode along this line	Header
0.0,0.0	Coordinates of the first electrode
Line direction (0=X,1=Y)	Header
0	Number specifying line direction
Line sign (0=positive,1=negative)	Header
0	Specify whether electrode coordinates increase or decrease
File 2 parameters	Same set of parameters for second file
Name of data file in RES2DINV format	
d:\test\FILE2D_2.DAT	
X and Y location of first electrode along this line	
0.0,-0.5	
Line direction (0=X,1=Y)	
0	
Line sign (0=positive,1=negative)	
….	Same for third file
….	
Name of Output file in RES3DINV format	Header
d:\test\FILE_3D.dat	Name of 3-D data file
End of file	Header for end of file

The second method is combined a number of 2D data files into a single 3D data file by use many text editor programs such as NOTEPAD, WORDPAD and Microsoft Office Excel program. In this method, the data are entered into one of these programs as a text file that can be read by the RES3DINV program. The detailed description of the data format is given as follows. As an example, the part of field data from Al-Zubedi (2015), is shown below with some comments.

Table (3-2):- The data file with part from field data with some comments, (Al-Zubedi ,2015).

3D Imaging Station	
60	*Number of electrodes in x direction*
4	*Number of electrodes in Y direction*
10	*x unit electrode spacing*
10	*Y unit electrode spacing*
7	*Array type, 7 Wenner-Schlumberger*
3156	*Number of data points*
300.00 0.00 330.00 0.00 310.00 0.00 320.00 0.00 112.00	
300.00 0.00 350.00 0.00 320.00 0.00 330.00 0.00 144.18	
300.00 0.00 370.00 0.00 330.00 0.00 340.00 0.00 45.80	
300.00 0.00 390.00 0.00 340.00 0.00 350.00 0.00 93.72	
300.00 0.00 410.00 0.00 350.00 0.00 360.00 0.00 7.80	
300.00 0.00 430.00 0.00 360.00 0.00 370.00 0.00 97.86	
300.00 0.00 460.00 0.00 370.00 0.00 390.00 0.00 80.60	
300.00 0.00 480.00 0.00 380.00 0.00 400.00 0.00 92.70	
.	
.	
.	
.	
.	
0	
0	
0	
0	

3-3-2 Interpretation of 3D Imaging Data.

Research and development on forward and inverse modeling methods for 3D resistivity imaging technique are underway. The principles are the same as those for the 2D case, but the demand on computational power is much higher and the practical application of 3D techniques is still in its infancy (Li, 1992; Oldenburg and Li, 1994; Loke and Barker, 1996b).

In the interpretation of data from 2D resistivity imaging surveys, it is assumed that the subsurface geology does not change significantly in the direction that is perpendicular to the survey line. In areas with very complex geology, there could be significant variations in the subsurface resistivity in this direction (i.e. the geology is 3D), which could cause distortions in the lower sections of the 2D model obtained. Measurements made with the larger electrode spacings are not only affected by the deeper sections of the subsurface, they are also affected by structures at a larger horizontal distance from the survey line. This effect is most pronounced when the survey line is placed near a steep contact with the line parallel to the contact, (Loke, 2012).

One model used to interpret the 3D data set is shown in figure (3-14a). The subsurface is divided into several layers and each layer is further subdivided into a number of rectangular blocks. A 3D resistivity inversion program, RES3DINV, is used to interpret the data from 3D surveys. This program attempts to determine the resistivity of the blocks in the inversion model that will most closely reproduce the measured apparent resistivity values from the field survey. Within the RES3DINV program, the thickness of the layers can be modified by the user. Two other alternative models which can be used with this program are shown in (Figures 3-14b and c). The second inversion model subdivides the top few layers vertically as well as horizontally by half. Another alternative is to subdivide the top few layers by half only in the horizontal directions figure (3-14c). Since the resolution of the resistivity method decreases rapidly with depth, it has been found that subdividing the blocks is only beneficial for the top two layers only. In many cases, subdividing the top layer only is enough. By subdividing the blocks, the number of model parameters and thus the computer time required to invert the data set can increase dramatically, (Loke, 2012).

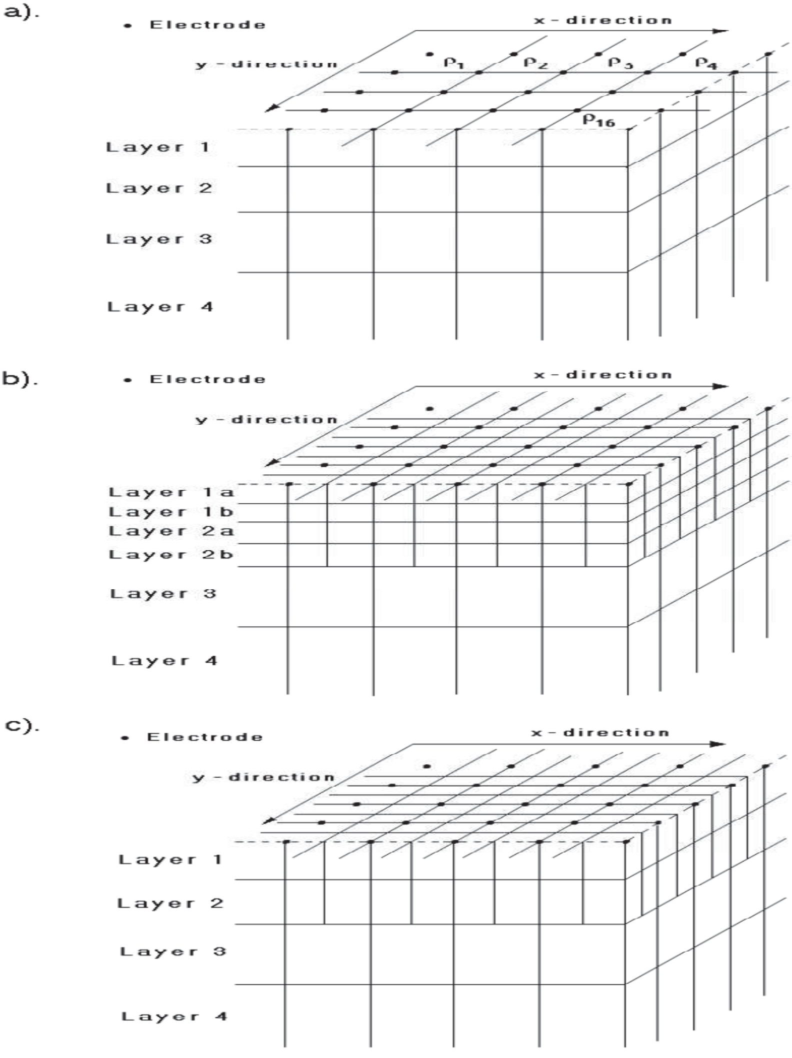

Figure (3-14):- The models used in 3D inversion. (a) Standard model where the widths of the rectangular blocks are equal to the unit electrode spacings in the x- and y-directions. (b) A model where the top few layers are divided by half, both vertically and horizontally, to provide better resolution. (c) A model where the model blocks are divided in the horizontal directions but not in the vertical direction, (Loke, 2014).

Please refer to the instruction manual for the RES3DINV program for the data format. An online version of the manual is available by clicking the "Help" option on the Main Menu bar of the RES3DINV program. The set of files that comes with the RES3DINV program package has a number of field and synthetic data files. You can carry out an inversion of some of these files to get a feel of how the program works. The following figures (3-15) shows the output from the RES3DINVsoftware. However, there are many programs can be used to display the 3D imaging data as 3D view, as shown in figure (3-16).

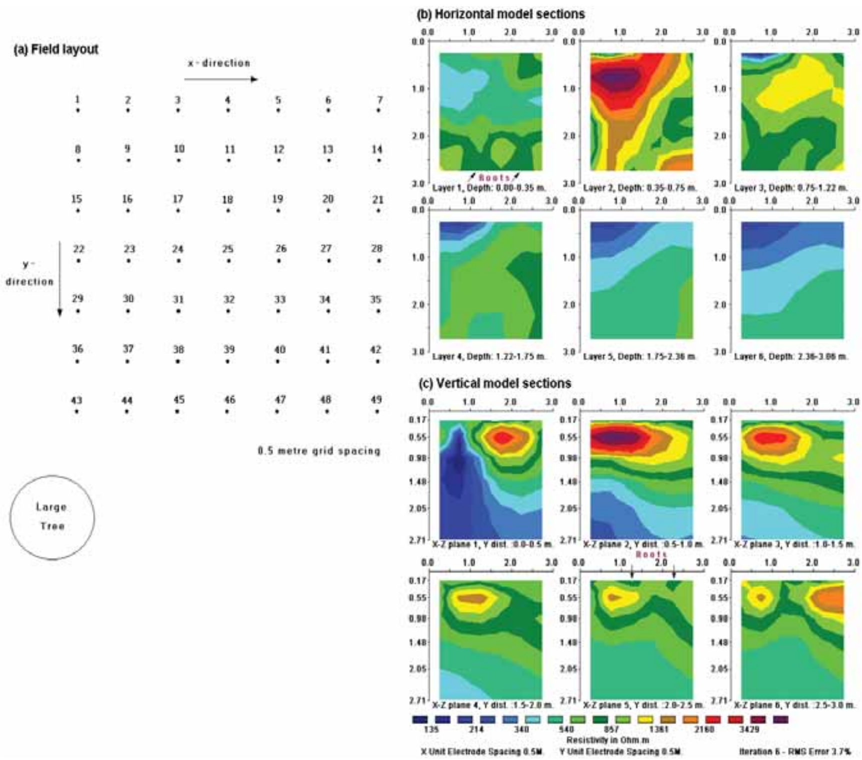

Figure (3-15):- (a) Arrangement of electrodes in the Birmingham 3-D field survey. (b) Horizontal and (c) vertical cross-sections of the model obtained from the inversion of the Birmingham field survey data set. The locations of observed tree roots on the ground surface are also shown, (Loke, 2014).

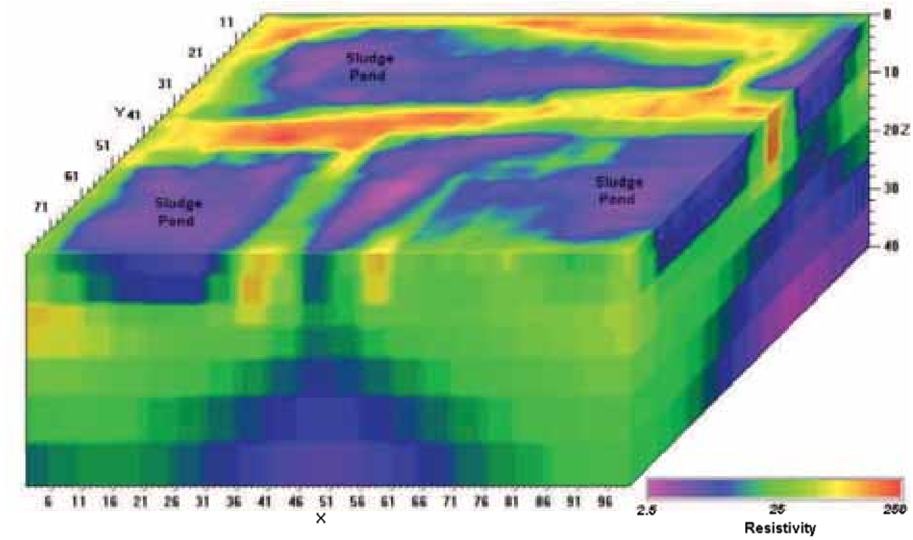

Figure (3-16):- A 3-D view of the model obtained from the inversion of the Lernacken Sludge deposit survey data set displayed with the Slicer/Dicer program. A vertical exaggeration factor of 2 is used in the display to highlight the sludge ponds. Note that the color contour intervals are arranged in a logarithmic manner with respect to the resistivity, (Loke, 2014).

3-4 Time-lapse And 4D Surveys .

Resistivity imaging surveys have not only been carried out in space, but also in time. The change of the subsurface resistivity with time has important applications. Time-lapse has been adopted as a new technology for long-term embankment warning systems (Gunn et al., 2010a; Chambers et al., 2011a; b; Gunn et al., 2014). Modern multi-electrode systems have effectively been used to map water content changes in earthworks such as embankments, (Hassan, 2014). For instance, Jackson et al. (2002) mapped a rapid build-up of moisture on embankment shoulder a few days before a shallow failure. As the seasonal changes in water content control the seasonal resistivity changes, water content anomalies can be extracted from time-lapse measurements, figure (3-17), that can be used as an early warning of moisture build-up in engineered earthworks (Chambers et al., 2009). According to Loke, (2012), a simple, but very interesting, experiment to map the flow of water from the ground surface downwards through the unsaturated zone and into the water table was described by Barker and Moore (1998).

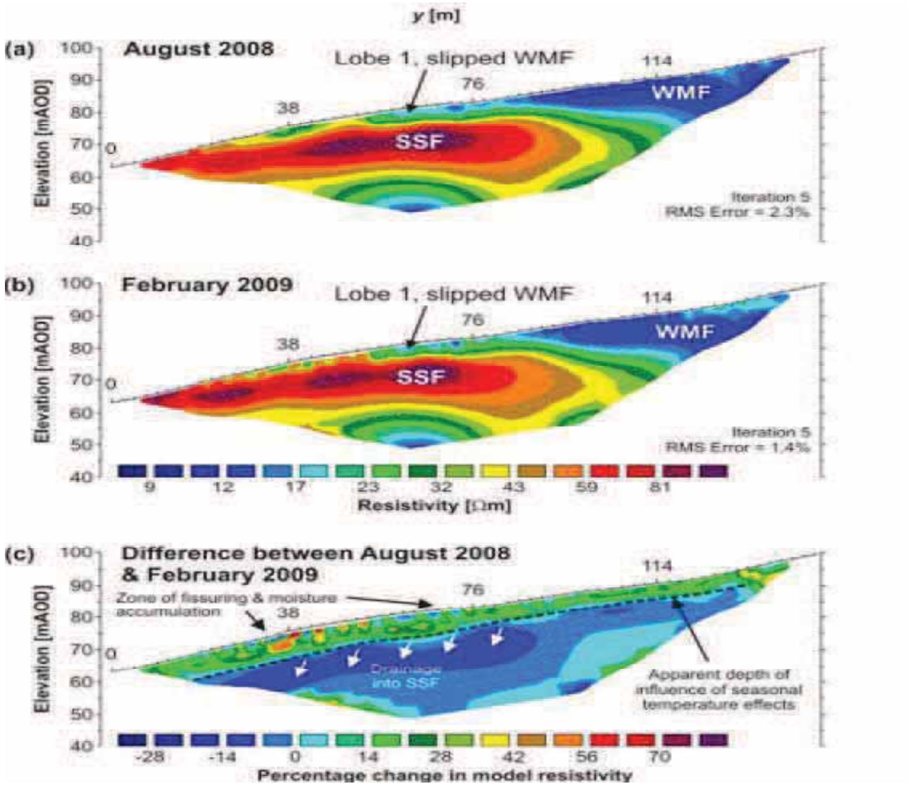

Figure (3-17):- Time-lapse 2D resistivity sections (Chambers et al., 2009).

Time-lapse surveys can be conducted using standard equipment used in 2D and 3D surveys, a number of dedicated automatic monitoring systems with permanently installed cables and electrodes have been developed, (Loke, 2014).

In 4D imaging surveys, the change of resistivity in both space and time is measured. Measurements are repeated at different times using the same 2D survey line or 3D survey grid. A number of techniques have been proposed for the inversion of time-lapse and 4D data, more information about this can be found in (Loke et al., 2013).

3-5 Pulled Array Recording System.

The dynamic type of resistivity instruments that used for resistivity surveys were described in the chapter one. If the available system does not offer enough electrodes to cover a full grid, a series of closely spaced parallel lines may suffice. Sørensen (1996) has developed a pulled-array recording system (PACEP) that adapts the well-known streamer concept from off-shore seismic surveying. A set of eight heavy steel electrodes connected to a heavy-duty cable is pulled by a small caterpillar over areas of interest. While two electrodes inject current, data are recorded continuously from the other six electrodes in three different arrays, figure (3-18). Shallow images extending over distances of several kilometers can be recorded during a single day with this system.

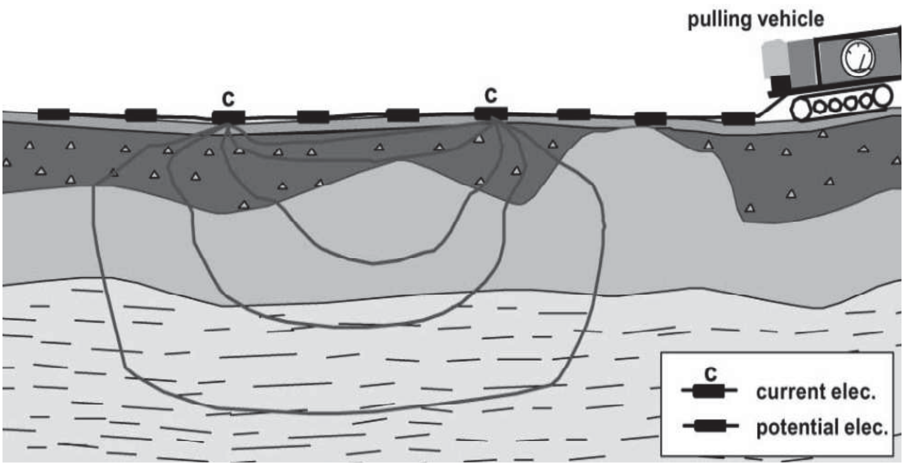

Figure (3-18):- Sketch of pulled array system (Christensen and Sørensen, 1998).

3- 6 Electrode Arrays Characteristics in 2D Imaging Surveys.

Data acquisition techniques in resistivity method were described in an earlier in this and previous chapters. It is based on the response of the earth to the flow of electrical current. Where electrical current is passing into the ground surface by two current electrodes and the potential difference is measured between second couples of electrodes. The arrangement of these electrodes for resistivity surveys is not always the same: sometimes the two potential electrodes are placed between the two current electrodes, other times they are placed outside or apart from the two current electrodes. Also, the distance (electrode spacing) between the four electrodes or each pair of electrodes is not always the same, (Tamssar, 2013). Therefore, these arrays have different sensitivities, different depths of investigation, different resolutions, different horizontal data coverage and different signals strengths.

Some arrays have high resolution in shallow investigation, and they might be appropriate or not to be used in deep investigation, while other arrays have high resolution in deep investigation. Where the resolution is the ability to distinguish separate features; the minimum distance between two features, so that the two can be defined separately rather than as one feature. Normally we think of resolution in the vertical sense, but there is also a limit to the horizontal width of an object that we can interpret from data. Therefore, the choice of best array for a field survey depends on different factors, such as the investigation depth, sensitivity function of array that is connected with the type of structure to be mapped, vertical and horizontal data coverage and the resolution of the array, in addition to, the sensitivity of resistivity meter and background noise level (Roy, and Apparao, 1971; Loke, 2012).

Depends on these factors there are many studies carried out to dilate which of these arrays respond best in mapping targets in different situations such as: (Zhou et al., 2002; Seaton and Burbey, 2002; Dahlin and Zhou, 2004; Reiser et al., 2009; Ahmad et al., 2010; Tamssar, 2013; Abrahem, 2013; Al-Hameedawie ,2013; Al-Zubedi, 2015). The results of these studies showed some important results, and as in the following:-

1- Zhou et al. (2002) investigated the success of different electrode arrays used during 2D imaging surveys for mapping karst hazards (at depths 15-20 m). Three commonly arrays were used during this investigation: the Wenner, the Schlumberger, and the Dipole-Dipole arrays. The aim of the study was to determine which of these arrays respond best in mapping karst hazard areas. The survey was carried out where a sinkhole had occurred. The results showed that the Dipole-Dipole array provides the highest precision of locating the sinkhole feature and has the greatest sensitivity to vertical resistivity boundaries. One drawback of the Dipole-Dipole array is that it does not provide a very high signal for measurement, and therefore it can produce somewhat noisy data. Other array geometries may provide a better signal-to-noise ratio but they do not have the resolving power of the Dipole-Dipole array.

2- Seaton and Burbey (2002) evaluated 2D resistivity technique in fractured crystalline-rock terrain, in the Blue Ridge Province, Southwest Virginia, using the Wenner, Wenner-Schlumberger, Dipole-Dipole and Pole-Pole arrays. The goal of the research was to determine which electrode array will produce the highest data quality from the hydrogeological investigation within the crystalline bedrock aquifers (at depths 25-35 m). For that research, synthetic data (output of numeric modelling of synthetic geologic structures using forward modelling program) and field data of the apparent resistivity were used.

Conclusions of the research showed that:

- The arrays that have the potential electrodes placed inside the current path (Wenner and Wenner-Schlumberger) have a shallower depth of investigation, generally less resolution and sensitivity to geologic detail than arrays with the potential probes outside of the current path (Dipole-Dipole). The Pole-Pole array has significantly greater depth of investigation than the other arrays but lower resolution and sensitivity than the other arrays.
- The Dipole-Dipole array reproduced the shallow and the intermediate depth resistivity structures accurately.
- The Dipole-Dipole is very sensitive even to small structures with anomalously high and low resistivities in the subsurface.
- The Dipole-Dipole has 20-25% greater depth penetration than the Wenner and Wenner–Schlumberger array.
- The higher resolution, greater depth of investigation, and high sensitivity to geologic detail offered by the Dipole-Dipole array outweighed the fact that it used more measurements than the Wenner or Wenner-Schlumberger array.
- The Dipole-Dipole array has low signal strength.

3- Dahline and Zhou (2004) used five synthetic geological models to compare the resolution and efficiency of 2D resistivity imaging survey for ten electrode arrays. These arrays were pole-pole, pole-dipole, half-Wenner, Wenner-α, Schlumberger, dipole-dipole, Wenner-β, γ-array, multiple or moving gradient array, and midpoint-potential-referred measurement arrays. Also he investigated the responses of variation in the data density and noise sensitivities of these electrodes using robust inversion and smoothness-constrain least-square inversion. They provide that the γ-array and Wenner-β are less contaminated by noise than the others electrode arrays. And the dipole-dipole, pole-pole, moving gradient and Schlumberger arrays can yield better resolution images than that of others.

4- Reiser et al. (2009) examined the imaging resolution of four different arrays for mapping of fracture zones in bedrock, (Dipole-Dipole, Gradient, Pole-Dipole and Wenner). The best results were achieved with Gradient and dipole-dipole especially for mapping fracture zones with various depth and width. The Gradient array gives the best response for mapping steeply dipping structures and different contrast, whereas Wenner is good at illustrating horizontal layers. Dipole-Dipole and Pole-Dipole show the most accurate results for situations where a low resistivity top layer is present.

5- Ahmad et al. (2010) investigated the performances of the Wenner and the Dipole-Dipole arrays in mapping an underground three-dimensional cavity using the 3-D resistivity imaging. The objective of the study was to compare the Wenner and the Dipole-Dipole arrays in delineating an underground cavity at a site near the University of Malaya in Malaysia. The results illustrate the superiority of the Wenner array over the Dipole-Dipole array for the determination of the vertical distribution of subsurface resistivity. Note that this research was done by the 3D imaging technique.

6- Tamsser, (2013) evaluated the suitability of different electrode arrays (Wenner, Schlumberger, Pole-Pole and Dipole-Dipole) during 2D surveys, south Africa, to image dykes, sills, fault and fractures (at depths 40-95m). Theoretical results showed that the Wenner array is very sensitive to vertical changes, has the strongest signal strength, yet the smallest depth of investigation and the narrowest horizontal data coverage. The Schlumberger array might not be the most suitable array in resolving dipping structures, but its performance when mapping sills intruded by dykes is good; it has a moderate depth of investigation and is less contaminated by noise compared to the Dipole-Dipole array. The Pole-Pole array has the largest depth of investigation, the widest horizontal data coverage, yet the lowest signal strength and is therefore inherently sensitive to noise.

Based on the results of the modelling investigations, it was decided to employ only the Wenner, Schlumberger and Dipole-Dipole arrays for the field surveys.

The inverse resistivity model obtained from the Schlumberger array imaged the vertical and horizontal changes in resistivity more sharply than the Wenner and Dipole-Dipole arrays.

7- Abrahem, (2013) used three arrays (Wenner-Schlumberger, Wenner, and Dipole – dipole arrays) to determine the best array in delineation the Archaeological targets in Uruk Archaeological Site ,Iraq. Dipole- dipole array is found to be the best array compared to Wenner and Wenner- Schlumberger arrays for detecting archaeological targets.

8- Al-Hameedawi ,(2013) evaluated the four arrays (Wenner-Schlumberger, Wenner , Schlumberger reciprocal and dipole – dipole arrays) in delineating aquifer boundaries (at depths 100-225m) in North Badra Area Eastern Iraq. The results of 2D imaging show that the Dipole-Dipole array is highly affected by near surface inhomogeneity (NSI) and lateral inhomogeneity, so that it's inverse model fails in delineating layers and aquifers. Its vertical resolution decreases with increasing depth and/or increasing inhomogeneity. The Wenner array shows good quality apparent resistivity measurements in comparison with the others electrode arrays, because it is less affected by inhomogeneity. Its ability in delineating aquifers (or layers), however, decreases with increasing the array length and/or increasing inhomogeneity. The apparent resistivity measurements of Schlumberger reciprocal array show good quality compared with the Dipole-Dipole array, and the inverse models of Schlumberger reciprocal array succeed in delineating the aquifers. Furthermore, it gives more depth of investigation than does other arrays. However, Wenner and Schlumberger reciprocal arrays give significant results in delineating layers and aquifers especially with small survey line and/or low inhomogeneity, but they do not show an optimal correspondence with the lithological sections of wells. However, their resolution is still less than that of Wenner-Schlumberger array

The Wenner-Schlumberger array gives the best results in delineating layers and aquifers, and shows the best resolution. Therefore, it is useful in determining the aquifers especially in areas with high background noise.

9- Al-Zubedi, (2015) tested through synthetic model three important electrode arrays in 2D imaging surveys to determine which array is the most successful in defining the vertical and horizontal geological structures that locate at different depths (10-110m). These arrays are Wenner-Schlumberger, Wenner and Dipole - dipole. The results showed that the Wenner-Schlumberger is the most suitable electrode array when both vertical and horizontal structures are present in the subsurface. It is the best in defining both the vertical and horizontal contacts and represented the vertical fracture zone and cavities more accurately than the Wenner and Dipole-dipole arrays.

The results of these studies indicated a higher resolution and high sensitivity to geologic detail for shallow investigation offered by the Dipole-dipole than other arrays, while the Wenner-Schlumberger is the best than other arrays for deep investigation.

3-7 Array Optimization Methods.

The development of automated data acquisition and inversion in recent years has increased the practical applicability of resistivity imaging tremendously, (Dahlin, 2001). There has been significant progress in automatic techniques to find the optimum set of electrode array configurations (Stummer et al., 2004; Maurer et al., 2010) in recent years, (Loke et al., 2015).The optimization methods are used the arrays to generate the maximum amount of information of the subsurface with 2D resistivity imaging surveys for a limited number of four-electrode measurements, (Alfuozan, 2008). Therefore, the optimized arrays can significantly improve the resolution obtained with 2D and 3D surveys (Wilkinson et al., 2012; Loke et al., 2014c).

The first attempt to apply resistivity data optimization in geological surveying was made by Cherkaeva and Tripp (1996), who applied a system of pole-pole configurations to current distribution on features at particular depths and locations. They applied theoretical works into geological setting. The study showed how the numerical experiments could discover optimal perturbations determined from priori model. Therefore, they concluded that the optimal method can be used as imaging technique based on either two applications. One application is for calculating the impedance matrices by using the suitable forward algorithm model to find the corresponding currents numerically, while the second application is considered to have insufficient information of the inclusion, so it could use the measured impedance matrix then find the optimal intensity distribution over the electrodes (Cherkaeva and Tripp, 1996).

Wilkinson et al. (2006) proposed a new optimization methods, which named the (Compare R) developed by British Geological Survey directly compares the model resolution matrices produces the best results but is much slower. British Geological Survey developed the second method (BGS). It uses linear approximations based on the modifications in the Jacobian matrix. Stummer et al. (2004) present method called (ETH), which uses the sensitivity distributions to calculate evaluation of the model resolution matrix. This provides a measure of how strongly the apparent resistivity data determines each model's cell. Loke et. al., (2007) present a new method called Combined (BGS-CR), which uses a combination of the (BGS) and (Compare R) methods. However, the (Compare R) method proved to provide arrays with the highest resolution among the other methods, (Loke et al. 2015).

Loke (2014) give a description of the array optimization methods procedures of the 2D resistivity technique. The number of possible array combinations (M) with 4 electrodes is

$$M=N(N-1)(N-2)(N-3)/8$$

As an example, for a system with 30 electrodes, there are 82215 possible configurations. We can reduce the number by rejecting all configurations with the Gamma arrangement (with interleaved current and potential electrodes), and those with very high geometric factors (i.e. low potentials) of greater than the dipole-dipole with a=1 and n=6. This reduces the total number of possible array configurations to 51283, which is called the (comprehensive) data set (Wilkinson et al. 2006b). If we make measurements with all these possible array configurations, we should get the best possible resolution.

Although taking all the 51283 possible readings will give the maximum possible resolution, this is not practical in actual field survey. We want to take a small subset of the possible readings that gives almost the same resolution. A possible algorithm (Stummer et al. 2004, Wilkinson et al. 2006b) is as follows:-

1. Start with a small set, the (base) data set, such as the dipole-dipole readings with a=1 and n=1 to 6 (147 readings).
2. Calculate the increase in the model resolution as each new array is added to the (base) set (there are several alternatives for this step with differences in speed and accuracy). Add the arrays that give the highest increase to the model resolution (and are sufficiently independent of each other) to the base set. After each iteration, increase the base set by about 9%.
3. Use the new set (base plus new arrays) as the base set, and repeat the procedure. Stop when the desired maximum number of arrays (eg. 5000) is reached.

To illustrate the performance of the different array configurations in detecting subsurface structures, a test model with four rectangular blocks at different depths (Wilkinson et al. 2006b) is used, figure (3-19).

Synthetic data sets were generated for the Wenner, Wenner-Schlumberger, dipole-dipole and optimized arrays. The data sets were then inverted to recover back the subsurface resistivity.

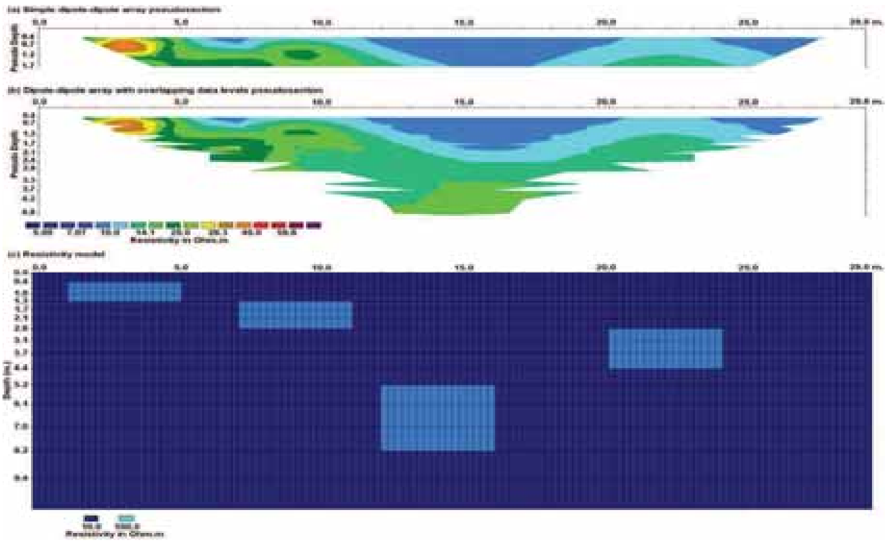

Figure (3-19):- Test inversion model for the different arrays. (a) Apparent resistivity pseudosection for the simple dipole-dipole array with a dipole length '*a*' of 1.0 meter with the dipole separation factor '*n*' of 1 to 6. (b) Apparent resistivity pseudosection for the dipole-dipole array with overlapping data levels. (c) The synthetic model with 4 rectangular blocks of 100 Ω.m embedded in a medium of 10 Ω.m. as used by Wilkinson et al. (2006b) from (Loke, 2014).

Figure (3-20a) shows the resulting inversion model for the Wenner array data set. The two topmost blocks are well resolved while the third block is poorly resolved. The deepest block is completely unresolved. The Wenner-Schlumberger array data set, figure (3-20b) performs slight better in resolving the third block but still cannot resolve the deepest block. The simple dipole-dipole array data set with a single dipole length (a=1.0m.) performs significantly better than even the Wenner-Schlumberger array data set where the third block is well resolved, figure (3-20c), even though it has fewer data points (147 compared with 292). However, it still cannot resolve the deepest block. The dipole-dipole array data set with multiple dipole lengths (all possible data points with a=1.0 to 3.0m. and n=1 to 6, with the restriction that the geometric factor cannot exceed that for a=1.0 and n=6) shows higher resistivity values at he location of the deepest block but it is not able to resolve the block, figure (3-20d).

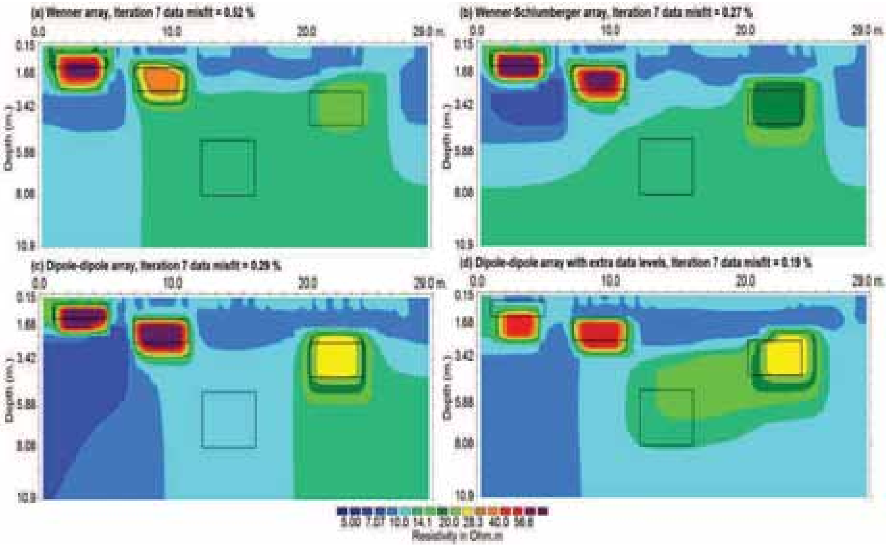

Figure (3-20):- Inversion results with the (a) Wenner array, (b) Wenner-Schlumberger array, (c) simple dipole-dipole array and (d) dipole-dipole array with overlapping data levels,(Loke, 2014).

The deepest block is fairly well resolved in the inversion model for the optimized data set with 4462 data points, figure (3-21a) where the shape and dimensions are close to the true structure. It might be argued that the better performance of the optimized data set compared to the dipole-dipole array with multiple dipole lengths is due to the much larger number of data points (4462 compared to 342). Next we use a truncated subset of the optimized data set with only 413 data points that is comparable to the dipole-dipole array data set. The inversion model with the truncated optimized data set, figure (3-21b) still shows significant better resolution for the deepest block compared to the dipole-dipole array model, figure (3-21d). While the shape of the deepest block is significantly less sharp compared to the large optimized data set, it still is better defined compared to the dipole-dipole array model. The third deepest block is also much better resolved by both optimized data sets with resistivity values of over 50 Ohm.m at the center compared to less than 30 Ohm.m for the dipole-dipole array model.

The simple example shows that there can be significant improvements in the depth resolution by using an optimized data set. An old rule of thumb in resistivity sounding is that the maximum depth of investigation is about one-sixth (17%) the line length, i.e. slightly less than 6 meters near the center of the line in the above examples. However, using an optimized data set has pushed this limit close to 8 meters or slightly more than one-fifth (about 28%) the line length. for more details, please refer to (Loke et al. 2015) and (Loke, 2014).

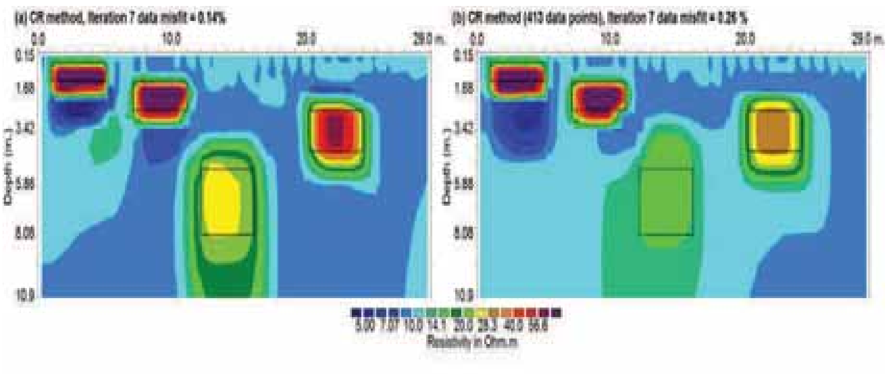

Figure (3-21):- Inversions models with the (a) optimized data set with 4462 data points and (b) a truncated optimized data set with 413 data points,(Loke, 2014).

References

ABEM, 2010. ABEM Terraloc Operators manual. Bromma, Sweden, 85P.

Abrahem, S.N., 2013. Comparison Between The Ground Penetration Radar (GPR) and 2D Imaging in Delineation and Identification Subsurface Archaeological Structures in Uruk Site , Al – Muthanna Governorate . Ph.D. Thesis, (Unpublished), University of Baghdad, college of Science. 131p.

Ahmad, N., Wan Abdullah, W.A.T., Samsudin, T. and Behrang, N., 2010. Comparison of Wenner and Dipole–Dipole arrays in the study of an underground three-dimensional cavity. *Journal of Geophysics and Engineering* **7**, 30–40.

Aizebeokhai, A. P., and Olayinka,A.I., 2010. Anomaly effects of arrays for 3D geoelectrical resistivity imaging using orthogonal or parallel 2D profiles. *African Journal of Environmental Science and Technology* **7**, 446-454.

AL-Ane, J. M., 1998. Theoretical and Application Consideration for the effect of the geometry on Schlumberger and dipole configuration. Ph.D. Thesis, (Unpublished), University of Baghdad, college of Science, 144p.

Alfouzan, F.A., 2008. Optimization Strategies of Electrode Arrays Used In Numerical and Field 2D Resistivity Imaging Surveys. Ph.D. Thesis, University Sains Malaysia. 254p.

Al-Hameedawie, M. A., 2013. Comparison between different electrode arrays in delineating aquifer boundary by using 1D and 2D techniques in north Badra area eastern Iraq. M.sc. Thesis, (Unpublished), University of Baghdad, college of Science. 142p.

Alpin,L.M., 1950. The Theory of Dipole Sounding, Moscow, Gostoptekhizdat,89P. (In Russian), English Translation in Keller,G.V.,1966, Dipole Methods for Measuring Earth Conductivity, Consultant Bureau, Plenum Press ,New York, 61-78.

Al-Zubedi, A. S., 2009. Application of Vertical Electrical Sounding and 2D Imaging for Delineation of Part of Aquifers South and Southwest Samawa City, Southern Iraq. M.Sc. Thesis (Unpublished), University of Baghdad, college of Science.125p.

Al-Zubedi, A.S., and Thabit, J.M., 2014. Comparison between 2D imaging and vertical electrical sounding in aquifer delineation: a case study of south and south west of Samawa City (IRAQ), *Arabian Journal of Geosciences* 7(1), 173 – 180.

Al-Zubedi, A. S., 2015. Delineation of Subsurface Fracture Characteristics Using 2D Azimuthal Resistivity Imaging in Dammam Aquifer Within and Out of Abu-Jir Fault Zone , Southwest of Karbala City, Central Iraq. Ph.D. Thesis, (Unpublished), University of Baghdad, college of Science. 147p.

References

Amin, A. K., 2008. Aquifer delineation and evaluation of hydraulic parameters from surficial resistivity measurements in sharazoor basin- north east Iraq. Ph.D. Thesis, (Unpublished), University of Baghdad, college of Science .181P.

Barker, R.D., and Moore, J.,1998. The application of time lapse electrical tomography in ground water studies. *Leading Edge*, 17,1454-1458.

Barker, R.D., 1992. A simple algorithm for electrical imaging of the subsurface. First Break 10, 53-62.

Barker, R.D., 1991. Depth of investigation of collinear symmetrical four-electrode arrays. *Journal of Geophysics* 54, 1031-1037.

Bentley, L. R., and Gharibi, M., 2004. Two- and three-dimensional electrical resistivity imaging at a heterogeneous remediation site. *Journal of Geophysics*, 69 (3), 674–680.

Bhattacharya, P. K., and Patra, H.P., 1968. Direct Current Geoelectrical Sounding, *Elesvier Publishing Company*, Amsterdam, 131p.

Bobachev, C., 2002. "IPI2Win" A Windows Software for an Automatic Interpretation of Resistivity Sounding Data, Ph.D. Moscow State University, Moscow, Russia, 320p.

Burger, H. T., Sheehan, A. F., Jones, C.H., 2006. Introduction to Applied Geophysics: Exploring the Shallow Subsurface. W.W. Norton & Company, London.

Busby, J. P., 2000. The effectiveness of azimuthal apparent resistivity measurements as a method for determining fracture strike orientations, *Journal of Geophysical Prospecting* 48, 677–695.

Busby, J. P. and Jackson, P., 2006. The application of time-lapse azimuthal apparent resistivity measurements for the prediction of coastal cliff failure, *Journal of applied Geophysics* 59, 261–272.

Carpenter, E.W. and Habberjam, G.M., 1956. A tri-potential method of resistivity prospecting. *Journal of Geophysical Prospecting* 29, 128-143.

Chambers, J. E., Meldrum, P. I., Gunn, D. A., Wilkinson, P. B., Kuras , O., Weller , A. L., and Ogilvy, R.D., 2009. Hydrogeophysical monitoring of landslide processes using automated time-Lapse electrical resistivity tomography (ALERT), *15th European meeting of environmental and engineering geophysics*, Dublin, Ireland.

References

Chambers, J. E., Wilkinson, P.B., Kuras, O., Ford, J. R., Gunn, D. A., Meldrum, P.I., Cherkaeva, E. & Tripp, A. C., 1996. Optimal Survey Design Using Focused Resistivity Arrays. *Ieee Transactions On Geoscience And Remote Sensing* 34, 358–366.

Chambers J E, Wilkinson P B, Weller A L, Ogilvy R D, Meldrum P I, and Caunt, S, 2007. Mineshaft imaging using surface and cross-hole 3D electrical resistivity tomography: A case history from the East Pennine Coalfield, UK. *Journal of Applied Geophysics* 62, 324-337.

Chitea F., and Georgescu P., 2009. Sensitivity function for various geoelectric arrays. Geophysical Research Abstracts. University of Bucharest, Faculty of Geology and Geophysics.

Christensen, N.B., S_rensen, K.I., 1998. Surface and borehole electric and electromagnetic methods for hydrogeological investigations. *European Journal of Engineering and Environmental Geophysics* 3 (1), 75–90.

Compagnie General de Geophysique, 1963. Abaques de sounding electrique, Master curve for electrical sounding, European association of exploration geophysicists.

Dahlin, T., 1996. 2D resistivity surveying for environmental and engineering applications. First Break 14 (7), 275–283.

Dahlin, T., 2001. The development of DC resistivity imaging techniques. *Computers and Geosciences* 27 (9), 1019–1029.

Dahlin, T. and Bernstone, C., 1997. A roll-along technique for 3D resistivity data acquisition with multi-electrode arrays, Procs. SAGEEP'97 (Symposium on the Application of Geophysics to Engineering and Environmental Problems), Reno, Nevada, March 23-26 1997, Vol. 2, 927-935.

Dahlin, T. and Zhou, B., 2004. A numerical comparison of 2D resistivity imaging with 10 electrode arrays. *Journal of Geophysical Prospecting* 52, 379-398.

Dahlin, T., Bernstone, C., Loke, M.H., 2002. A 3D resistivity investigation of a contaminated site at Lernacken in Sweden. *Geophysics* 60 (6), 1682–1690.

Dahlin, T., Loke, M.H., 1998. Resolution of 2D Wenner resistivity imaging as assessed by numerical modelling. *Journal of Applied Geophysics* 38 (4), 237–249.

Dahlin, T., Zhou, B., 2006. Multiple gradient array measurements for multi-channel 2D resistivity imaging. *Near Surface Geophysics* 4 (2), 113–123.

deGroot-Hedlin, C., Constable, S., 1990. Occam's inversion to generate smooth, two-dimensional models from magneto telluric data. *Geophysics* 55 (12), 1613–1624.

Dey, A., Morrison, H.F., 1979b. Resistivity modeling for arbitrarily shaped three - dimensional shaped structures. *Geophysics* 44 (4), 753–780.

Edwards, L.S., 1977. A modified pseudosection for resistivity and IP. *Journal of Geophysics* 42 (5), 1020-1036.

Flathe, H., 1955. Possibilities and limitation in applying geoelectrical methods to hydrogeological problems in the coastal area of the North West Germany, *geophysical prospecting* 14 (14) , 195-206.

Gerard, R. and Tabbagh, A., 1991. A mobile four electrodes array and its application to electrical survey of planetary grounds at shallow depths. J. *Geophys*. Res., 96 (B-3), 4117-4123.

Griffiths, D. H., and King, R. f., 1981. Applied Geophysics for Geologist and Engineers, Pergamon Press., Second Edition, 223p.

Griffiths, D.H. and Turnbull, J., 1985. A multi-electrode array for resistivity surveying. First Break3, (7), 16-20.

Griffiths, D.H., Turnbull, J. and Olayinka, A.I., 1990. Two-dimensional resistivity mapping with a computer- controlled array. First Break 8, 121-129.

Gunn, D. A., Chambers, J. E., Uhlemann, S., Wilkinson, P. B., Meldrum, P. I., Dijkstra, T. A., Haslam, E., Kirkham, M., Wragg, J., Holyoake, S., Hughes, P.N., Hen-Jones, R. and Glendinning, S., 2014. Moisture monitoring in clay embankments using electrical resistivity tomography. *Construction and Building Materials*, 1-13.

Gunn, D. A., Ogilvy, R., Chambers, J. and Meldrum, P., 2010a. ALERT-ME New technologies for embankment warning systems. *Rail Technology Magazine*, Oct/Nov 2010, 80-82.

Gunther, T., Rucker, C., and Spitzer, K., 2006. Three-dimensional modeling and inversion of dc resistivity data incorporating topography-II. Inversion. *Geophysical Journal International* 166, 506–517

Habberjam, G. M. and Watkins, G. E., 1967. The use of a square configuration in resistivity prospecting, *Journal of Geophysical Prospecting*15, 445–467.

Hallof, P. G., 1957: On the interpretation of resistivity and induced polarization measurements. PhD Thesis, Massachusetts institute of technology.

Hagrey, S. A., 1994. Electric study of fracture anisotropy at Falkenberg, Germany, *Journal of Geophys*. 59, 881–888.

Hassan, A.A., 2014. Electrical Resistivity Method for Water Content Characterisation of Unsaturated Clay Soil. Ph. D. Thesis, Durham University. 303p.

Keller, G. V. and Frischknecht, F. C., 1966. Electrical Methods in Geophysical Prospecting, Pergamon Press Inc., Oxford, 519p.

Keller, G. V. and Frischknecht, F. C., 1970. Electrical methods in geophysical

Keller, G. V., and Frischknecht, F. C., 1982. Electrical methods in geophysical prospecting, Third edition, Pegamon press Inc., Oxford, 523P.

Kemna, A., Kulessa, B., Vereecken, H., 2002. Imaging and characterisation of subsurface solute transport using electrical resistivity tomography (ERT) and equivalent transport models. *Journal of Hydrology* 267 (3–4), 125–146.

Kirch, R., 2006. Groundwater geophysics. Springer-Verlag Berlin Heidelberg. 489p.

Kunetz, G., 1966. Principle of direct current resistivity prospecting. Borntrager, Berlin, 106 p.

Lashkaripour, G.R., and Nakhaei, M.,2005, Geolecatrical Investigation for the Assessment of Groundwater Conditions: a Case Study. *Annals of Geophysics* 48, 937-944.

Leonard, M. P., 1984. A surface resistivity method for measuring hydrologic characteristics of jointed formations, U.S. Bur. Mines Report of Investigations. No. 8901.

Li Y, and Oldenburg D.W., 1992. Approximate inverse mappings in DC resistivity problems. *Geophysical Journal International* 109, 343-362.

Loke, M. H., 1999.Tutorial: 2-D and 3D Electrical Imaging Surveys, 111p.

Loke, M.H., 2004. Tutorial: 2-D and 3D Electrical Imaging Surveys, 127p.

Loke, M. H., 2010. Tutorial: 2-D and 3D Electrical Imaging Surveys, 145p.

Loke, M. H., 2012. Tutorial: 2-D and 3D Electrical Imaging Surveys, 172p.

Loke, M. H., 2014. Tutorial: 2-D and 3D Electrical Imaging Surveys, 188p.

Loke, M. H., Alfouzan, F. A. and Nawawi, M. M., 2007. Optimisation of Electrode Arrays Used In 2d Resistivity Imaging Surveys. In: Aseg (Australian Society of Exploration Geophysicists), *19th Geophysical Conference and Exhibition*. Perth, Western Australia, 18- 22 November 2007, Extended Abstract.

Loke, M.H. and Barker, R.D., 1995. Least-square deconvolution of apparent resistivity pseudo-sections. *Journal of Geophysics* 60(6), 499-523.

Loke, M.H., Barker, R.D., 1996a. Rapid least-squares inversion of apparent resistivity pseudosections by a quasi- Newton method. *Geophysical Prospecting* 44 (1), 131–152.

References

Loke, M. H., and Dahlin, T., 2010. Methods to reduce banding effects in 3-D resistivity inversion. Procs. 16th European Meeting of Environmental and Engineering Geophysics, 6-8 September 2010, Zurich, Switzerland, 16 p.

Loke, M. H., Chambers J.E., Rucker D.F., Kuras O., Wilkinson P. P., 2013. Recent developments in the direct-current geoelectrical imaging method. *Journal of Applied Geophysics* 95, 135–156.

Loke, M.H., Wilkinson, P.B., Chambers, J.E., Uhlemann, S.S. and Sorensen, J.P.R., 2014. Optimized arrays for 2-D resistivity survey lines with a large number of electrodes. *Journal of Applied Geophysics* 122, 136-146.

Loke, M.H., Wilkinson, P.B., Uhlemann, S.S., Chambers, J.E., Oxby, L.S., 2014c. Computation of optimized arrays for 3-D electrical imaging surveys. *Geophys Journal Intentional* 199, 1751–1764

Lowrie, W., 2007. Fundamentals of Geophysics. The Edinburgh Building, Cambridge CB2 8RU, UK. , Second Edition, 393p.

Maillet, R., 1974. Fundamental Equations of Electrical prospecting. *Geophysics* 12, 297-308.

Massoud, U., Qady ,G., Metwaly, and Santos,F., 2009. Delineation of Shallow Subsurface Structure by Azimuthal Resistivity Sounding and Joint Inversion of VES-TEM Data: Case Study near Lake Qaroun, El Fayoum, Egypt. *Pure and Applied Geophysics* 166, 701–719.

Maurer, H., Curtis, A., Boerner, D.E., 2010. Recent advances in optimized geophysical survey design. *Geophysics* 75, 177–194.

McGillivray, P.R. and Oldenburg, D.W., 1990. Methods for calculating Frechet derivatives and sensitivities for the non-linear inverse problem: A comparative study. *Journal of Geophysical Prospecting* 38, 499-524.

Merrick, N.P., 1997. A new resolution index for resistivity electrode arrays. *Exploration Geophysics* 28, 106-109.

Nimmer, R. E., Osiensky, J. L., Binley, A. M. & Williams, B. C., 2008. Three-dimensional effects causing artifacts in two-dimensional, cross-borehole, electrical imaging. *Journal of Hydrology* 359, 59-70.

Nunn, K. R., Barker, R. D., and Bamford, D., 1983. In-situ seismic and electrical measurements of fracture anisotropy in the Lincolnshire chalk, Quart. *Journal of Engineering Geology* 16, 187-195.

Oldenburg, D.W. and Li, Y., 1999. Estimating depth of investigation in dc resistivity and IP surveys. *Geophysics* 64 (2), 403–416.

References

Oldenborger, G.A., Routh, P.S. and Knoll, M.D., 2005. Sensitivity of electrical resistivity tomography data to electrode position errors. *Geophysical Journal International* 163, 1–9.

Orellana, E., and Moony, H. M.,1966. Master Tables and Curves for Vertical Electrical Sounding over Layered Structures, Interciencia, Costanilla de Los Angeles, 15, Madrid, Spain.

Overmeeren, R.A., van Ritsema, I.L., 1988. Continuous vertical electrical sounding. First Break 6 (10), 313–324.

Panissod, C., Dabas, M., Hesse, A., Jolivet, A., Tabbagh, J., Tabbagh, A., 1998. Recent developments in shallow depth electrical and electrostatic prospectingusing mobile arrays. *Geophysics* 63–5, 1542–1550.

Pavlova, A.M, and Shevnin, V.A., 2013. 3D Electrical Resistivity Tomography in Glacial Sediments. Near Surface Geoscience -19th European Meeting of Environmental and Engineering Geophysics Bochum, Germany, 9-11 September.

Pazdirek, O. and Blaha, V., 1996. Examples of resistivity imaging using ME-100 resistivity field acquisition system. EAGE 58th Conference and Technical Exhibition Extended Abstracts. Houten, the Netherlands: EAGE.

Pennington, C. V. L., Weller, A., L., Hobbs, P. R. N. and Ogilvy, R. D. 2011b. Threedimensional geophysical anatomy of an active landslide in Lias Group mudrocks, Cleveland Basin, UK. *Geomorphology* 125, 472-484.
prospecting, Second edition book, Pergamon press Inc., Oxford, 519P.

Reiser. F., Dalsegg. E., Dahlin. T., Guri. V., GanerØd., RØnning.J. S., 2009. Resistivity modeling of fracture zones and horizontal layers in bedrock. Geological survey of Norway. 120p.

Robinson, E.S. and Coruh, C., 1988. Basic Exploration Geophysics, Wiley, New York, 562p.

Roy, A. and Apparao, A., 1971. Depth of investigation in direct current methods. *Journal of Geophysics* 36, 943-959.

Rucker, D.F., Levitt, M.T., and Greenwood, W.J., 2009a. Three-dimensional electrical resistivity model of a nuclear waste disposal site. *Journal of Applied Geophysics* 69 (3–4), 150–164.

Sasaki, Y., 1992. Resolution of resistivity tomography inferred from numerical simulation. *Geophysical Prospecting* 40 (4), 453–464.

References

Seaton, W.J. and Burbey, T.J., 2002. Evaluation of two-dimensional resistivity methods in a fractured crystalline-rock terrain. *Journal of Applied Geophysics* 51, 21- 41

Shima, H., Sakashita, S. and Kobayashi, T., 1996. Developments of non-contact data acquisition techniques in electrical and electromagnetic explorations. *Journal of Applied Geophysics* 35, 167-173.

Sørensen, K., 1996. Pulled array continuous profiling. First Break 14 (3), 85–90.

Steinich, B.; Simon, I.; Chavarria, J.A. and Marin, L.E., 1997. Geological investigations of the vadose zone in the valley of Hermosillo aquifer, Sonora, Mexico. *Journal of Geophysics International* 36 (3), 191-200.

Stummer, P., Maurer, H., Green, A., 2004. Experimental design: electrical resistivity data sets that provide optimum subsurface information. *Geophysics* 69, 120–129.

Szalai, S., Szarka, L., 2008. On the classification of surface geoelectric arrays. *Journal of Geophysical Prospecting* 56 (2), 159–175.

Tamssar, A. Hamidou, 2013. An evaluation of the suitability of different electrode arrays for geohydrological studies in karoo rocks using electrical resistivity tomography. Ph.D. Thesis, university of Free State, faculty of natural and agricultural science, south Africa.183p.

Taylor, R. W. and Fleming, A. H., 1988. Characterizing jointed systems by azimuthal resistivity surveys. *Journal of Groundwater* 26, 464–474.

Telford, W.M.; Geldart, L.P.; Sheriff, R.E., and Keys, D.A., 1979. Applied Geophysics, Cambridge University Press, Cambridge, England, 451-455.

Van Overmeeren, R. A., 1989. Aquifer Boundaries Explored by Geophysical Measurements in the Coastal Plain of Yamen, A Case of Equivalence, *Geophysics* 54(1), 38- 48.

USGS, 2010. Surface Geophysics for Groundwater Exploration, Workshop, Erbil, Iraq.

Watson, K. A. and Barker, R. D., 1999. Differentiating anisotropy and lateral effects using azimuthal resistivity offset Wenner soundings. *Journal of Geophysics* 64(3), 1-7.

Wilkinson, P.B., Loke,M.H.,Meldrum, P.I., Chambers, J.E., Kuras, O., Gunn, D.A., Ogilvy, R.D., 2012. Practical aspects of applied optimised survey design for Electrical Resistivity Tomography. *Geophys Journal Intentional* 189, 428–440.

Wilkinson, P.B., Meldrum, P.I., Chambers, J.C., Kuras, O. and Ogilvy, R.D., 2006b. Improved strategies for the automatic selection of optimized sets of electrical resistivity tomography measurement configurations. *Geophys Journal Intentional* 167, 1119-1126.

Wilkinson, P.B., Meldrum, P.I., Chambers, J.E., Kuras, O., Ogilvy, R.D., 2006. Improved strategies for the automatic selection of optimized sets of electrical resistivity tomography measurement configurations. *Geophys Journal Intentional* 167, 1119–1126.

Wilkinson, P. B., Chambers, J. E., Lelliot, M., Wealthall, G. P. & Ogilvy, R. D., 2008. Extreme Sensitivity Of Crosshole Electrical Resistivity Tomography Measurements To Geometric Errors. *Geophysical Journal International* 173, 49-62.

Zhao, J.X., Rijo, L. and Ward, S.H., 1986. Effects of geologic noise on cross-borehole electrical surveys. *Geophysics* 51, 1978-1991.

Zhou, B. and Greenhalgh, S.A., 2000. Cross-hole resistivity tomography using different electrode configurations. *Geophysical Prospecting* 48, 887-912.

Zhou, QY, Matsui H, Shimada J., 2004. Characterization of the unsaturated zone around a cavity in fractured rocks using electrical resistivity tomography. *Journal Hydraulic Res*. 42, 25-31.

Zhou, W., Barry, F.B. and Angela, L.A., 2002. Effective electrode array in mapping karst hazards in electrical resistivity tomography. *Environmental Geology* 42, 922-928.

Zohdy, A. A. R., 1974. Electrical Methods Application of Surface Geophysics to Groundwater Investigations, Techniques of Water Resources Investigations of the United States Geological Survey (USGS), book 2, chapter D1, 66p.

Zohdy, A.A.R., Eaton, G.P., and Mabey, D.R., 1974. Application of surface geophysics to ground-water investigations; U.S. geological survey. Techniques of water resources investigation, 66p.